VARIATIONS OF THE FRASER RIVER PLUME; OBSERVATIONS AND COMPUTER SIMULATIONS

by

LOUISE ROYER

B.Sc., Université de Montréal, 1979

A THESIS SUBMITTED IN PARTIAL FULFILMENT OF

THE REQUIREMENTS FOR THE DEGREE OF

DOCTOR OF PHILOSOPHY

in

THE FACULTY OF GRADUATE STUDIES

Department Of Oceanography

We accept this thesis as conforming

to the required standard

THE UNIVERSITY OF BRITISH COLUMBIA

July 1983

In presenting this thesis in partial fulfilment of the requirements for an advanced degree at the University of British Columbia, I agree that the Library shall make it freely available for reference and study. I further agree that permission for extensive copying of this thesis for scholarly purposes may be granted by the head of my department or by his or her representatives. It is understood that copying or publication of this thesis for financial gain shall not be allowed without my written permission.

Department of Oceanography

The University of British Columbia
1956 Main Mall
Vancouver, Canada
V6T 1Y3

Date July 28, 1983

Abstract

Temporal and spatial variations of the Fraser River plume, in the central Strait of Georgia (British Columbia, Canada), are monitored by continuous salinity sampling of the engine cooling water on two B.C. ferries. Travelling along two different routes between Vancouver Island and the mainland the ferries provide eight crossings per day both north and south of the river outflow. From each crossing, characteristic measures of the plume are extracted, such as the average salinity and the maximum salinity gradient. These parameters are then formulated as time series and used to compute cross-correlations and cross-spectra with the probable driving forces of wind and river discharge. The effect of the tides is examined using harmonic analysis.

Periods of high river discharge lead to decreases in the average salinity for each section, and peaks in the magnitude of the maximum salinity gradient. The correlation of the plume characteristics (average salinity, maximum salinity gradient) on the southern section with the along-strait component of the wind is consistent with advection by the wind. Weak correlation is found between the plume characteristics on the northern section and the wind. Linear combination of the wind and the discharge variations reproduce the general trend of the average salinities but cannot explain the level of variability. A shift to a non-linear combination of the wind and discharge improves this comparison. The phases of parameter fluctuations at tidal frequencies, on the southern section, agree with the expected

effects of tidal currents and the modulation of the river discharge. The agreement is not as apparent for the northern section. The level of the discharge is seen to affect the tidal amplitudes of the salinity fluctuations on the southern section.

A numerical model, previously developed to examine the effect of tidal forcing on the plume, is modified to input the hourly wind and daily discharge data record. Equivalent average salinities along the ferry section are outputed and compared to the observed ferry data. Good agreement is reached after manipulating the entrainment velocity and the momentum transfer from the wind to the plume. The tides are seen to add a tidal modulation to the general salinity pattern resulting from the combined effect of the wind and the discharge. Horizontal distributions from the model and from CTD cruise results agree fairly well with each another.

Table of Contents

List of Tables

List of Figures

Acknowledgement

Among all the people that helped carrying through this thesis project, I would like, in particular, to acknowledge the suggestions and advice from all the committee members, and especially the guidance from my thesis supervisor, Dr W.J. Emery. I would also want to thank the many officers and employees of the B.C. Ferry Corporation who cooperated in the data collection, especially Messrs A. Ritchie and B. Bowring for their support and cooperation. The dedication of P. Nowlan contributed significantly to maintaining and processing the data. I am grateful to Dr J.A. Stronach for his permission to use his numerical model program and to Dr L.E. Giovando for sending me the lighthouse data. This research was supported financially by the Canadian Natural Sciences and Engineering Research Council under its Strategic Grants Program for Ocean (Grant No. G0353) and through a Science 1967 scholarship. This support is gratefully acknowledged. Finally, I would like to thank my husband, Philip Green, for his continued encouragement and moral support.

I. INTRODUCTION

A remarkable feature, in the central Strait of Georgia near Vancouver, B.C. is a strong salinity front marking the fresh water extent of the Fraser River plume. This front is often associated with a marked change in colour due to an abrupt increase in the suspended sediment concentration. Different aspects of the plume have been studied through aerial pictures (Tabata,1972), satellite pictures (Feely and Lamb, 1979; Duffus and Tilley, 1978), drogue tracking surveys (Giovando and Tabata,1970; Cordes, 1977) and a numerical model (Stronach,1981). In the introduction to his work, Stronach (1977) lists most of the relevant studies of the Fraser River plume and similar plumes and LeBlond in a latter review (waiting publication) updates the list. Among the pertinent work, papers by Waldichuk (1957) and Tully and Dodimead (1957) gave a first qualitative description of the Strait of Georgia waters. Other plumes have also been investigated. The Mississipi River plume received modelling attention (Wright and Coleman, 1971). The Connecticut River plume has been documented by Garvine (Garvine and Monk, 1974; Garvine, 1974 and 1977) who also gave analytical (Garvine, 1979 a and b, 1981) and numerical (O'Donnel and Garvine, 1983) model of frontal plume dynamics. All of these studies dealt mainly with short-term variations (over a day or two) of the plume properties. The present study investigates the causes of the plume property variations over a wide range of time scales. The variations of the plume's salinity front are measured along two across-strait sections by instruments on

British Columbia ferries. This data collection system provides the first fast sampling long-term data record of the plume fluctuations. An attempt is made to correlate these measured variations of the salinity front with possible driving mechanisms: the discharge of the River, the wind and the tides. Cross-correlations, cross-spectra and harmonic analyses will be used to quantify the possible relationships between variations in the plume characteristics and the forcing parameters. An existing numerical model will be modified to account for the long-term fluctuations of the forcing mechanisms and for easy comparisons with the ferry data.

II. DATA COLLECTION AND PROCESSING

2.1 Data Collection

British Columbia ferries offer platforms that make frequent trips (eight per day) crossing the Strait of Georgia all year long. The two tracks in the central Strait are shown in Fig. 1. Up to three ferries have been equipped with instruments to monitor the temperature and salinity of the engine cooling water. The sea water intake is located about two or three metres below the water line depending on ferry load. The instrument installed on each ferry was a Shipboard Salinity Recorder (SDL-12) made by Applied Microsystems Ltd. This instrument is specifically made for monitoring and recording temperature, conductivity and time every minute. The salinity measurements of the SDL-12 have an accuracy of ±0.1 o/oo and a range of 0 to 40 o/oo while the temperature range is -2 to 25°C with an accuracy of ±0.02°C. During each ferry crossing while the data are automatically recorded, the officers on the ferry filled out log sheets giving radar fixes at specific points along the ferry tracks. To estimate the time it takes for the near surface water to be taken into the sea chest and travel to the sensor, manual surface samples were taken from the deck of the ferry, two or three times a month.

Unfortunately the ferries do not run at night, leaving a 35% gap in the data every day. Various malfunctions of the instruments and extended dry docking of the ferries also increased the amount of missing data. Table I gives a list of

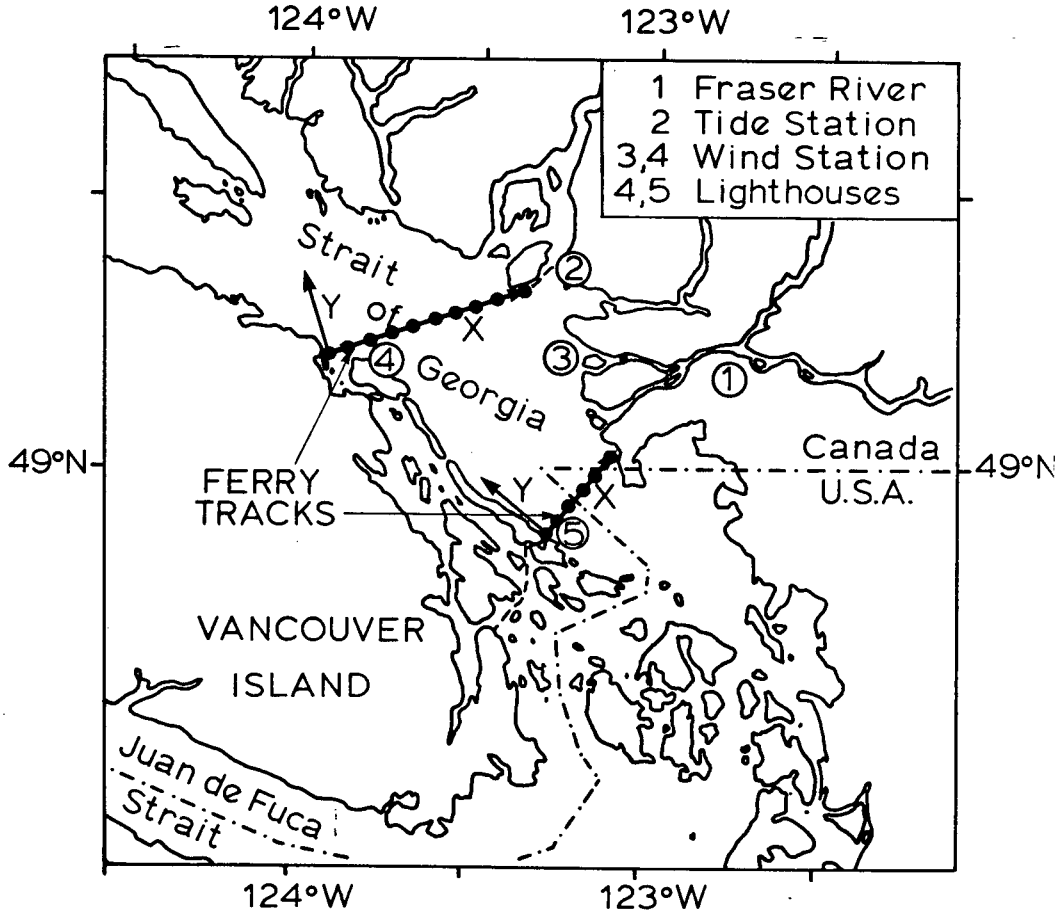

Figure 1 - Map of the Strait of Georgia with the following: 1: Fraser River, 2: Point Atkinson tide gauge, 3: Sand Heads wind station, 4: Entrance Island wind station and lighthouse station, 5: Active Pass lighthouse station. Dots on axes indicate the positions of CTD stations

periods for which the recording seems satisfactory. Julian days are set so that January 1,1980 corresponds to day 0 and that they continuously covered the two years of 1980 and 1981. Table I indicates that, for small periods of time, each section has been monitored by two ferries simultaneously.

The ferry data give a horizontal distribution of the plume

Table I - Periods where the ferry data are available

Name of the ferry and section monitored	Starting-finishing dates	Starting-Finishing julian days
Queen of Alberni (Southern section)	1980: March 21-July 16, Aug 1-Oct 21, Oct 24-Nov 23, Dec 18-Dec 24, Dec 26-Jan 9 1981. 1981: Jan 11-Feb 2,Feb 5-Feb 16,Feb 18-May 4, May 6, May 9-June 3, June 7-June 25, Sept 9-Nov 11.	80-197, 213-294,297-327,352-358, 360-374 376-398,401-412,414-489, 491,494-519, 523-541,617-680
Queen of Alberni (Northern section)	1981: June 26-Aug 28, Sept 1-Sept 8.	542-605, 609-616
Queen of Coquitlam (Northern section)	1980: Feb 22-March 12, March 15-March 20, March 25-July 4, July 8-Sept 7, Sept 10-Sept 30.	52-71, 74-79, 84-185,189-250,253-273
Queen of Cowichan (Northern section)	1980: Nov 21-Feb 20 1981 1981: March 24-April 4, April 16-Dec 16.	325-416 448-459, 471-715
Queen of Oak Bay (Southern section)	1981: July 24-Oct 6.	570-644

at one depth. In order to get some insight into the vertical distribution of the water properties of the plume, monthly CTD surveys have been carried out. Each survey consisted of 32 to 42 stations from which ten stations were along the northern ferry section and six stations covered the southern section (Fig. 1). The rest of the stations were dispersed in the area of the Strait between the two ferry sections. Conductivity and temperature were measured by a Guildline 8705 digital CTD down to 100 metres, water depth permitting. A survey usually took

about 20 hours. In addition to the CTD surveys, surface temperature and salinity were measured daily at two lighthouses close to the path of the ferries. They are located at Entrance Island and Active Pass (Fig. 1).

To evaluate the effects of the various forcing mechanisms, time series data of wind, tide and river discharge were acquired (Fig. 1). Hourly wind data are available from two stations maintained by the Atmospheric Environment Service: Entrance Island (4) and Sand Heads (3). The wind measurements are made to the nearest mile/hr with the direction specified by one of the eight directions of the compass card. The nearest tide gauge is located at Point Atkinson (Fig. 1) (Canadian tide and current tables 1980, and 1981). The sea level elevation given at this station can be used to characterize the tides for the entire study area (Crean,1976). The discharge of the Fraser river is measured daily by Water Survey of Canada at Mission City situated about 75 km upstream of the river mouth. There is no station closer to the river mouth and it was not possible to estimate the contributions of the small rivers discharging into the Fraser River between Mission City and the river mouth. By looking at the ratio of the areas drained by these smaller rivers to the area drained by the Fraser River, one can argue that the contributions of these tributaries are small and that most of the variations in the river discharge are monitored at Mission City.

2.2 Data Processing

2.2.1 Ferry Data

It was necessary to convert the raw data into time series of some plume characteristics that could be compared with coincident time series of wind, tide and discharge. The time recorded on the ferry was first corrected for a delay of about five minutes due to the travel time between the water surface and the instrument. This delay was evaluated by comparing the manual surface salinity samples to the salinity recorded by the instrument. This corrected time was then converted to a position across the Strait defined by a set of cartesian coordinates, unique to each section (Fig. 1). The x-axis follows the ferry track with x increasing towards the mainland. It should be noted that because of safety regulations, the track to Vancouver Island was set to be one nautical mile to the north of the one going to the mainland. The x-axes described here are set between these two tracks for each section; in other words, the y-coordinates of the ferry position averaged out to zero if summed up over a long period of time. The length of the x-axes are 18 and 40 km for the southern and northern section, respectively. A particular position was usually normalized as the ratio of its x-coordinate in kilometres to the length of the axis. The y-coordinate was neglected.

Assuming a constant speed between radar fixes, the salinity as a function of position was plotted for the eight trips per day. The usual picture (Fig. 2) is a decrease of salinity with

increasing x (as expected, since the Fraser River is on the mainland). There is also a sharp salinity gradient on the order of 2 (o/oo)/km that marks the plume front. From each trip, the salinity values at the mid-point, at one-third and two-thirds were extracted along with the average salinity over the section and the magnitude, salinity and position of the maximum gradient. These were then plotted against time, selected to be an average of the times when the ferry was at the ends of the section.

Daily series of the characteristics are needed for comparison with the discharge. The two data records on periods where two ferries were monitoring the same section simultaneously were first combined to give one time series. To account for gaps at night, hourly series were first interpolated using a tensioned cubic spline function (Spath,1969) and then convolved with a 48-h wide Bartlett lag window. The value used for the daily series was the smoothed value at noon of each day. In obtaining this value, the averaging had put more weight on the measured values during the day than to the spline interpolated values during the night gaps. Interpolation of the daily series with a cubic spline over gaps of 10 days or less was performed to provide series that cover a longer time interval than the individual hourly series. Formulated also as a daily series was the variance of the salinity estimates for each day at one point. It consists of the average of the squared differences between the salinity at a fixed point and the daily average of the salinity at that point.

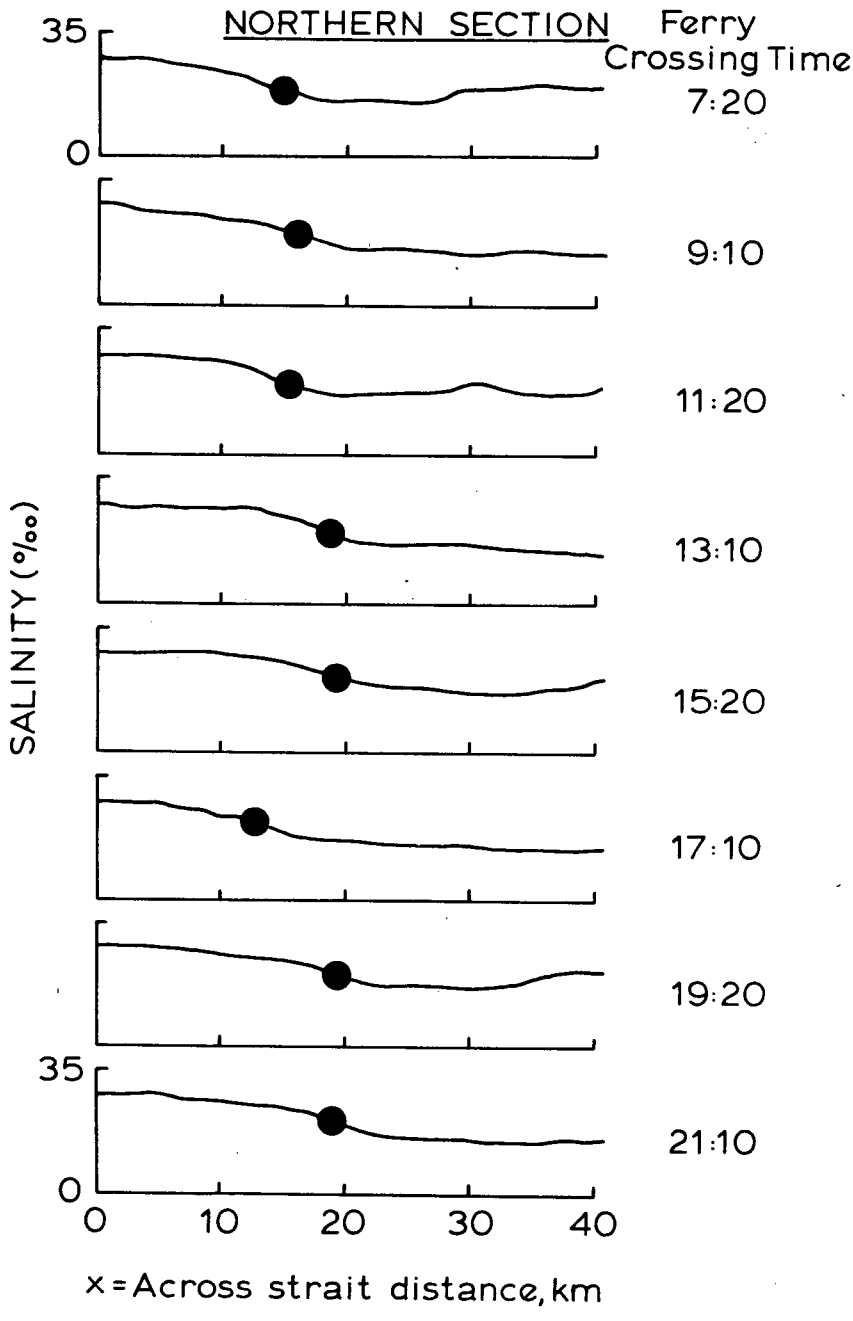

Figure 2 - Plots of salinity versus position for eight consecutive trips on the northern section on June 9, 1980. Dots indicate the positions of the maximum horizontal salinity gradients

Finally the plume characteristic series were plotted and compared with each other and with the concurrent forcing parameter series (discharge and wind). Cross-correlations and cross-spectra were computed for various combinations of the plume characteristics and the forcing parameters. Before computing each cross-correlation, a linear detrending of both time series was performed. The characteristics chosen for these computations were the average salinities and the magnitudes of the maximum salinity gradient for both sections. The longest possible daily series were used. They consist, for the southern section, of data for the periods from Julian days 80 to 327, 352 to 541 and 570 to 680. Similar time series for the northern section cover periods from Julian days 52 to 273, 325 to 416 and 448 to 715. Spectra were normalized (the power spectral estimates were divided by the variance of the series) to allow comparisons between spectra. In computing the spectra, a Bartlett taper function (Jenkins and Watts, 1968) with a width of 1/8 of the data series length was used as a filter. This procedure yielded 24 degrees of freedom for each spectral estimate. The noise level for the cross-spectra was estimated by using the null hypothesis (Groves and Hannan, 1968).

Harmonic analysis was used for comparisons at tidal frequencies, in place of the cross-spectra, to overcome the problem of interpolation. This analysis was intended to be carried out for all tidal constituents for which the length of the record would allowed resolution. The computer program used was developed by Foreman and Henry (1979). This program, when

used with series of a year or two was too costly. It was then decided to exclude all the constituents for which the amplitude of the sea level elevation at Point Atkinson was smaller than .8 cm. P_1 was inferred from K_1, ν_2 from N_2 and K_2 from S_2 whenever the length of the record did not allow their resolution. The harmonic analysis has been performed on the four chosen characteristics and for the sea level elevation at Point Atkinson. The latter will be used as a reference for the phases. These phases will be expressed as the difference between the Greenwich phase lag of one of the four characteristics and the Greenwich phase for the same constituent from the sea level elevation.

2.2.2 CTD Data

The data from each 100m CTD drop were first sorted by increasing depth (using both up and down traces) then interpolated every 0.01 m and finally smoothed by convolving the series of salinity as a function of depth with a Bartlett lag window of 1m width centered at each 0.5 m from 0.5 to 20 m.

2.3 Error Estimation

2.3.1 Wind Forcing Parameter

The aim of this subsection is to define a wind forcing parameter series that will be used in the cross-correlations with the plume characteristics. The prevailing winds are in general along the axis of the Strait, northwest and southeast as discussed in Waldichuk (1957). For this reason the wind data

were separated into along-strait (positive towards the northwest) and across-strait (positive towards the northeast) components.

Spectra, cross-spectra and cross-correlations have been evaluated for the available two years of hourly wind data at the two coastal stations. No statistical differences were found between the two years of data. Spectra indicated sharp peaks at the diurnal frequency with this frequency being relatively more important for the across-strait component. Broad peaks were also found at low frequencies. High values of the cross-correlation (0.8) near 0 lag, between the along-strait components at the two different stations, indicated the spatial uniformity of this component over the central Strait. The corresponding cross-spectra showed a restriction of this agreement to fluctuations with periods greater than 20 h. The across-strait components were not as well correlated (0.3) and high coherencies were restricted to periods between 31 h and 8 days with the exception of the diurnal frequency for which an out-of-phase relationship between the across-strait components on each side of the Strait seems to prevail. It was also found that the variance of the across-strait component is in general four times smaller than the along-strait component variance and that the two components were not independent. A small but significant out-of-phase correlation (0.2) was discovered for periods of the order of 3 to 10 days.

From all these considerations, a single representative time series of the along-strait wind component seemed to be the

appropriate quantity to simulate the global action of the wind over the Strait. The data from the wind station at Entrance Island will be generally used since it is the most complete record. Daily wind series were obtained from the hourly data the same way as the daily plume characteristic series.

2.3.2 Comparison Between The Ferry Data And The Lighthouse Data

The next question is how well do the ferry data describe the near-surface water properties. Sporadic and short series of manual surface sampling from the ferry deck gave an indication that the water monitored by the instrument had a higher salinity than the surface water by 1 to 2 o/oo. A comparison over a longer period can be carried out using the lighthouse data. Fig. 3 shows the lighthouse data along with the daily salinity at the closest point to the lighthouse on the ferry tracks, namely at x=0 on both sections. The erratic appearance of the salinities measured at the lighthouses comes from the fact that this daily measure is not smoothed and is taken at different times each day. The salinities measured by the ferry are usually higher (on the average, by 0.6 o/oo on the southern section and by 0.06 o/oo on the northern section) consistent with the realization that the ferry monitored water slightly below the surface. As could be seen by a visual inspection of the time series of Fig. 3, high values for the cross-correlations of the two different estimates of the surface salinity were obtained (0.7 for both sections). These results show that the Ferry salinity data are representative of the near

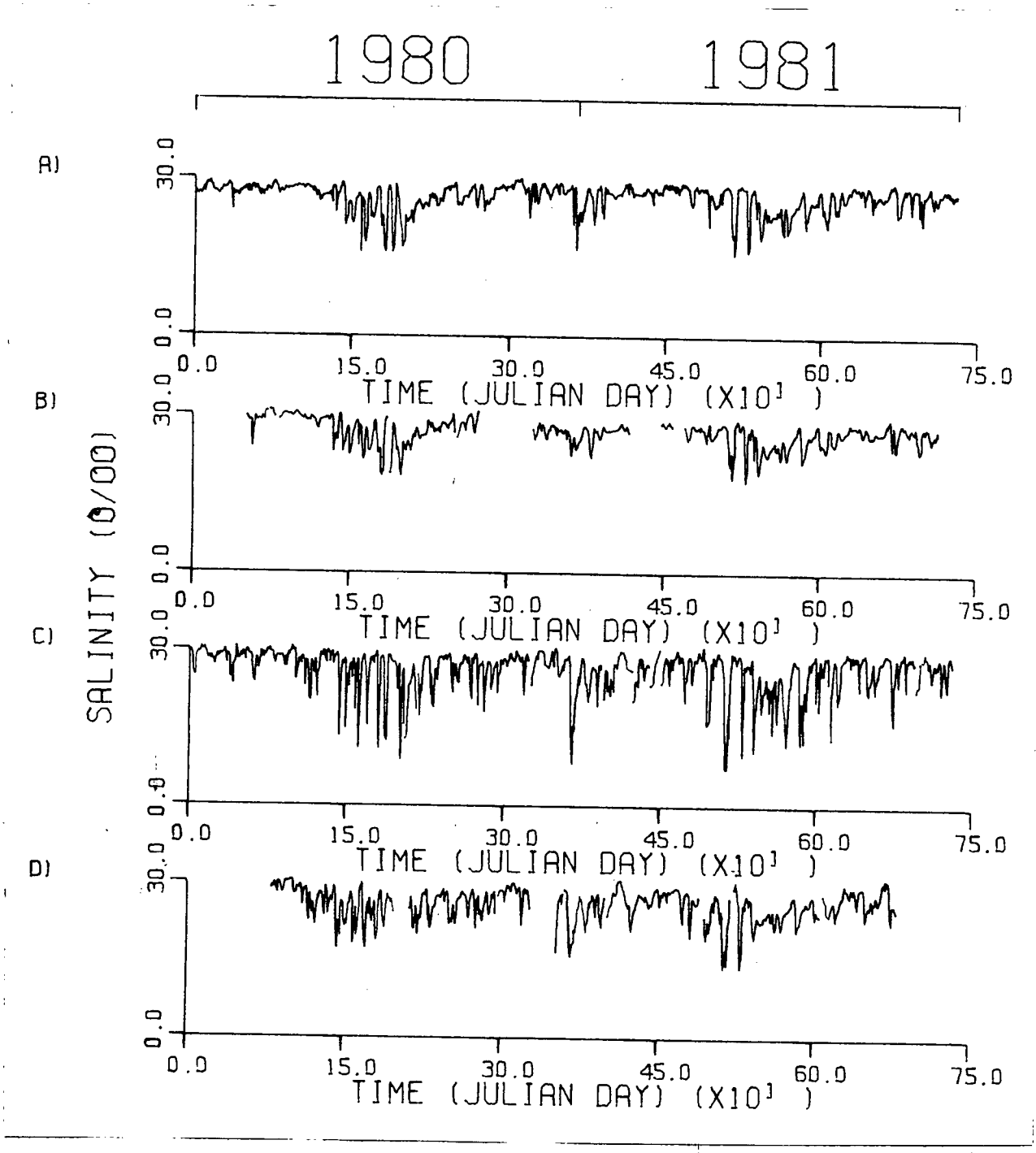

Figure 3 - Plots of salinity vs time from a) the data measured at Entrance Island lighthouse b) the northern section daily average ferry data at x=0 c) the data measured at Active Pass lighthouse d) the southern section daily average ferry data at x=0

surface salinity variations.

2.3.3 Comparison Between The Ferry Data And The CTD Data

The aim of this subsection is to establish the depth of the water monitored by the ferry. For this purpose an interpolated salinity value was computed from the ferry crossing at the time a CTD station was taken from the values of salinity along the ferry track from the two closest data points. A typical salinity depth profile (Fig. 4) monotonically increases with depth. From this profile, the 0.5m depth-interval, within which the interpolated ferry salinity is found,constitutes an estimate of the depth from which the water monitored by the ferry was taken. Two hundred and thirty one CTD stations were suitable for this calculation (they were deployed within the ferry period of operation). The histograms of Fig. 5 summarize the results. The solid line histogram gives the percentage of the 231 stations defining the depth of the ferry salinity for each 0.5m depth-interval within the first 20m of the water column. It shows that one third of the stations yielded a depth of the observed salinity within the first 0.5m, that 80 % of the time the depth of this salinity is within the first 7m and that the average depth is 3.5m. This clearly indicates that the water monitored by the ferry corresponds to a near surface water type. Since the ferry intake was about 2 to 3m below the water line, one could conclude that a great deal of vertical mixing by the ferry brings the fresh surface water to the depth of the intake.

A small fraction of the CTD stations yielded depths well

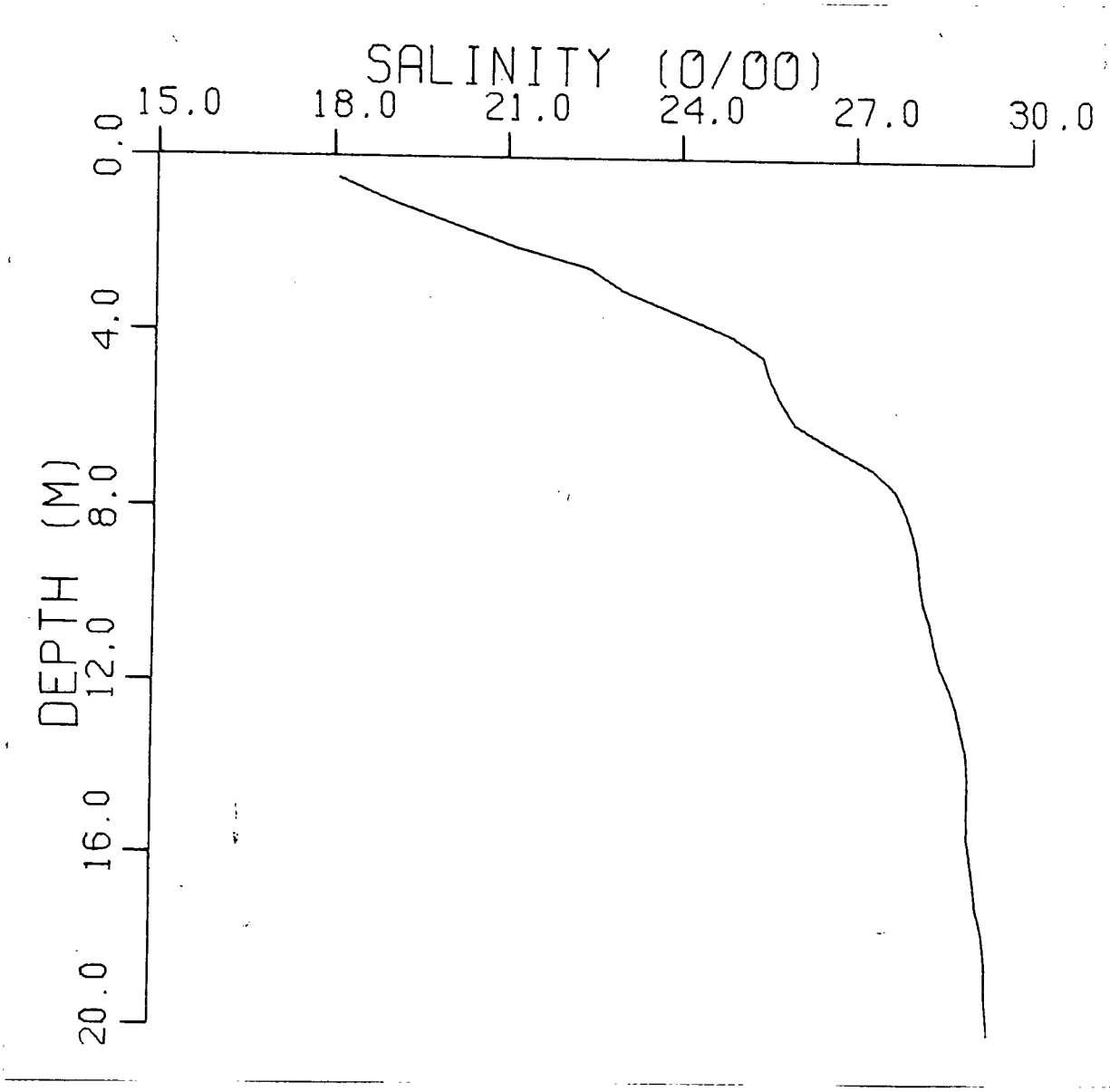

Figure 4 - Salinity depth profile obtained on May 11, 1981 at the second most eastern CTD station on the northern section

below the water intake (3% of the depths are below the 20 m line). These anomalous depths are associated with stations having low vertical salinity gradients. For these stations, a small error in the estimation of the interpolated ferry salinity produces a large variation in the estimated depth of the water

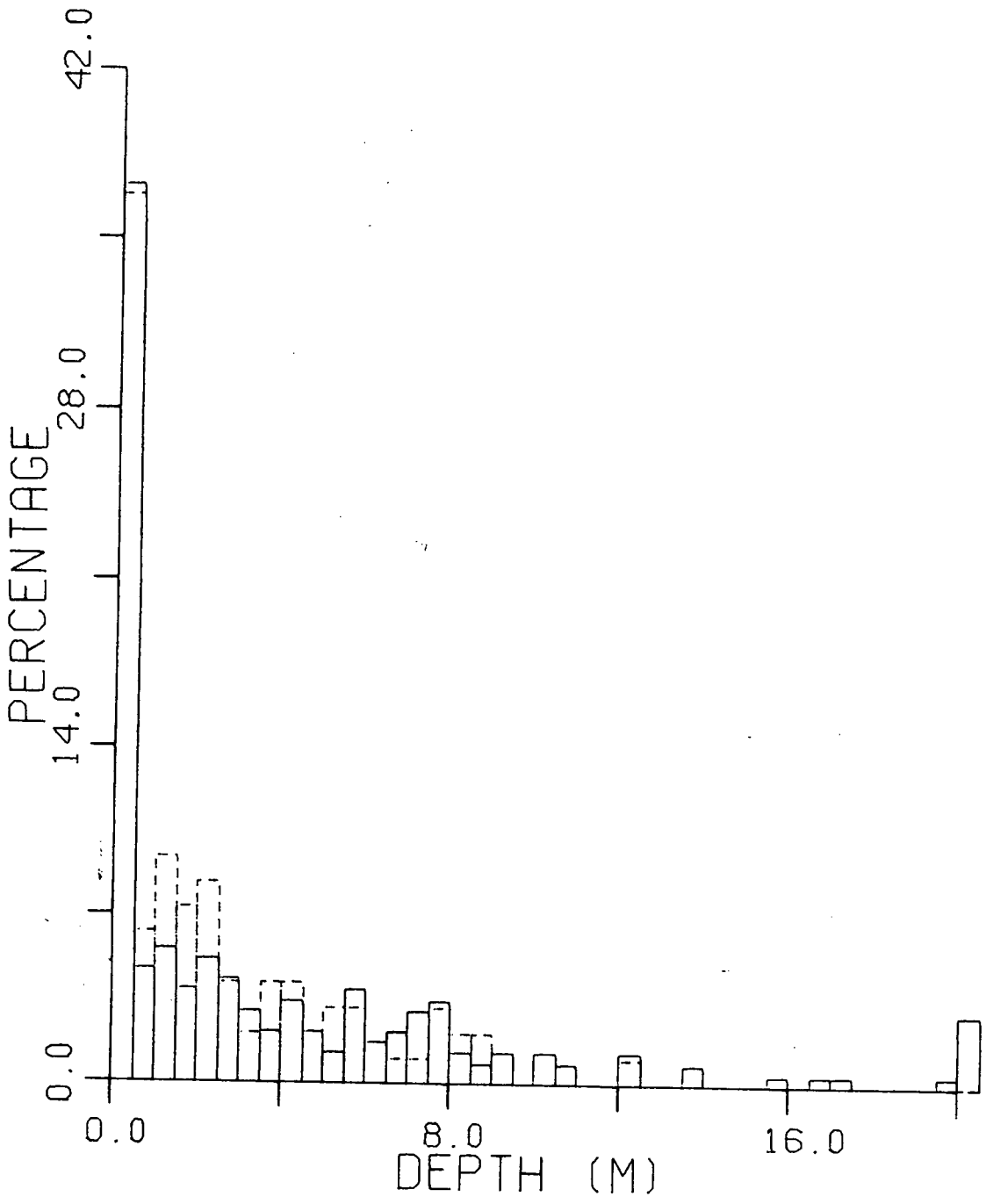

Figure 5 - Histograms of the distribution of ferry data salinity depths from the analysis of all 231 CTD stations (solid line) and of 95 CTD stations (broken line) characterized by a vertical salinity difference equal or greater than 4 o/oo

having this salinity. The variation of this depth can be well demonstrated for stations for which two salinity estimates are available because two ferries were monitoring the same section at the time of the deployement of the CTD station. The difference in the depths ranged from 0 to above 20 m with 80% of the differences between 0 and 6.5 m. A new histogram (broken line histogram of Fig. 5) was produced using only 95 stations for which a salinity difference of 4 o/oo and over was observed in the first 20 m. The proportion of the depths between 0 and 0.5 m did not change but the depths over 20 m disappeared because they corresponded to stations that monitored well mixed water. A larger fraction of the depth values than before were found at small depths (80% of them were above the 4.5 m depth line and the average depth was 2.5 m). These values of depth are known from CTD depth profiles to be within the depths influenced by the plume (Fig. 4).

2.3.4 Comparison Of Data From Two Ferries On The Same Section

It is crucial to know the errors associated with the variations of the ferry load, the change of the ferry tracks (along-strait fluctuations), the change of the ferry, changes in the sampling depth, etc. The reproducibility of the ferry results can be estimated by comparing the ferry data from two ferries monitoring the same section at the same time. As inferred from Table I, the northern section was simultaneously monitored by two ferries from Julian days 542 to 605 and 609 to 616 and the southern section from Julian days 617 to 644.

From the two average salinity series for each section, hourly and daily series were computed and the differences between the two salinity estimates evaluated (Table II). The

Table II - Results of the statistics of the average salinity difference between two series recorded on two different ferries on the same section

	Averaged difference of salinity (o/oo)	Root mean squared error (o/oo)
Southern section Alberni - Oak Bay Series series hourly series Julian days: 617-644	0.5	1.3
daily series Julian days: 617-644	0.5	1.0
Northern section Cowichan - Alberni Series Series hourly series Julian days: 542-605	-0.2	1.0
hourly series Julian days: 609-616	-0.5	1.2
daily series Julian days: 542-616	-0.2	0.5

average difference of 0.5 o/oo for the southern section indicates that the salinity values given by the instrument on the Queen of Alberni were slightly higher than the ones from the Queen of Oak Bay. The two values of -0.2 and -0.5 o/oo of the average differences for the northern section account also for

the higher salinity measured by the Queen of Alberni than by the Queen of Cowichan. This systematic error does not account for the root mean squared error between the two series. The daily averaging process, by smoothing the series, decreases the RMS error. The error for the southern section is in general higher than for the other section. This can be explained by the proximity of the southern section to the Fraser river mouth that provides the possibility of strong salinity differences between the measurements from the two different ferries. In summary, the overall salinity error estimate is on the order of 1 o/oo, which is one order of magnitude larger than the accuracy of the instrument. This error depends on the smoothing and on the ferry section used and is still small compared to the salinity fluctuations which can be on the order of 10 o/oo.

Cross-spectra between the two salinity estimate series were then computed to investigate the range of frequencies for which the two series agree with each other. Cross-spectra with hourly series indicated coherencies well above the noise level for periods higher than 30 hours. The cross-correlation coefficients between the daily series were above 0.96 at day lag 0. Confidence from these results is acquired since, for periods above 30 h, the ferry salinities give reproducible measurements and the fluctuations recorded at these frequencies are independent of the ferry used. For the time period when two ferries were monitoring the same section, one daily series can be computed from a combination of the series from the two ferries since both series display the same fluctuations at the

same time. Prior to the combination, one of the series is altered by the small amount identified as the systematic error between the two ferry measurements.

For periods lower than 30 hours, such as tidal frequencies, harmonic analysis was used on the salinity estimate series for each section. The results of these computations are compiled in table III for the constituents which at some point had an

Table III - Amplitudes (A) and phase (ϕ) from the harmonic analysis of the average salinity series from different ferries on the same sections

	Alberni series (S. Section) Julian days: 617-644		Oak Bay series Julian days: 617-644		Cowichan series Julian days: 542-616		Alberni series (N. Section) Julian days: 542-616	
	A (o/oo)	ϕ (°)	A (o/oo)	ϕ (°)	A (o/oo)	ϕ (°)	A (o/oo)	ϕ (°)
MSf	1.3	136	0.7	101	0.9	235	0.8	219
$2Q_1$	0.6	158	0.2	127	0.2	219	0.3	239
NO_1	1.1	175	0.9	179	0.3	71	0.3	63
P_1	0.2	-21	0.5	-37	0.2	32	0.2	-20
K_1	0.6	-21	1.5	-37	0.5	32	0.6	-20
J_1	0.9	-38	0.6	-9	0.1	-68	0.1	-67
OO_1	0.6	273	0.4	236	0.0	110	0.2	93
N_2	0.5	-34	0.1	-45	0.1	130	0.2	157
M_2	0.7	-34	0.2	22	0.1	167	0.1	140
S_2	0.1	19	0.4	74	0.3	240	0.5	176

amplitude equal to or greater than 0.5 o/oo. For an error of 1 o/oo, in the salinity measurements, only amplitudes equal to or above 0.5 o/oo could be thought of as being something other than noise. The similarity between the results of the P_1 and the K_1 constituents are due to the inference of P_1 from K_1. The absolute value difference between the two phase estimates for

each constituent never exceeds 64°. This value gives us an estimate on how well the phases from the harmonic analysis of the average salinity can vary due to the sampling method.

The exact same procedure can be applied to the two series of the magnitude of the maximum salinity gradient from different ferries on each section. The accuracy of the instrument to measure horizontal salinity gradients can be computed from the distance travelled by the ship during a sampling interval of 1 minute (0.7 km) and from the accuracy of the salinity measurement (0.1 o/oo) to give an accuracy for the salinity gradient of 0.1 (o/oo)/km. Table IV shows the analogous results to table III for the magnitude of the maximum gradient. As for the salinity, the root mean squared error for the gradient is above the accuracy of the instrument but the average error difference is not significantly different from 0. This means that each ferry does not introduce an offset relative to the measurements of salinity gradient from another ferry. As before the daily averaging reduces the RMS error by smoothing. Both sections seem to produce the same error, that is about 0.5 (o/oo)/km for hourly value series. Relative to the size of the maximum salinity gradient that usually never exceeds 2 (o/oo)/km, this error of 0.5 (o/oo)/km is quite substantial.

The cross-spectra between the two salinity gradient estimates reached coherencies lower than those between the corresponding salinity series. The coherencies stay above the noise level for periods larger than 24 h for the northern section and 45 h for the southern section and the correlation

Table IV - Results of the statistics of the maximum salinity gradient difference between two series recorded on two different ferries on the same section

	Averaged difference of salinity gradient (o/oo)/km	Root mean squared error (o/oo)/km
Southern section Alberni - Oak Bay Series series		
hourly series Julian days: 617-644	0.1	0.5
daily series Julian days: 617-644	0.1	0.2
Northern section Cowichan - Alberni Series Series		
hourly series Julian days: 542-605	-0.1	0.5
hourly series Julian days: 609-616	0.3	0.4
daily series Julian days: 542-616	-0.1	0.3

coefficients for the daily series are 0.8 and 0.86 for the northern and southern section respectively. This supports the assumption that the variations of the magnitude of the maximum gradient, with periods over two days, are significantly well described by the ferry data.

The harmonic analysis of the maximum salinity gradient gave poor results. According to the RMS error, only tidal amplitudes

over 0.25 (o/oo)/km can be differentiated from noise. It only occured twice; that is, for the K_1 constituent for the Oak Bay salinity gradient series and the MSf constituent for the southern section Alberni series. A phase difference of 134° between the K_1 constituent of the Oak Bay series and the analogous Alberni series rules out the usefullness of this characteristic at this tidal frequency. The MSf constituent leads to phase differences of 59° and 21° between the analogous salinity gradient series for the southern and northern section, respectively. This constituent still holds the possibility of giving significant information.

It was then supposed that a better salinity gradient characteristic, for short term variations, would be the magnitude of the salinity gradient following a particular front instead of taking the maximum salinity gradient for the whole section. This would differentiate between the 1 to 3 fronts possibly present over a section at any one time. Such particular fronts were followed for the period of time when two ferries were monitoring the same section. The salinity gradient and the position of the front were recorded as a time series. This procedure cuts the period of observation into small series of the length of the life-time of each front i.e. of the order of 10 days. The small length of these series makes them useless in the determination of long term variations but harmonic analysis can still be used. The analysis done with the frontal magnitude of the salinity gradient did not show any improvement over the previous salinity gradient characteristic. The MSf

constituent could not be resolved in the case of the frontal southern section salinity gradient and position series and a large phase difference (106°) between the analogous frontal northern section salinity gradient series was found. The last statement does not hold for the northern section frontal position series for which a phase difference of 17° was computed. The RMS errors for the position series were evaluated as being 4.7 and 3.3 km for the northern and southern section, respectively.

III. VISUAL INTERPRETATION OF THE FERRY DATA

3.1 Comparison Of The Plume Characteristics With Discharge

Marked effects of the fluctuations in the Fraser River discharge on the average salinity for both ferry sections can be seen by comparing the three daily time series of Fig. 6. In general, both average salinities show the same response, with lower salinities corresponding to higher discharges in the springs and summers. Increases in river discharge occur rather rapidly in April and May (Julian days 110 to 130 and 475 to 515) while the adjustment to lower salinities along the ferry sections is somewhat slower. All three curves exhibit peaks (drops in salinity) in the early summer (Julian days 130 to 180 and 515 to 525) with a more gradual decrease in river discharge in the fall accompanied by gradual increases in salinity.

Along with the general decrease in average salinities, both ferry sections display higher variability during periods of high discharge. The amplitude of this variability is larger for the southern section reflecting its nearness to the Fraser River. This sharp response on the southern section to the discharge makes it easier to see the effects of small peaks in the river discharge. Secondary peaks in discharge on Julian days 234, 254, 269, 278, 393 and 675 correspond to simultaneous drops in the southern section average salinity. Similar drops are not evident in the northern section salinity series except perhaps for the drop on day 675 that is a relatively large secondary peak. Some of the variability of these salinity estimates is

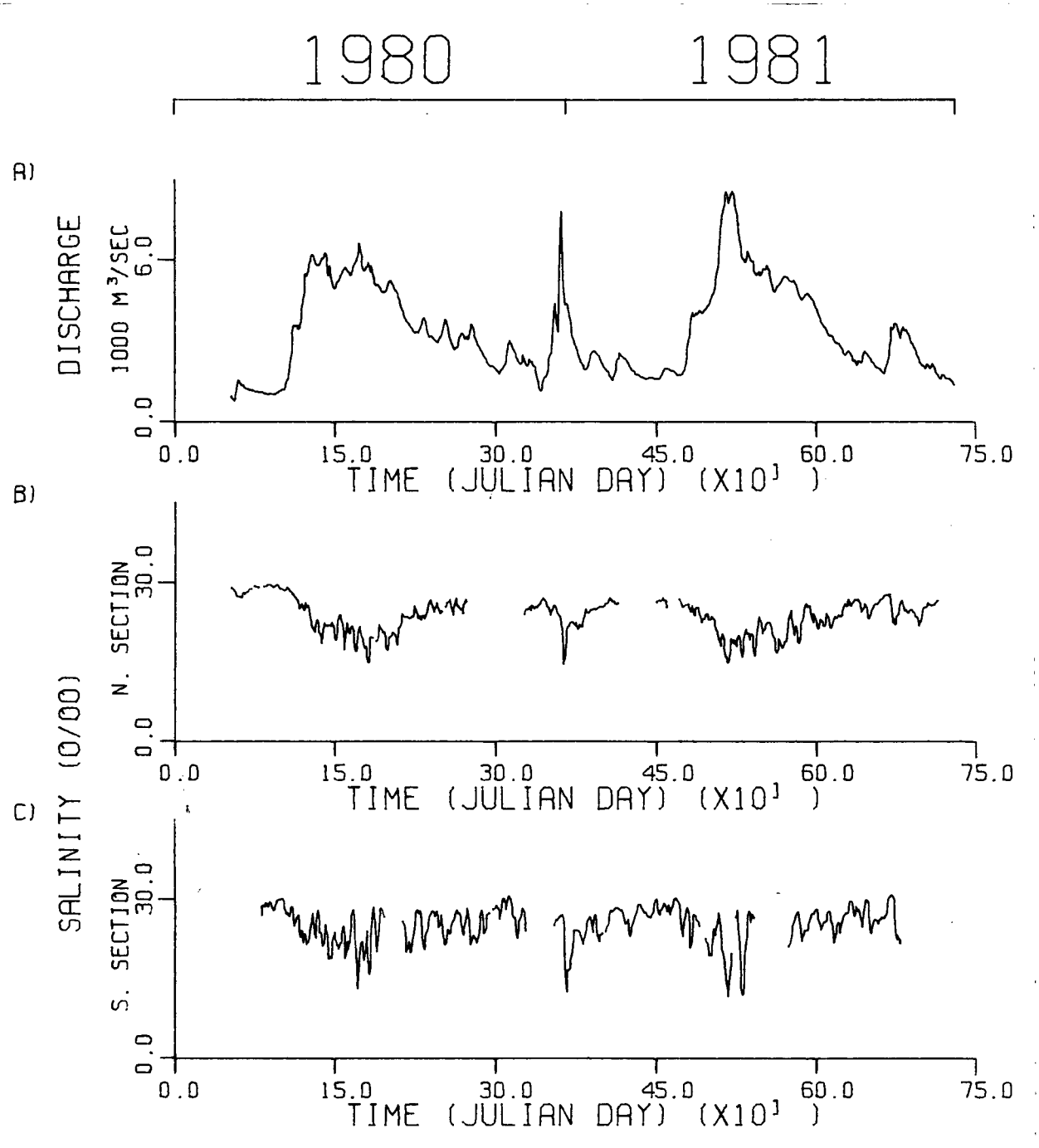

Figure 6 - Plots of the a) Fraser River discharge, b) the average salinity on the northern section and c) the average salinity on the southern section versus time

due to wind forcing. The wind, as will be seen later, contributes fluctuations ranging from 11.5 to 28 o/oo for the average salinity on the southern section during the period of highest discharge for these two years (Julian days 515 to 525).

An unusual feature of the curves in Fig. 6 is the abnormally high discharge in December 1980 and the corresponding drops in average salinity along each ferry section. This event was due to anomalous rains and flooding in the winter of 1980/81. It is interesting to note that although the maximum Fraser River discharge occured at day 361, the salinity minima occured at days 365 and 363 at the southern and northern sections, respectively. With the close proximity of the southern section to the Fraser River mouth, it is a surprise that the more distant northern section responded first. In a subsequent subsection, this particular event will be discussed in detail relating the combined effects of discharge and wind.

The river discharge not only influences the average salinities in the Strait but also the horizontal gradients of salinity, as can be seen in Fig. 7. In general, the magnitude of the maximum gradient on the southern section is larger than that on the northern section. This again reflects the proximity of the southern section to the Fraser River mouth. The previously mentioned secondary peaks in the discharge (on days 234, 254, 269, 278, 393 and 675) cause relatively stronger magnitudes of the maximum gradient on the southern section. Other qualitative patterns of the discharge are reproduced in the variations of the magnitude of the maximum gradient, like

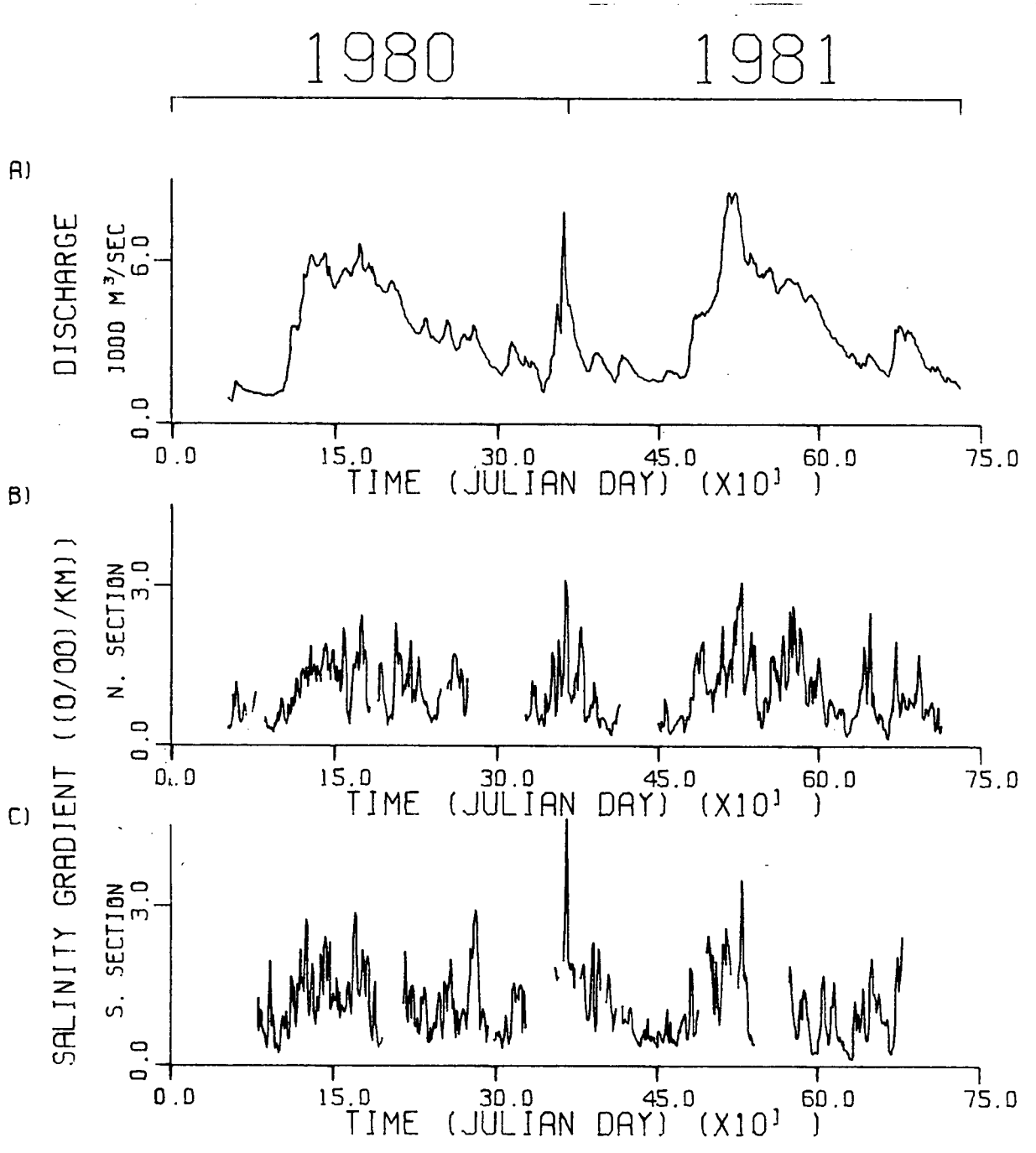

Figure 7 - Plots of the a) Fraser River discharge, b) the maximum salinity gradient along the northern section and c) the maximum salinity gradient along the southern section versus time

the sharp peak around day 360 and the low gradients around days 100, 300, 450 and 710 coincident with the lowest values of the discharge for the two years.

3.2 Comparison Of The Salinity At Different Points Along The Sections

The same pattern as that for the average salinity is reproduced in the salinities at some fixed points across each section. They are presented in Figs. 8 and 9 for five points along each of the southern and northern sections, respectively. Qualitative agreement between the variations of the salinity at different points along the sections suggests that the average salinity was a good choice as a characteristic that summarizes the salinity for the whole section.

In general, the salinities increase from the mainland to Vancouver Island with the exception of the salinity at the eastern end of the southern section that is noticeably higher than the average salinity for that section in spite of its proximity to the Fraser River mouth. It is likely that the plume turns north, deflected by the Coriolis acceleration, advecting the fresh water away from the southeast coast. The salty surface water close to the east-end of the southern section has also been observed during the CTD surveys done in this area and is predicted by a numerical model as will be seen in chapter 5. Another possible explanation for the high salinities measured by the ferries at the southeast terminus, depends on the operation of the ferry. As can be seen from the

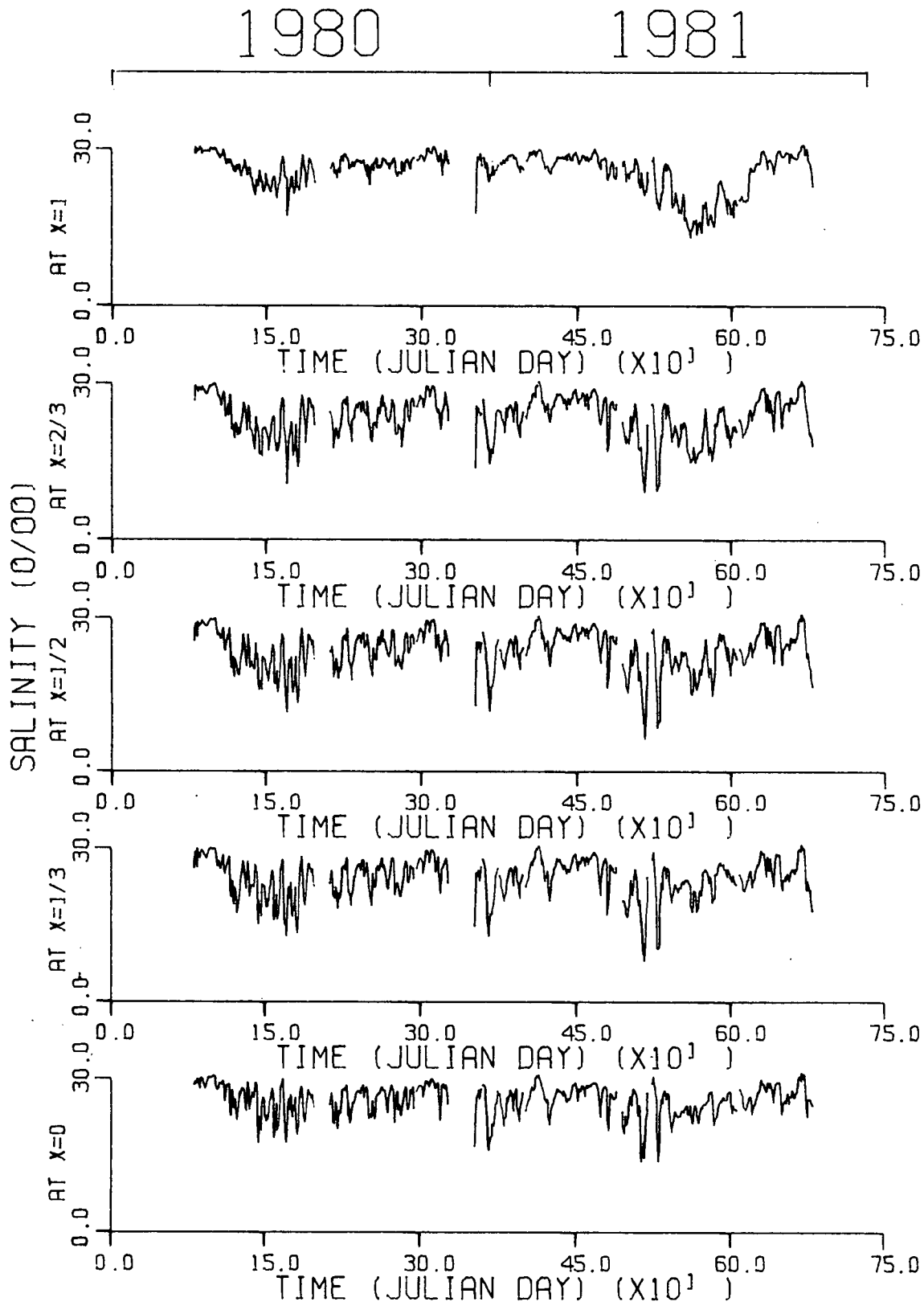

Figure 8 - Plots of salinity versus time for five different points along the southern section (x=0,1/3,1/2,2/3,1)

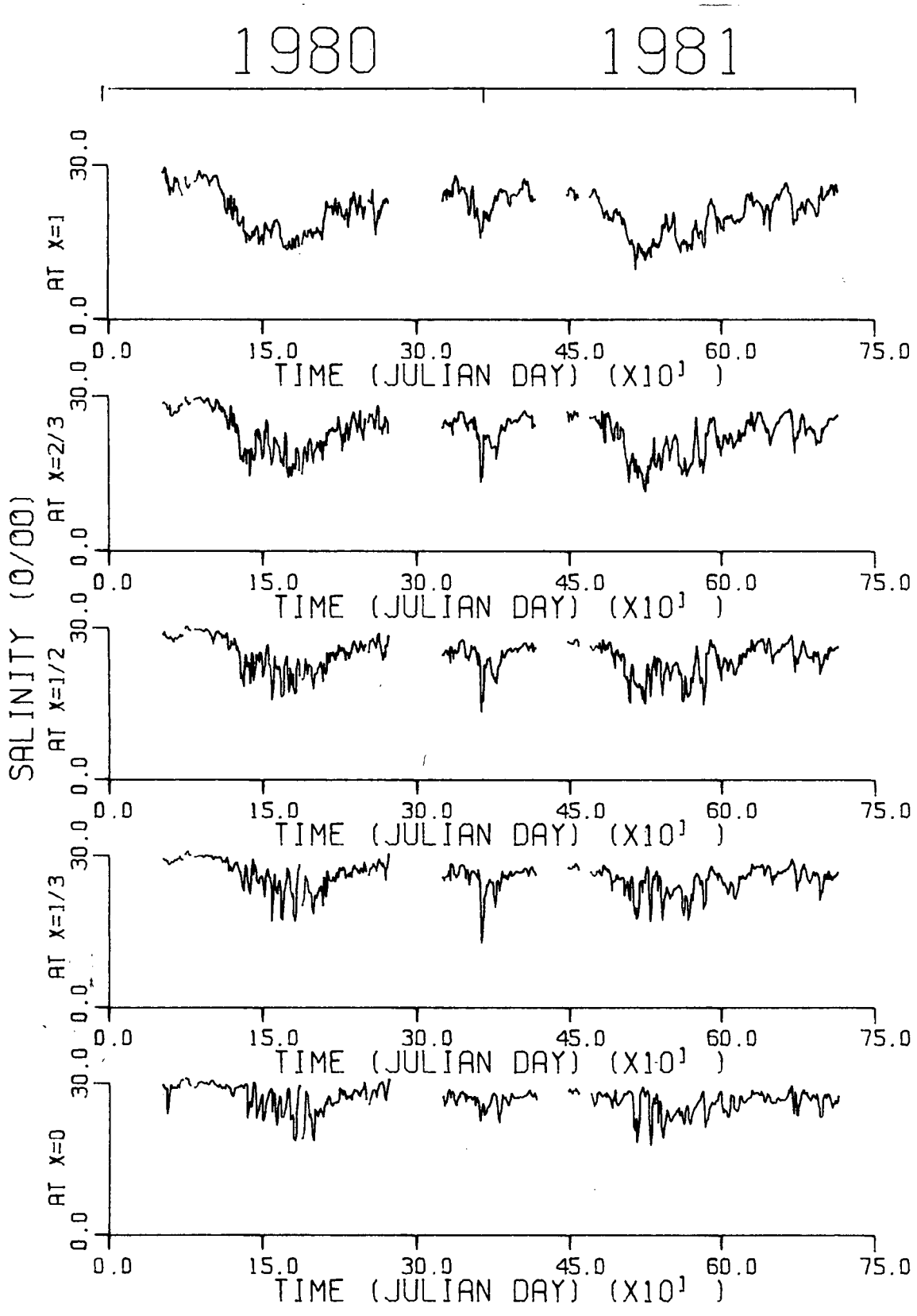

Figure 9 - Plots of salinity versus time for five different points along the northern section (x=0,1/3,1/2,2/3,1)

map in Fig. 1, this is the only point where data were obtained close to a ferry terminal. When the ferry is docked, the engines are kept running to position the ferry. Held at a fixed position, the sea water coolant is heated up and an increase in engine room temperature takes place. A corresponding increase in salinity was measured by the instruments. In addition, it was observed that salinities were higher when the ferry was leaving compared with its arrival 20 minutes earlier. This is most likely an artifact of the heating in the engine room following the docking. In an effort to avoid contamination from this effect, it was decided to look at data at one-third rather than at quaterly intervals along each section.

Coming back to Fig. 9, one can see that for the northern section the discharge effect is less apparent near Vancouver Island. This is understandable since this is farthest from the Fraser River mouth. It is interesting to notice that on the northern section during the anomalous discharge in December 1980 however, the salinities at x= 1/3, 1/2 and 2/3 seem to be most affected, with the minimum salinity around x=2/3. During the high summer discharges, the plume first affects the salinity at the point closest to the mainland and as the discharge increases, slowly advances towards Vancouver Island. This progression will be clearly seen in the daily variance to be discussed in the next subsection.

3.3 Comparison Of The Daily Variance Series

In addition to causing a strong salinity gradient (the front), high discharges should introduce more variability in the estimate of salinity at a point. Figs. 10 and 11 show the daily variance of the salinities at fixed points across the Strait for the southern and northern sections, respectively. Most of the variance is during periods of high discharge (Julian days 120 to 180, around day 361 and between Julian days 480 and 620). For the northern section, the interval of time over which the variance is significant, varies with position along the section. At x=1, the variance becomes significantly above 0 around Julian day 111. The time of this change in variance progressively increases as x decreases to about Julian day 135 at x=0 near Vancouver Island. After the spring-summer discharge maximum, the plume retreats, ceasing to influence the salinity at x=0 around Julian day 210. The same progression is seen for the spring-summer 1981 discharge. The time limits of influence of the plume at x=1 are about from Julian days 480 to 620 while the analogous time limits at position x=0 are Julian days 510 and 545. It seems to indicate that a discharge of 3000 m^3/s and over is needed to have the plume reach the northern section. This across strait progression is not evidenced on the southern section. It might be because this section is so close to the Fraser River mouth that the plume influences the whole section at the same time starting around Julian days 110 and 495 for the spring discharges of 1980 and 1981, respectively. The large daily variance at x=1 on the southern section is probably

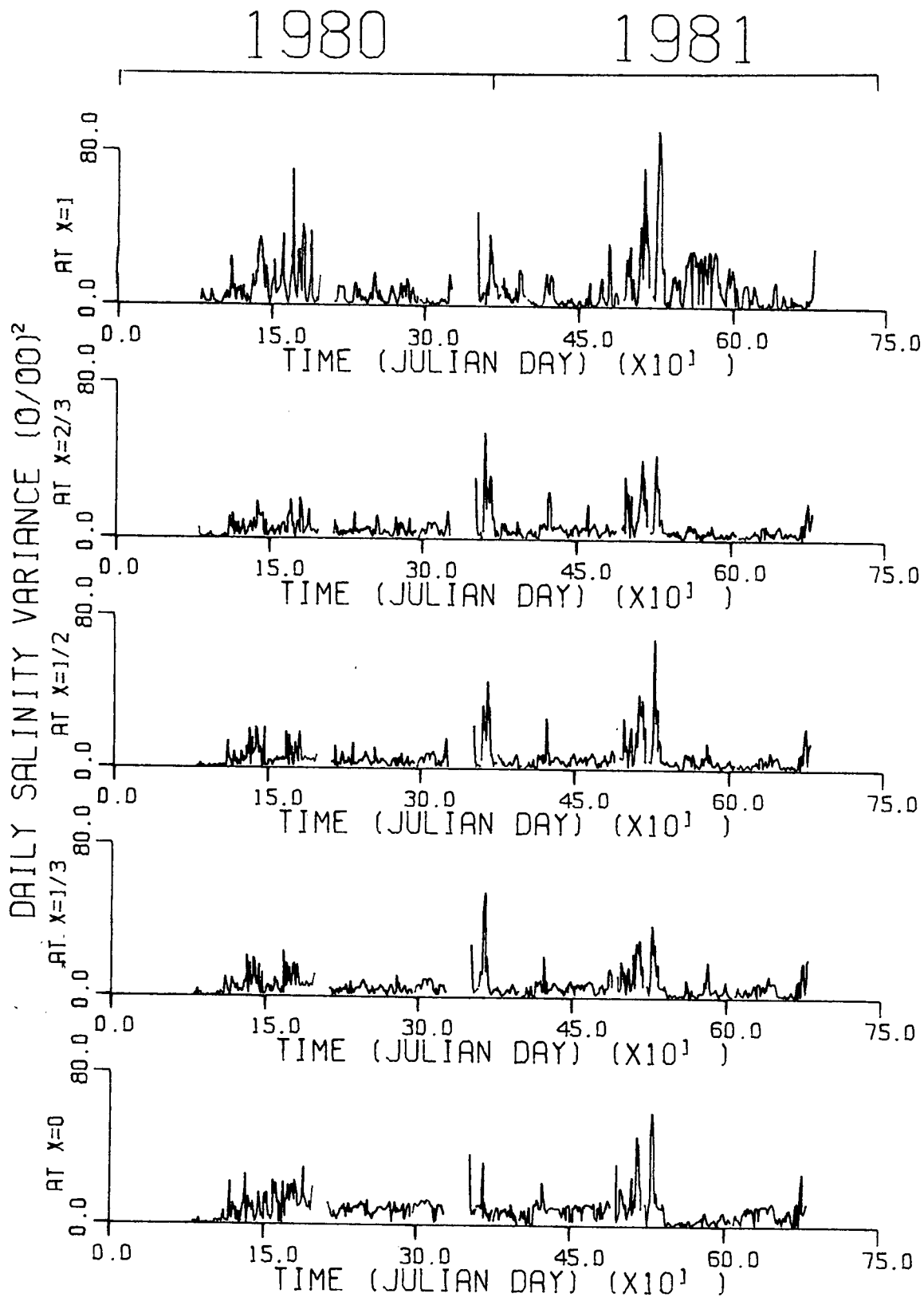

Figure 10 - Plots of the daily variance of salinity versus time for five different points along the southern section (x=0,1/3,1/2,2/3,1)

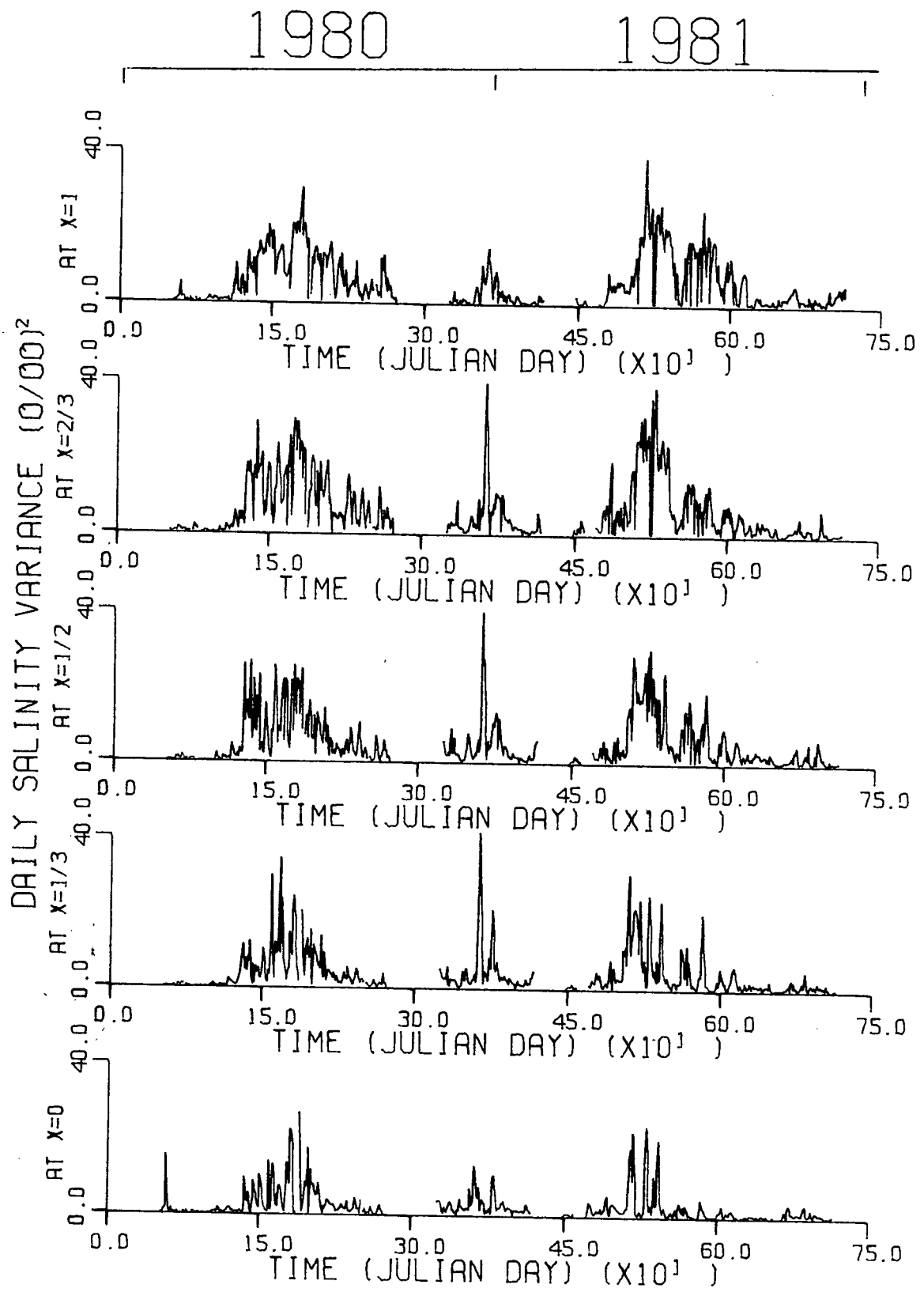

Figure 11 - Plots of the daily variance of salinity versus time for five different points along the northern section (x=0,1/3,1/2,2/3,1)

partly due to the problem of the ferry docking previously described. It is interesting to note that on the northern section, during the anomalous discharge of December 1980, the daily salinity variances at x=1/3, 1/2 and 2/3 seem to be the greatest while at the ends of the section they are relatively low.

3.4 Combined Effects Of The Wind And Discharge On The Plume Characteristics

No obvious visual correlations could be found by comparing the time series of the wind with those of the plume characteristics for the two year period as was done for the discharge in Figs. 6 and 7.. Some insight may be gained by analysing the effect of the wind during short intervals of time (20 to 30 days), the order of the important wind fluctuation periods. Three intervals of time are examined; they also correspond to the cases for which extensive numerical modelling is described in chapter 5. The December Peak discharge is given special attention and the two sharp increases in discharge in the springs will be the subjects of the two other cases.

3.4.1 Spring 1980

This period is characterized by an increasing discharge that leads to the general decreasing trend in the northern section salinity (Fig. 12). Such a decreasing trend is not evidenced in the southern section salinity. After three days of variable wind (Julian days 119 to 122), three days of

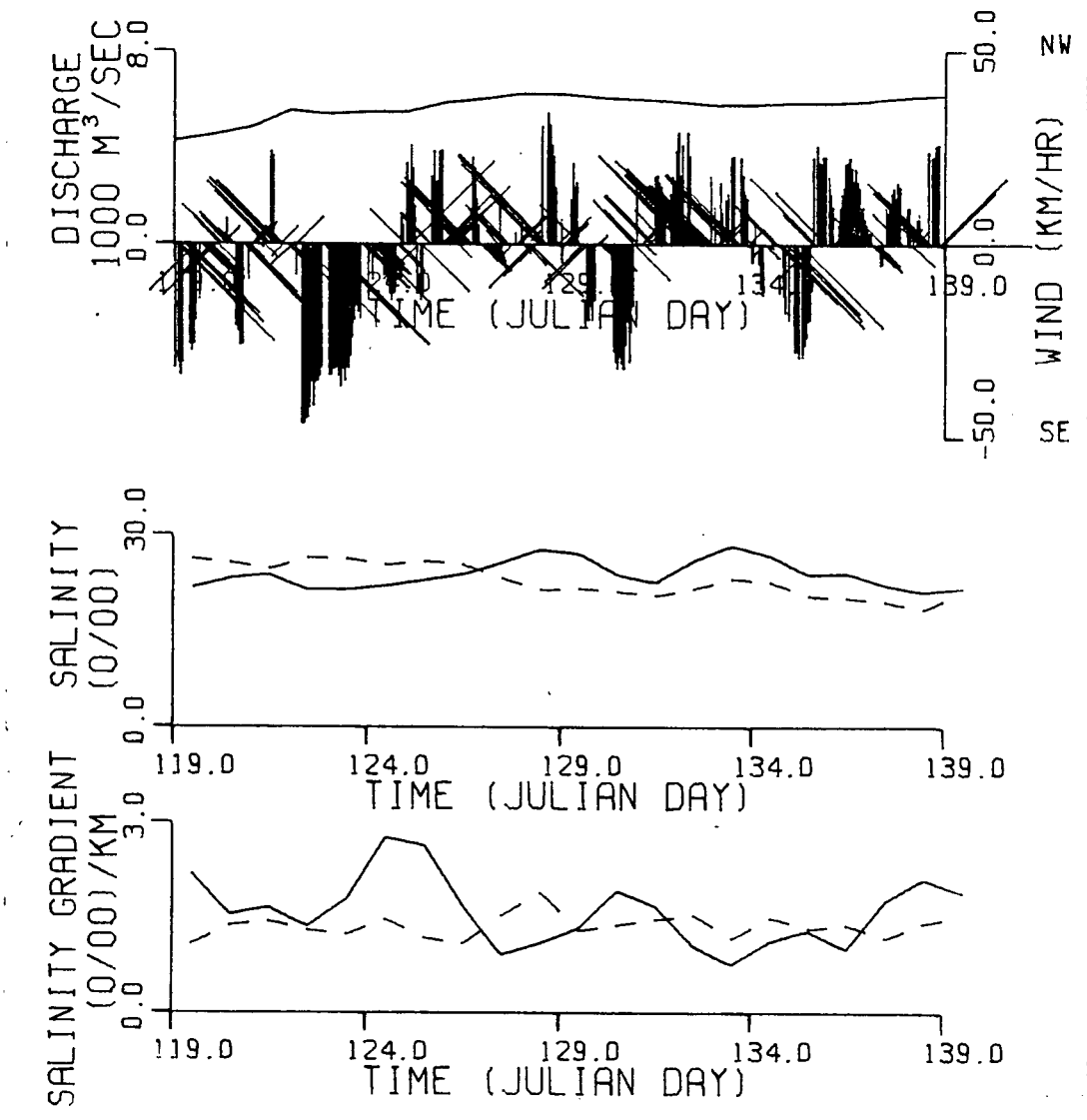

Figure 12 - Plot of the River discharge (solid line,top), stick diagram of wind (top), and plots of average salinities (middle) and salinity gradients (bottom) for the southern (solid line) and northern (broken line) sections vs time during the Spring 1980

northwesterly winds (Julian days 122 to 125) do not seem to have much effect on the plume characteristics except an increase in the salinity gradient on the southern section. On the other hand, the four following days (125 to 129) show the effect of southeasterly wind advection that brings the fresh water close

to the northern section and away from the southern section. Accordingly, the salinity on the northern section is seen to decrease while the salinity on the other section is seen to significantly increase. A peak in the salinity gradient is reached for the northern section while this characteristic on the southern section drops from the peak it attained previously due to the negative along strait wind.

Two days (129 to 131) of negative along strait wind that pushes the plume towards the southern section, are enough to cease the decrease of salinity on the northern section and cause a drop in the southern section salinity. It is accompanied by an increase in salinity gradient on that section while this characteristic for the northern section drops from its highest value for that period, reflecting the mixing that eliminates the salinity difference. A return of southeasterly wind for the next three days (131 to 134) did not give rise to a significant response on the northern section while the predicted rise of salinity and drop of salinity gradient are observed on the southern section. The drop of southern section salinity and the increase of salinity gradient, subsequent to this event, might have been partly initiated by the northwesterly wind on day 135, but the stretch of positive along strait wind after that day should have brought the salinity up again. The effect of the high discharge level at that time might have counteracted this wind effect. The combined effects of the wind and discharge helped decrease the salinity at the northern section.

3.4.2 December Peak

The signature of the discharge pattern is clearly visible in all four characteristics shown in Fig. 13. The high discharge induced drops in average salinity and sharp peaks in

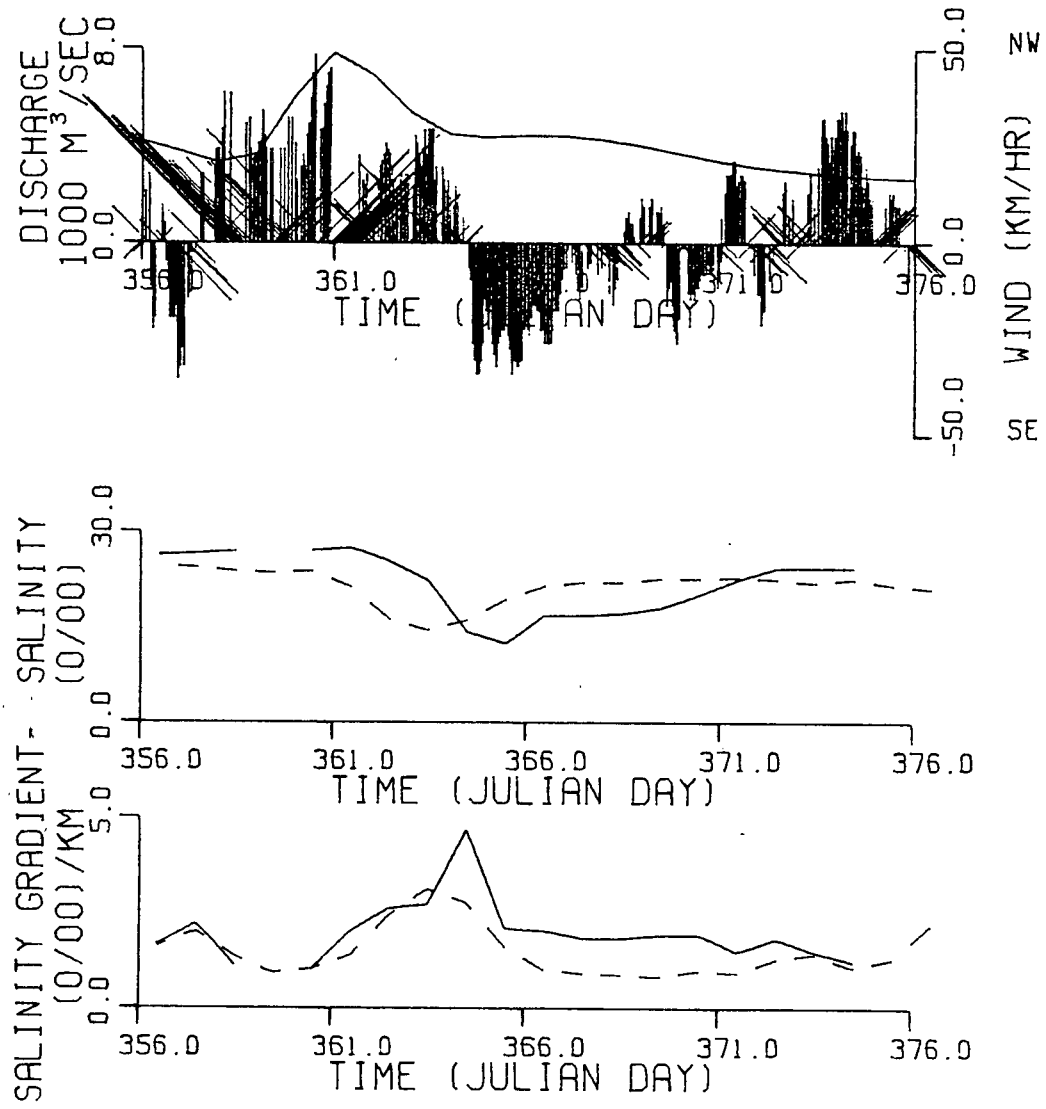

Figure 13 - Plot of the River discharge (solid line,top), stick diagram of wind (top), and plots of average salinities (middle) and salinity gradients (bottom) for the southern (solid line) and northern (broken line) sections vs time during the December Peak

the salinity gradients. It is seen in Fig. 13 that the high peak discharge occurs mainly during a period of positive wind (south-east) that should push the fresh plume water towards the northern section. This combination of wind and discharge is responsible for the salinity drop on the northern section at days 361-362, a time of only gradual salinity decrease on the southern section. It is only when, on day 364, the wind reverses direction that there is a significant salinity drop on the southern section while the salinity on the northern section is seen to increase. The magnitudes of the maximum gradient respond sharply to the discharge and the wind. They also show the delay in the response of the southern section in comparison to the response of the northern section. After the discharge disturbance is over, the salinities and the salinity gradients slowly go back to the level they were at before the event.

3.4.3 Spring 1981

As for the spring 1980 case, the discharge is progressively increasing throughout the interval of time studied (Fig. 14). The general decreasing trend of the salinity on the northern section, supported by the gradual increase of salinity gradient shows the overall freshening effect of the discharge. On the other hand, the large increase of the southern section salinity between Julian days 516 and 524 can not be discharge-related. A look at the wind record identifies the cause of the salinity increase as being high southerly winds that take the plume away from the southern section, reducing at the same time the

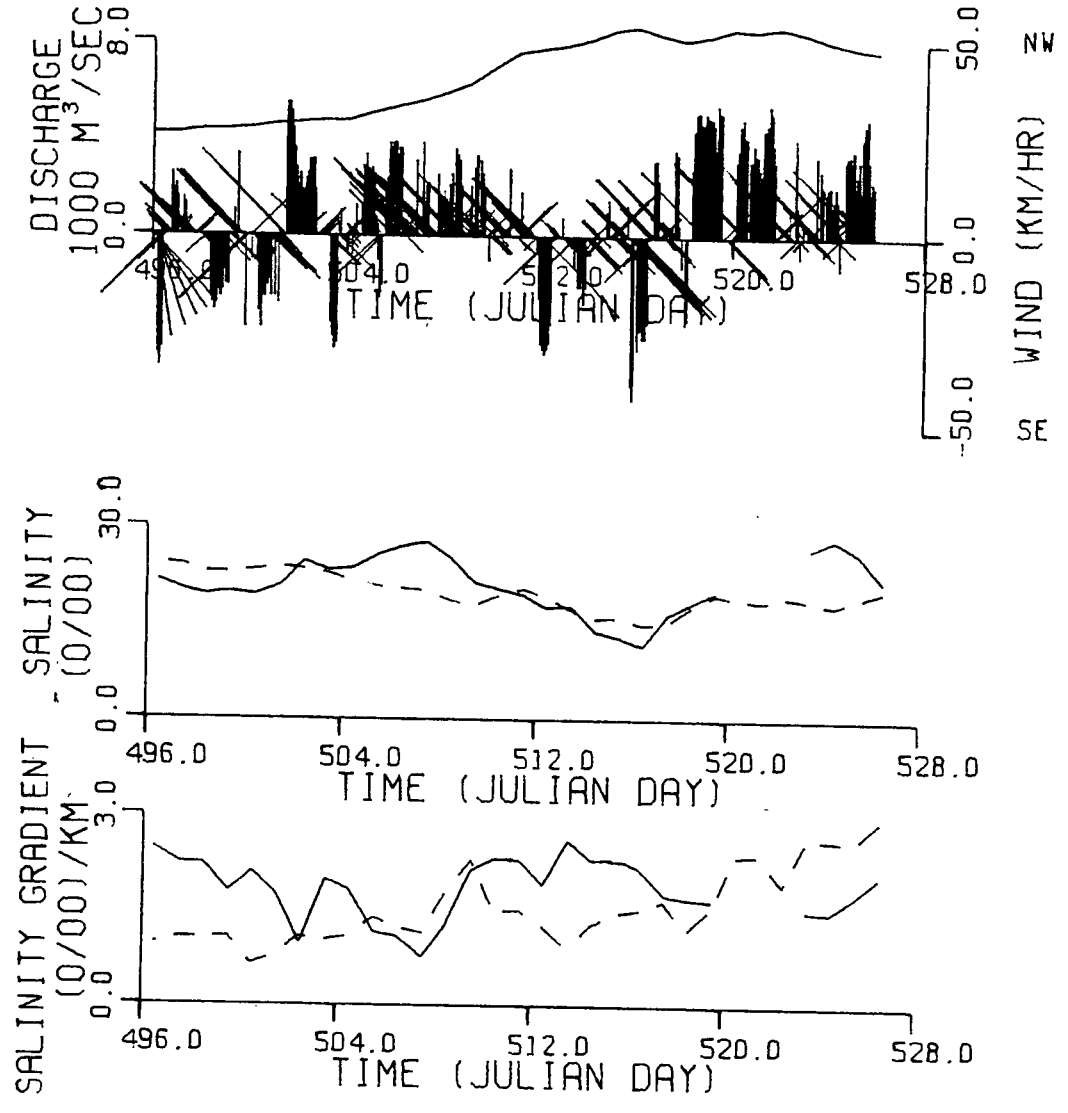

Figure 14 - Plot of the River discharge (solid line,top), stick diagram of wind (top), and plots of average salinities (middle) and salinity gradients (bottom) for the southern (solid line) and northern (broken line) sections vs time during the Spring 1981

salinity gradient. Low salinities and high gradients are encountered on the southern section during a combination of high discharge and northwesterly winds (Julian days 512 to 516). The burst of negative wind on day 512 might be responsible for the peak in the northern section salinity on that day accompanied by

a slight decrease of salinity gradient magnitude. The long stretch of positive wind between Julian days 501 and 512 is certainly responsible for the salinity variation on the southern section from days 501 to 508. On that day (508), due to a weakening of the wind or to a greater importance of the discharge, salinity starts to drop and the salinity gradient to rise. During the period from Julian days 498 to 501, low salinities and relatively high gradients of salinity on the southern section were maintained by negative winds pushing the plume towards that section while high salinities were found on the northern section.

The analysis of these three cases is effective in showing the effects of the wind in producing variations of the plume characteristics. While these effects have been predicted by many workers (Feely and Lamb, 1979; Duffus and Tilley, 1978; Stronach, 1981), the ferry data provides the first set of time series which allow this assumption to be verified.

IV. STATISTICAL ANALYSIS

4.1 Cross-correlations

Cross-correlations can be used as a tool to quantify the suspected relation between the forcing parameters (wind and discharge) and the plume characteristics (average salinity and magnitude of the maximum salinity gradient). Table V summarizes the cross-correlation computations for the longest possible daily series (three series per section). The computations were performed with the plume characteristic and the forcing parameter in such an order so as to give a peak in the correlation function at a negative lag when the forcing parameter is leading the plume characteristic fluctuations. The peak correlations were tabulated along with the corresponding time lags. If two significant peaks are present in the cross-correlation function, they are both written in Table V.

4.1.1 Discharge

As can be seen from Table V, the time lags in the discharge correlations are negative (or 0.) indicating that the discharge leads the variations of the plume characteristics. The exact value of the lag (fluctuates between -7 and 0 days) is, however, not statistically significant at the 99 % level and is seen to vary from one data period to the other for the same section. This conclusion of non-significant differences between the different data periods also holds for the correlation coefficients. The correlations themselves are fairly high and

Table V - Results of the cross-correlation computations between the plume characteristics and the forcing parameters

	Discharge		Along-strait wind component	
	Cross-correlation coefficient	Day lag	Cross-correlation coefficient	Day lag
AVERAGE SALINITY				
Southern section Julian days:				
80-327	-0.65	-1	0.42	-1
352-541	-0.69	-4	0.40	5
570-680	-0.37	-3	0.56	-2
Northern section Julian days:				
52-273	-0.87	-7	-0.18	-4
325-416	-0.86	-2	-0.19	-4
			0.33	2
448-715	-0.83	0	0.24	6
MAGNITUDE OF THE MAXIMUM GRADIENT				
Southern section Julian days:				
80-327	0.43	-1	-0.18	-1
352-541	no sig. correlation		no sig. correlation	
570-680	0.42	-2	-0.42	-2
Northern section Julian days:				
52-273	0.59	-1	0.17	-2
			-0.19	2
325-416	0.67	-2	0.34	-3
			-0.30	2
448-715	0.64	0	-0.25	13

significant at the 99 % level except for the magnitude of the salinity gradient on the southern section during the Julian day period 352-541. The correlations are suprisingly higher on the

northern section than on the southern section for both plume characteristics. This might be due to the Coriolis force which could favor the northern section by deflecting fresh water towards it. Also, the southern section is closer to the input of salty ocean water through the Strait of Juan de Fuca. The northern section, however, is fairly well removed from any strong sources of sea water. Thus, some of the fluctuations at the southern section, may be responses to variations in sea water input and be unrelated to changes in river discharge.

A lower correlation with the magnitude of the maximum gradient than with the average salinity was expected because the former is not continuous. For example, on the southern section, at high discharge, the front can go beyond x=0, through a pass (Fig. 1) so that the gradients on the section itself are low. The sign of the correlation indicates that, as expected low salinities and high gradients are related to and follow high discharges as seen in the time series of chapter 3.

4.1.2 Wind

Unlike the discharge correlations, the wind cross-correlation coefficients and time lags fluctuate greatly from one time period to another for a particular plume characteristic. This is a first hint at the effect that the wind causes salinity variations that are not independent of the general water properties and discharge level present at the time.

The along-strait wind component is only weakly correlated

(table V) with the plume characteristics. In this case, positive time lags are nearly as frequent as negatives ones. They occur in such a way that a quadrature relationship between the forcing parameter and the plume characteristic is suspected. Cross-spectra between those two parameters constitute a better tool to investigate the phase difference between the two series.

The correlation coefficients with the wind are low but are still significant at the 99 % level. The effect of the wind is more strongly felt at the southern section than at the other section. This is in contrast to the effects of the discharge on the two sections. If we think of positive along-strait winds as advecting the fresh water of the plume towards the northern section then, for strong positive winds, high salinities can be expected at the southern section and low salinities at the northern section. Thus, a positive correlation of the average salinity on the southern section with the along-strait wind component and a negative correlation with the same characteristic on the northern section are expected. Moreover, if the proximity of the plume to a section increases the salinity gradient then high gradients on the southern section should be seen when the plume is advected towards this section i.e. with a negative along-strait wind component. This process predicts a negative correlation between the magnitude of the maximum gradient on the southern section with the along-strait wind component and a positive one on the northern section. These assertions regarding the signs of the correlations for the southern section plume characteristics are verified as can be

seen from table V but the quadrature property of the relationship between the northern section characteristic and the wind parameter do not allow any statements about the phase until cross-spectra are computed.

4.2 Linear And Non-linear Combination Of The Wind And Discharge

In this section, an attempt will be made to state how much of the variations of the average salinity and the magnitude of the maximum gradient can be explained by a linear combination of the wind and the discharge parameters. If such a combination of wind and discharge is found to describe reasonably well the ferry data, it could then be used to interpolate during periods of missing data and to extrapolate for other years.

The notation will follow essentially that of Jenkins and Watts (1968). Let's suppose that the detrended output X_{t3} (that will be either the average salinity or the salinity gradient) can be written as:

$$X_{t3} = h_1 X_{(t-r)1} + h_2 X_{(t-s)2} + Z_t$$

$$\text{for } t = 1,2...N \qquad 3.1$$

where h_1 and h_2 are linear coefficients,

r is the lag time of the effect of the series X_{t1} (that will be the discharge series) on the output X_{t3},

s is the lag time of the effect of the series x_{t2} (that will be the along-strait wind component series) on the output X_{t3},

Z_t is a noise term that will be assumed to be white.

The previous equation can be written in matrix form:

$$x = Xh + Z \qquad 3.2$$

where

$$X = \begin{bmatrix} x_{(1-r)1} & x_{(1-s)2} \\ \vdots & \vdots \\ x_{(N-r)1} & x_{(N-s)2} \end{bmatrix}$$

$$h' = (h_1 \quad h_2)$$

$$x' = (x_{13} \quad x_{23} \quad \ldots x_{N3})$$

$$Z' = (z_1 \quad z_2 \quad \ldots z_N)$$

By multiplying the matrix equation by X'/N, one gets:

$$(1/N)X'x = (1/N)(X'X)h + (1/N)X'Z. \qquad 3.3$$

Each element of the matrix $(1/N)X'Z$ is a cross-covariance estimate between the inputs and the noise. This is essentially zero. The matrix $(1/N)X'X$ can be rewritten in terms of the cross-correlation coefficient matrix of the inputs:

$$((1/N)X'X)_{11} = (1/N)\sum_{k=1}^{N} x_{(k-r)1}\, x_{(k-r)1}$$

$$= VAR(X_1),$$

$$((1/N)X'X)_{22} = (1/N)\sum_{k=1}^{N} x_{(k-s)2}\, x_{(k-s)2}$$

$$= VAR(X_2),$$

$$((1/N)X'X)_{12} = ((1/N)X'X)_{21} = (1/N)\sum_{k=1}^{N} x_{(k-r)1}\, x_{(k-s)2}$$

$$= r_{12}(r-s)(VAR(X_1)VAR(X_2))^{1/2} \qquad 3.4$$

where $r_{12}(r-s)$ is the cross-correlation coefficient at lag $(r-s)$ between time series 1 and 2. The matrix $(1/N)X'x$ can be written in terms of the cross-correlation coefficients between the inputs and the output:

$$((1/N)X'x)_{11} = (1/N)\sum_{k=1}^{N} x_{(k-r)1}\, x_{k3}$$

$$= r_{13}(r)(VAR(X_1)VAR(X_3))^{1/2}$$

$$((1/N)X'x)_{21} = (1/N)\sum_{k=1}^{N} x_{(k-s)2}\, x_{k3}$$

$$= r_{23}(s)(VAR(X_2)VAR(X_3))^{1/2}. \qquad 3.5$$

Finally the matrix equation can be rewritten and solved for h_1 and h_2. The results are

$$h_1 = (VAR(X_3)VAR(X_1))^{1/2}\ \frac{r_{12}(r-s)r_{23}(s)-r_{13}(r)}{r_{12}^2(r-s)-1}$$

$$h_2 = (VAR(X_3)VAR(X_2))^{1/2}\ \frac{r_{12}(r-s)r_{13}(r)-r_{23}(s)}{r_{12}^2(r-s)-1}. \qquad 3.6$$

The linear combination should attempt to describe the data as a whole and not only small sections of it. The various estimates of cross-correlation coefficients and variances needed to compute h_1 and h_2, should characterize the statistics of both years of data. In view of the uniformity of the cross-correlation coefficients of Table V and the insignificant

variations of the time lag for different time periods for a particular section and plume characteristic, an arithmetic average of the three (two in the case of the southern section salinity gradient) cross-correlation coefficients should give the desired estimates for r_{13} and r_{23}. In cases where two cross-correlation coefficients at different time lags are discussed, the highest one of the two is used in the computation of the averaged cross-correlation coefficients. These are given in Table VI and they exhibit the same general properties described in the previous section concerning the size and the

Table VI - Averaged cross-correlation coefficients between the plume characteristic (Series 3), the discharge (Series 1), the wind (Series 2) and the linear combination (Series 4)

	r_{13}	r	r_{23}	s	r_{43}	r^2_{312}
AVERAGE SALINITY						
Southern section	-0.57	1	0.46	1	0.66	47 %
Northern section	-0.85	2	0.13	0	0.88	72 %
MAGNITUDE OF THE MAXIMUM GRADIENT						
Southern section	0.43	1	-0.3	0	0.47	25 %
Northern section	0.63	2	-0.03	2	0.63	40 %

sign of the values of the correlations for the different plume characteristics. The values of r_{23} are low and insignificant for the northern section characteristics and also carry the opposite sign to that predicted by wind advection. The cross-correlation between discharge and wind (r_{12}) produced a uniform value of -0.13 around 0 day lag. This value is very low and not significant as expected. The time lags r and s associated with

the average cross-correlation estimates of Table VI were obtained by finding the combination of r and s that gives the highest cross-correlation at lag 0 between the plume characteristic data and the linear combination. The values of the latter cross-correlation coefficients (r_{43}) are shown in Table VI along with the percentage of the data series variance explained by the linear combination, a value also known as the multiple correlation coefficient (r^2_{312}). The multiple correlation coefficient is expressed as follows:

$$r^2_{312} = (r^2_{13} + r^2_{23} - 2r_{12}r_{13}r_{23})/(1 - r^2_{12}). \qquad 3.7$$

The conclusions to be drawn from these correlations are that in general the correlation is better between the data and the linear combination than with the two forcing parameters separately, and that the average salinity is a better characteristic compared to the salinity gradient to see the influence of wind and discharge. A reconstruction of the plume characteristic series from the detrended output of the linear combination is shown in Figs. 15 and 16. This reconstruction used the slopes and intercepts from the earlier detrending procedure done on the plume characteristics. The detrending procedure yielded a value of 0 for the slopes and of 24.7 o/oo for the average salinity intercepts. Intercept values for the salinity gradient trends are 1.3 and 1 (o/oo)/km for the southern and northern sections, respectively. These linear reconstructions (Fig. 15 b,d and 16 b,d) show a lack of fluctuations compared to the data series of Fig.15 a,c and 16 a,c. A large portion of the variance (in most of the cases,

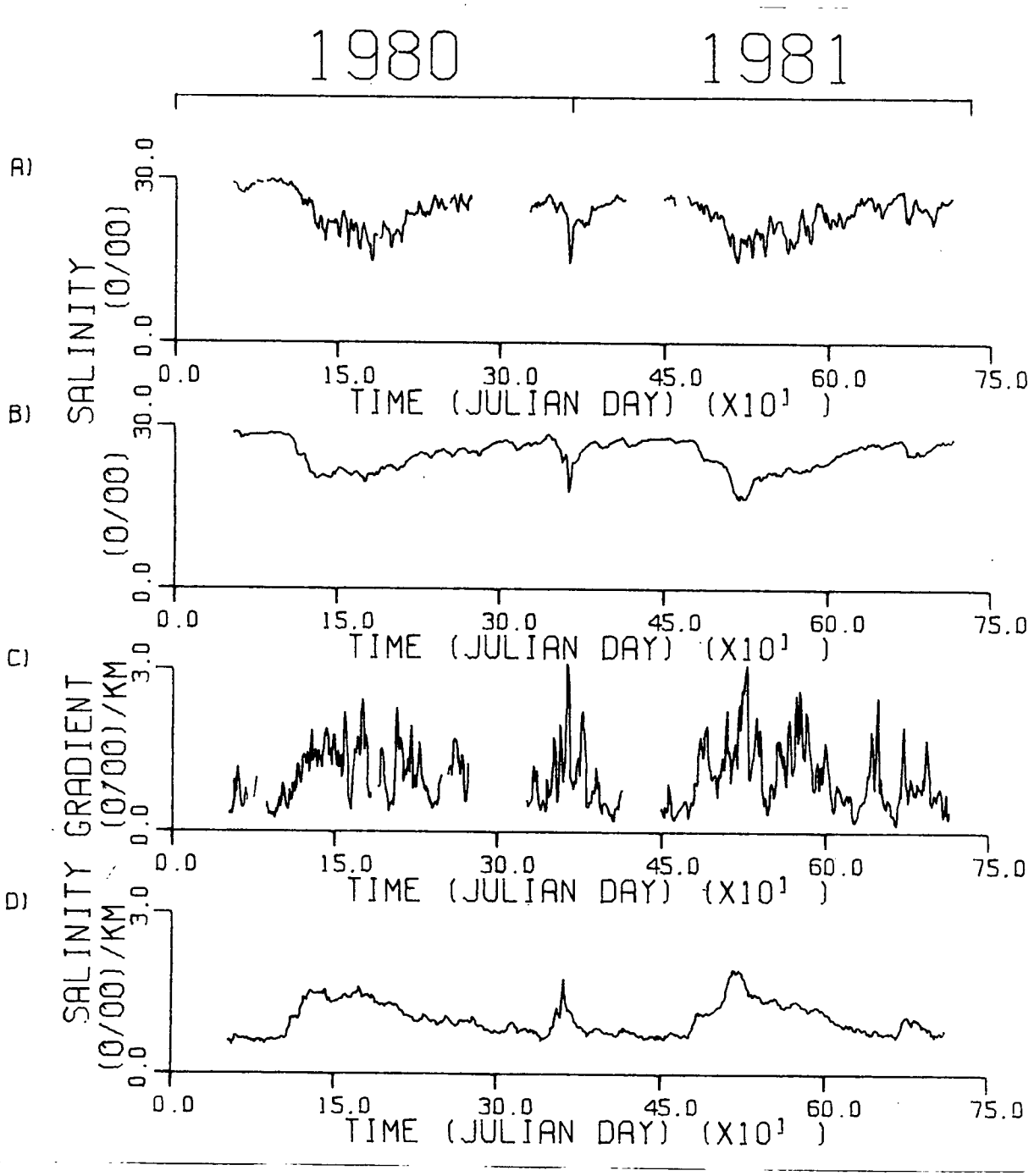

Figure 15 - Plots of northern section plume characteristics versus time: a) average salinity ferry data, b) average salinity from linear combination, c) maximum salinity gradient ferry data, d) maximum salinity gradient from linear combination

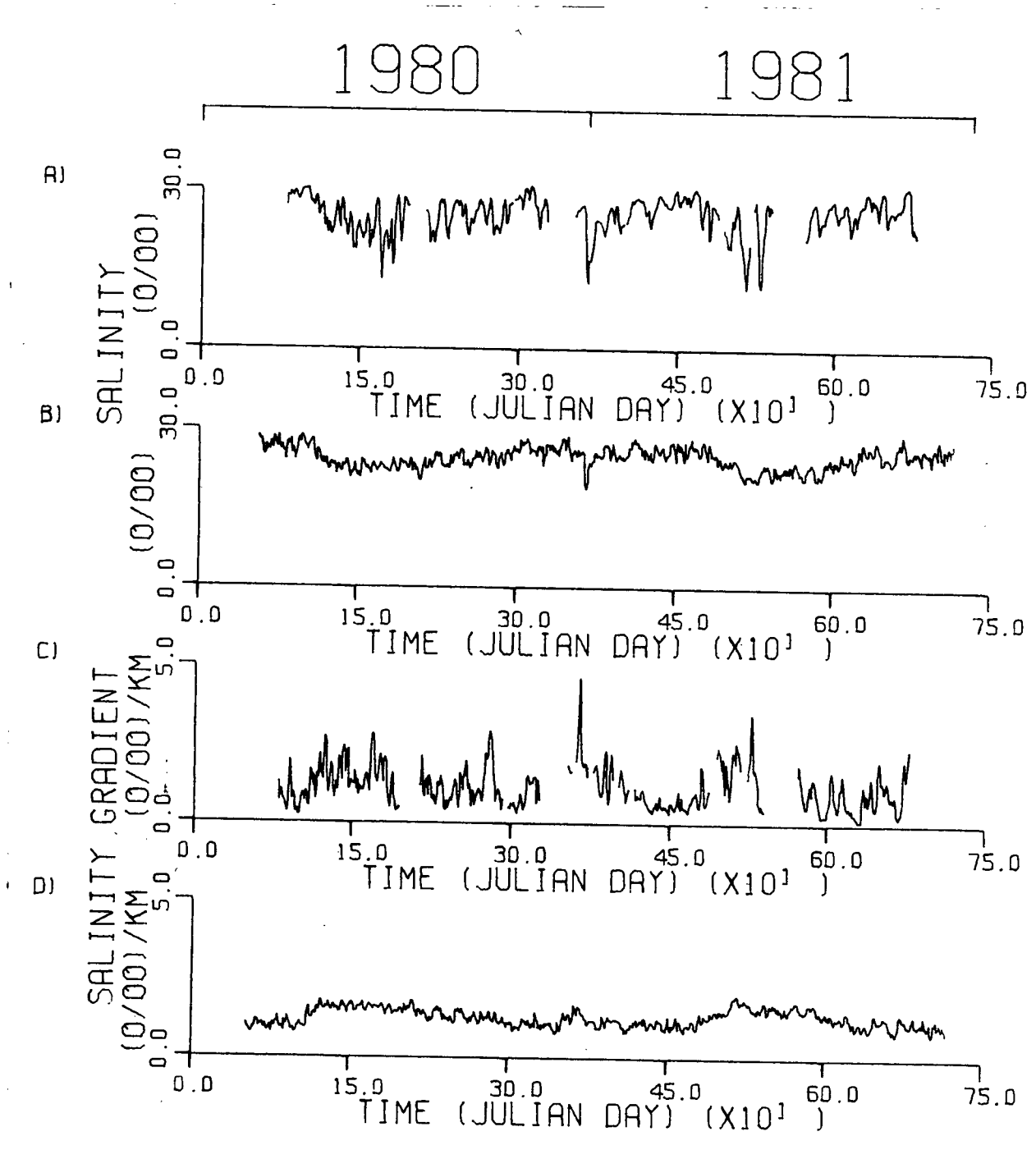

Figure 16 - Plots of southern section plume characteristics versus time: a) average salinity ferry data, b) average salinity from linear combination, c) maximum salinity gradient ferry data, d) maximum salinity gradient from linear combination

more than 50 %, Table VI) is still unexplained by the wind and the discharge or cannot fit into the linearity assumption of the combination of the two forcing parameters.

In view of the increased variability of the plume characteristics during high discharge (Fig. 6 and 7), it was thought that a better combination of the wind and the discharge would be to make the contribution due to the wind (h_2X_{t2}) dependent on the discharge by multiplying it by a factor of the form $C \exp(kX_{(t-r)1})$ where $X_{(t-r)1}$ has units of 10^3 m^3/s. By slowly varying the value of k and finding the corresponding value of C that minimized the squared differences between the resulting combination and the average salinity data, sets of two number (k and C) were found that maximized the correlations between the non-linear combination and the ferry data. The optimized k values were 0.4 and 0.6 for the southern and northern sections, respectively. The resulting cross-correlations for the non-linear combination were slightly above the corresponding correlations for the linear combinations. No improvement in the variability in the reconstructed series from the non-linear combination of wind and discharge was found and this reflected the effect of the optimization procedure in trying to minimize the wind contributions (the optimized values of C were quite low). By arbitrarily increasing the value of C by a factor of 3 for the non-linear combination of the southern section average salinity, the resultant series (Fig 17 b) shows a better qualitative agreement of the variability level between

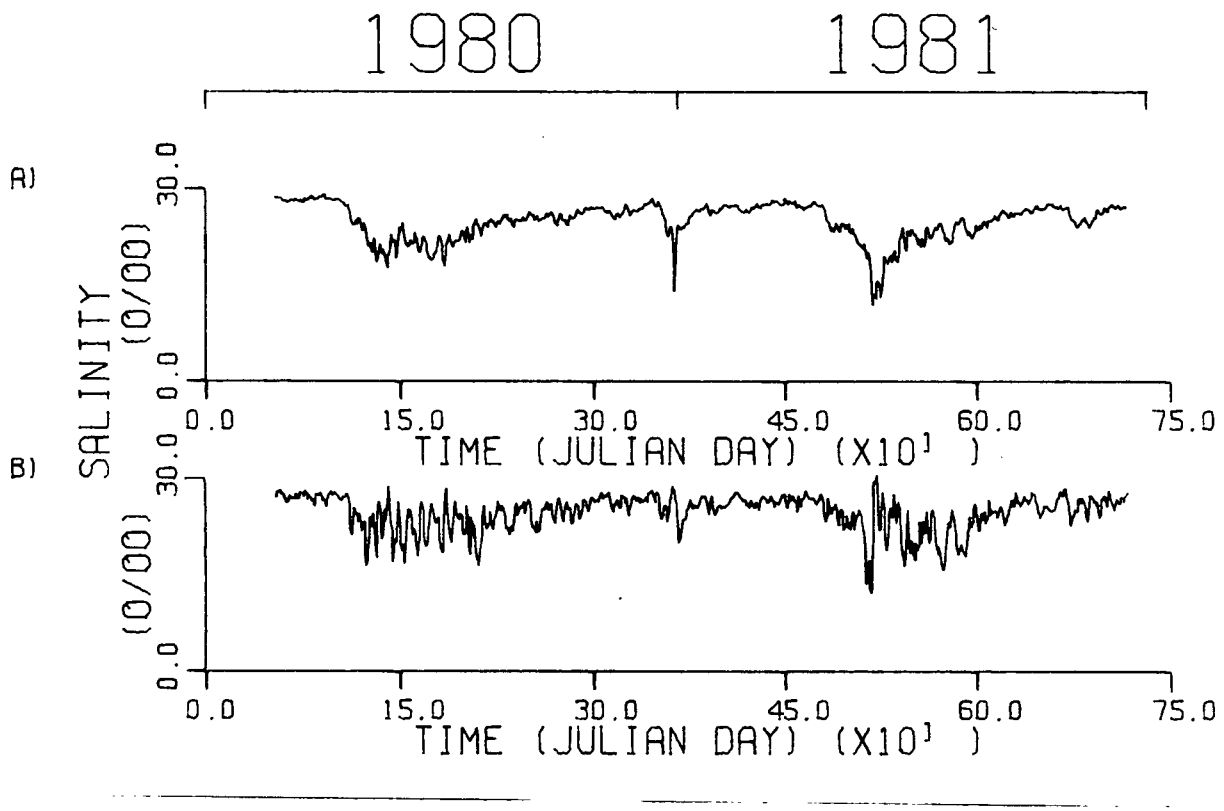

Figure 17 - Plots of the average salinity versus time for the a) northern and b) southern sections as given by a non-linear combination of wind and discharge

the combination and the data. Nevertheless, it is accompanied with a slight decrease in the actual cross-correlation coefficient (0.62). When the value of C for the combination resulting in the estimation of the northern section salinity, is optimized with k=0.4, C becomes negative and increases by a factor of 14 compared to the optimized C value with k=0.6. This different set of k and C effectively increases the wind contribution to a level that improves the qualitative accord between the combination series and the data (Fig. 17 a). The cross-correlation computation quantifies this accord to a value of 0.80. The fact that the constant C is now negative brings

the sign of the wind contribution in agreement with the effect of wind advection for salinity near the northern section.

4.3 Spectra And Cross-spectra

In an attempt to achieve maximum spectral resolution and use the full length of the data as a single time series, the gaps between the three daily series for each plume characteristic and each section were filled with the appropriately reconstructed linear combination of the wind and the discharge described in the previous section. It was felt that the time intervals covered by these gaps were small compared to the total length so that they would not modify the spectral results. To support this assumption, an overall comparison between the spectral results from the three different portions of the data record and the results from the full data record did not show any major differences.

Spectra of the daily forcing parameters and the plume characteristics are displayed in Fig 18. The major contributions to the spectrum of the discharge are at periods longer than 20 days while the periods of the wind fluctuations are mostly shorter than 20 days with a sharp peak at 6 days and a broad one between 10 and 20 days. This nicely separates the possible effects of the discharge from those of the wind in frequency space. Looking now at the spectra of the plume characteristics, one sees that only the spectrum of the northern section average salinity clearly appears red similar to the discharge spectrum. Peaks at 6 days for the southern section

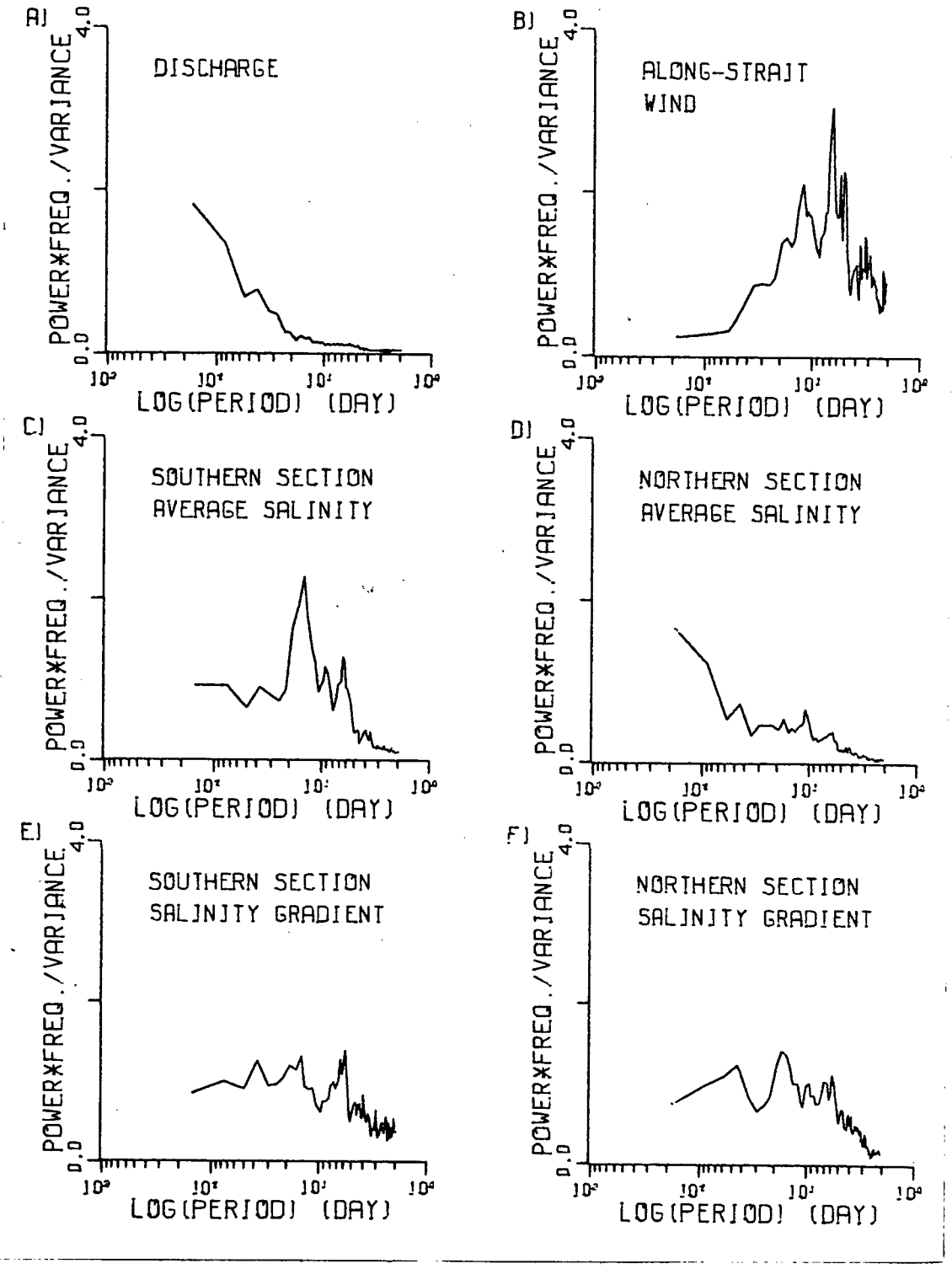

Figure 18 - Plots of normalized spectra of a)the Fraser River discharge, b) the along-strait wind component, c)the southern and d) northern section average salinities and the e) southern and f) northern section maximum salinity gradient

spectral estimates and the broad peak over the period interval of 10 to 20 days for all characteristics (except the northern section salinity spectrum) are quite similar to the corresponding peaks in the wind spectrum. To quantify this similarity between the spectral representation of the forcing parameters with the plume characteristics, cross-spectra have been computed and the peaks in coherency are tabulated in Tables VII and VIII.

4.3.1 Cross-spectra With The Discharge

One should notice that in the cross-spectra of Table VII, the highest squared coherency occured at the lowest computed

Table VII - Results of the cross-spectra between the plume characteristics and the river discharge

	Maximum Squared Coherency	Corresponding Period (days)	Phase lag
AVERAGE SALINITY			
Southern section	0.82	149	179°± 8°
Northern section	0.92	165	-171°± 2°
MAGNITUDE OF THE MAXIMUM GRADIENT			
Southern section	0.50	149	-20°±20°
Northern section	0.87	165	0°± 4°

frequency. This frequency depends on the length of the record and the averaging taper. The values of the squared coherency are high, except for that of the southern section salinity gradient and are above the noise level for periods over 30 days. The order of importance of the maximum coherency follows the

same order as the cross-correlation coefficients (r_{13}) of Table VI: higher coherencies found with the northern section characteristics than with the southern ones and a more coherent relation between the average salinities and the discharge than between the salinity gradients and the discharge. The phases of Table VII also agree with the signs of the correlations given in Table VI. The uncertainties in the phases are taken from Fig. 9.3 of Jenkins and Watts (1968). An exact lag value (to the closest day) of the effect of the discharge on the plume characteristics cannot be determined. It is only in the case of the northern section salinity that a tendency of the discharge to lead this plume characteristic by a few days is found.

4.3.2 Cross-spectra With The Wind

As suggested above, one may be able to identify the small peaks in the spectra of the characteristics (for periods below 20 days) as possible wind effects. Cross-spectra of the plume characteristics with the along strait wind component were computed (Table VIII). This type of computation shows a weak but significant coherence for the wind not only with the southern section plume characteristics but also with the northern section. The peaks in coherence occur at different frequencies for each section. The sharp peak at 6 days in the wind spectrum appeared to influence the southern section cross-spectra but not those for the northern section. On the other hand, the broad peak between 10 and 20 days seemed to influence fluctuations of all four characteristics. As expected from the

Table VIII - Results of the cross-spectra between the plume characteristics and the along strait wind component

	Maximum Squared Coherency	Corresponding Period (days)	Phase lag
AVERAGE SALINITY			
Southern section	0.63	6	60°±20°
	0.51	19	-20°±20°
Northern section	0.31	10	-30°±30°
	0.31	12	-90°±30°
MAGNITUDE OF THE MAXIMUM GRADIENT			
Southern section	0.34	6	-110°±30°
	0.41	19	-170°±20°
Northern section	0.46	12	140°±20°

shape of the spectra, the worst correlation with the wind was for the northern section salinity. The phase differences for the average salinities and magnitudes of the maximum gradients for each section at corresponding periods is close to 180° indicating an out of phase relationship between the two plume characteristics on each section. Numerous phase values are close to the quadrature values of 90° or -90°. This could be explained as follow. Let's assume the along-strait wind component to be a sinusoidal function of either 6 or 12 days (periods corresponding to the periods of highest coherencies in the cross-spectra). One can think of this along-strait wind component as advecting the body of fresh water as a whole in the same direction as the wind. During the positive part of the cycle, the water is advected to the north so the southern section salinity is progressively increasing (while it is decreasing on the northern section) until the wind changes

direction and brings the fresh water back towards the southern section. Under these conditions, the salinity maximum on the southern section should occur when the wind is zero and changing from a positive wind component to a negative one. The preceding explanation predicts a phase lag of 90° between the southern section average salinity and the wind component and -90° between the northern section salinity and the wind. The computed phases of 60° and -90° are not far from the expected phase lags.

4.4 Harmonic Analysis

In order to evaluate fluctuations at tidal frequencies the average salinity series were divided into two portions: the 1980 data and the data for 1981. Each portion was harmonically analysed and only the constituents listed in Table III were given special attention since they are the only constituents simultaneously monitored by two ferries on the same section. The list of constituents to receive attention is further reduced by eliminating the constituents for which the amplitude does not exceed the noise level of 0.5 o/oo for the yearly harmonic analysis. Table IX summarizes the harmonic analysis for these constituents for the two years of data. Two constituents (Ssa and Mf) that could not be resolved in the analysis leading to Table III, have been added to the list. They both respect the critera of having amplitudes above the noise level. If one excludes the results of S_2 for the southern section for which amplitudes are below the noise level and the difference between the phases of the two different years is 115°, no significant

difference between the phases for the different years is noticed. The highest phase difference is 56° and is lower than the fluctuation of the phases noticed to occur between two series obtained by two ferries on the same section (64°). On the other hand, the amplitudes of the fluctuations vary from one year to another.

Small tidal amplitudes for the northern section are usually found in comparison to the corresponding amplitudes for the southern section. The proximity of the river mouth to the southern section, that leads in general to the presence of high horizontal salinity gradients, might be responsible for this

Table IX - Amplitudes (A) in o/oo and phases (ϕ) from the harmonic analysis done on the average salinity series for the two years of the data

	Southern section				Northern section			
	1980		1981		1980		1981	
	A	ϕ	A	ϕ	A	ϕ	A	ϕ
SSa	1.7	46°	3.1	32°	3.4	53°	2.3	52°
MSf	0.5	-26°	1.9	3°	0.2	-52°	0.4	-108°
Mf	0.5	128°	1.5	127°	0.2	65°	0.3	105°
P_1	1.5	-17°	0.6	0°	1.1	18°	1.0	35°
K_1	1.7	18°	0.7	2°	1.2	56°	1.0	53°
M_2	0.6	-27°	0.4	-19°	0.0	180°	0.1	126°
S_2	0.3	168°	0.1	-77°	0.5	-167°	0.4	-127°

difference between the two sections. Stronger tidal currents near the southern section than near the northern section, have also been measured (Data Record of Current Observations, 1969-1970) and might be responsible for high tidal salinity fluctuations on that section. The high amplitude of the Ssa

constituent, which has a half-year period, can hardly be related to the almost negligible corresponding constituent in the sea level elevation. The fact that the frequency of this constituent lies within the frequency band of the discharge, suggested that the large amplitudes at this tidal frequency may be due to a discharge effect. It is not as clear for the MSf and Mf constituents that happen to have frequencies in the range of the spectral peaks of the wind. One can hardly separate the effects of the two forcing mechanisms, but some hints favor the wind as the primary forcing. First, the northern section tidal amplitudes for these constituents are not above the noise level. Secondly, the phases of the amplitudes of the southern section fluctuations vary widely from MSf to MF.

Both years indicate that for high frequencies tidal constituents (diurnal and semi-diurnal constituents) K_1 and M_2 are the major constituents for the southern section salinity. On the northern section, K_1 is again a major constituent but M_2 no longer is, and is even below the noise level. This is surprising since the tides in the Strait are classified as of the mixed dominantly semi-diurnal type (Crean, 1976). The high frequency constituent phases for the average salinity on the southern section are close to 0° or at least between -90° and 90° except in the case of the S_2 constituent that has an amplitude below the noise level. Two processes might be invoked to explain a relation between the tides and the salinity variations: the advection of the plume by the underlying water and the modulation of the discharge. It is known (Crean, 1976)

that from the ebb- to the flood-tide, the water is moving towards the northwestern part of the Strait of Georgia and, conversely, to the southeast from high to low tides. Another effect of the tides is the modulation of the river discharge. This occurs by changing the heights of the water in the river and in the Strait. High discharges can occur at low tides while the river is effectively shut off at high tides. Both processes (the advection of the plume and the modulation of the discharge) bring fresh water (thus lower salinity) to the southern section at low tides. This may be why the phases indicate an in-phase relationship between the average salinity on the southern section and the sea level elevation at Point Atkinson. On the northern section, the two processes act against each other. This leads to a more confused picture. As a consequence, there is no clear cut pattern in the phases relationship recorded that would favor an out-of-phase or an in-phase relation between the tidal forcing and the salinity fluctuations.

When the same analysis is carried out for the magnitude of the maximum gradient series, remembering that MSf was the only constituent for which the analysis done in chapter 2 left some hope of being useful, it turned out that for the yearly analysis none of the amplitudes of the MSf constituent were above the noise level. By examining the harmonic results at tidal frequency that could not be resolved in the analysis of section 1.3.4, only the SSa constituent acquires amplitudes above the noise level. The phases for that constituent are essentially identical for both years and have a difference of 180° with the

phases recorded for the SSa salinity fluctuations. As mentionned before, the discharge more than the tides seems to be the forcing mechanism responsible for fluctuations at the SSa frequency.

When harmonic analysis is performed on yearly frontal salinity gradient series, none of the constituent amplitudes are above the noise level. The only significant amplitudes are obtained by the yearly analysis of the frontal position. It occurs at the MSf frequency for the 1981 northern section series. The phase computed is 182°. The same problem of this constituent being at a frequency of a wind peak is still present but regardless of the mechanism causing the fluctuation, the phase indicates that the frontal position is nearly in phase with the salinity (182° compared to -108°, (Table IX)); that is, low salinities on the northern section are recorded when the plume front is near Vancouver Island. The frontal position and the salinity are in phase on the southern section even though the amplitudes of the MSf fluctuations in position are below the noise level.

As for the wind, it is suggested that the amplitudes of the induced tidal fluctuations might depend on the strength of the river discharge. To investigate this assumption, the data record was separated into nine portions, divided so that each portion is characterized by a certain level of discharge. Portions of the record during which the discharge is between 0 and 3000 m^3/s are characterized by a low discharge (L). This occurs for data portions 1,4,6 and 9 covering in terms of Julian

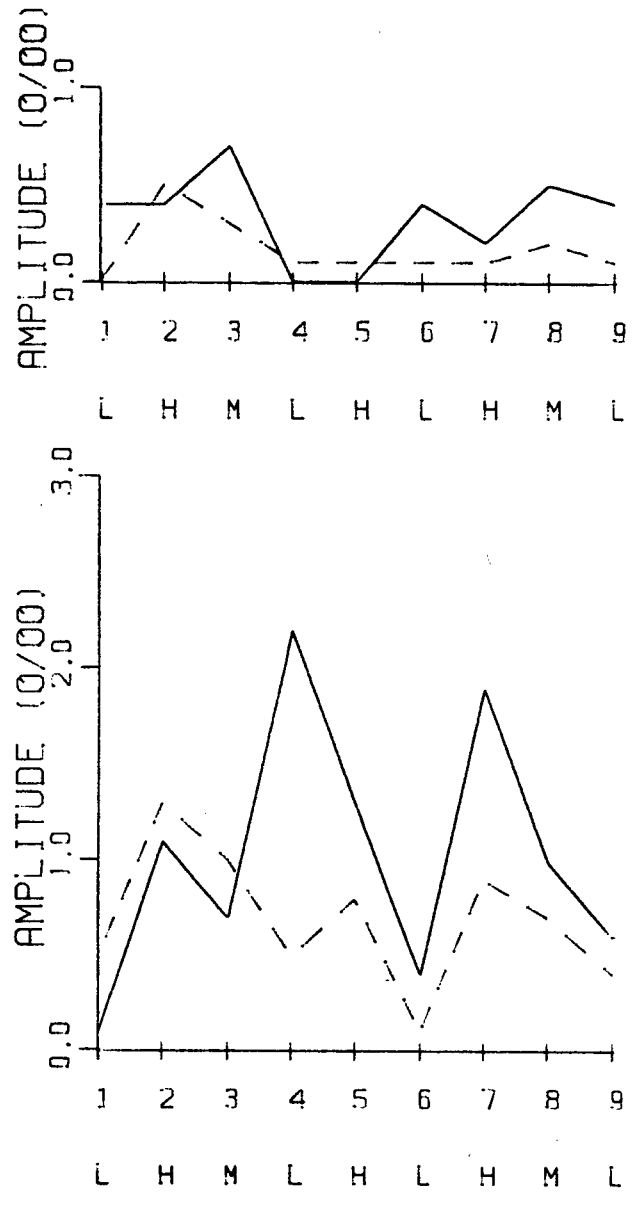

Figure 19 - Northern (top) and southern (bottom) section salinity fluctuation amplitudes for the K_1 (solid line) and M_2 (broken line) constituents from harmonic analyses done on nine different data portions characterized by a discharge level (L,M,H)

days the periods 52 to 109, 283 to 353, 373 to 479 and 618 to 669. Records with discharge between 3000 and 5000 m^3/s are coded as medium discharge portions (M). Data portion 3 and 8 are characterized by this type of discharge. They correspond to periods between Julian days 206 and 282 and also 583 and 617. Finally, when the discharge is over 5000 m^3/s, the portions of the data are associated with high discharge (H). These are data portions 2,5 and 7 with corresponding Julian day periods: 121-205, 354-372 and 504-582. Harmonic analyses have been performed on each of the nine individual portions of the average salinity record for each section. The comparison between the amplitudes of the K_1 and M_2 constituents for the nine portions of data is displayed in Fig. 19. The letters on the x-axes correspond to the level of the discharge during that portion. Series 5 corresponds to the anomalous December Peak. Fig. 19 clearly shows the dominance of K_1 over M_2 for both sections. It also shows that the northern section amplitudes are rarely above the noise level (0.5 o/oo) and because of that do not show any definite relation with the level of the discharge. On the other hand, the southern section amplitudes, while being in general above the noise level, reproduce the pattern of the discharge level for both constituents. Low discharges correspond to amplitude minima and high discharges to amplitude maxima. The only exception is the K_1 amplitude of series 4 that exhibits an anomalous high value for a low discharge level.

V. COMPUTER SIMULATIONS

5.1 Description Of An Existing Model Of The Fraser River Plume

Stronach (1977) developed a numerical model of the thin layer of the Fraser River Plume. It is worthwhile to go over the principles and equations on which that numerical model is based before introducing any changes. It consisted of a two layer model in which the bottom layer was driven solely by the barotropic tides as given by Crean's (1978) numerical tidal model of the Strait of Georgia. The area covered by the model was bounded by Vancouver Island, the mainland and two open boundaries, one along a transect about 8 km to the northwest of Nanaimo and another one about 10 km to the southeast of Boundary Pass. Boundary Pass itself was left open. The timestep and the grid size were respectively 120 sec and 2 km in the final version of the model.

The governing equations for the upper layer were expressed as follow:

$$\partial h/\partial t+\partial U/\partial x+\partial V/\partial y = w_p - w_n \qquad 4.1$$

$$\partial S/\partial t+\partial(US/h)/\partial x+\partial(VS/h)/\partial y = w_p s_o - w_n S/h \qquad 4.2$$

$$\partial U/\partial t+\partial(U^2/h)/\partial x+\partial(UV/h)/\partial y+\partial(g'h^2/2)/\partial x-fV$$
$$+KU_R (U_R^2+V_R^2)^{1/2}/h^2+h\partial(A\partial(U/h)/\partial x)/\partial x$$
$$+h\partial(A\partial(U/h)/\partial y)/\partial y = u_o w_p - (U/h)w_n - gh\partial\zeta/\partial x \qquad 4.3$$

$$\partial V/\partial t+\partial(UV/h)/\partial x+\partial(V^2/h)/\partial y+\partial(g'h^2/2)/\partial y+fU$$

$$+KV_R(U_R^2+V_R^2)^{1/2}/h^2+h\partial(A\partial(V/h)/\partial x)/\partial x$$

$$+h\partial(A\partial(V/h)/\partial y)/\partial y = v_o w_p -(V/h)w_n -gh\partial\zeta/\partial y \qquad 4.4$$

where

U,V are vertically integrated transports for the upper layer (cm^2/s),

$g'=g\Delta\rho/\rho$, the specific gravity (cm/s^2),

A= horizontal eddy viscosity (cm^2/s),

ζ= barotropic tidal elevation (cm),

S= vertically integrated salinity (cm(o/oo)),

u_o, v_o= tidal streams (cm/s),

U_R, V_R = relative transports =$U-u_oh$, $V-v_oh$ (cm^2/s),

K= quadratic friction coefficient,

w_p = entrainment velocity (cm/s),

w_n = depletion velocity (cm/s),

s_o= constant salinity of the water underneath the plume (o/oo),

h= plume thickness (cm),

f= Coriolis parameter (sec^{-1}).

This system of equations was solved for h,U,V and S. Reflecting the strong dependence of density on the salinity of the plume water, an empirical equation of state was used:

$$g' = 24.0-(0.8S/h). \qquad 4.5$$

The entrainment velocity took the final form:

$$w_p = 0.0001(U_R^2+V_R^2)^{1/2}/h. \qquad 4.6$$

This expression was similar to the one given by Keulegan (1966) for the arrested salt wedge entrainment:

$$w_p = 0.000212\ (u-u_c) \qquad 4.7$$

where u_c for the Fraser river is about 3 cm/s (Cordes et al., 1980). This was a departure from a suggested expression for the entrainment velocity that included a dependence on the local Richardson number (Ellison and Turner, 1959). The depletion velocity (the vertical velocity associated with the water going from the plume to the bottom layer) was introduced to thin the plume in the outer regions (away from the Fraser River mouth). This velocity was then made dependent on the salinity through the expression:

$$w_n = (1-\exp(S/(10h)))h/200 \qquad 4.8$$

This expression had no observational or theoretical support. It was the result of a suspected dependence of the depletion on the stratification in the outer regions and of various modelling tests introducing this term (Stronach, 1977). The terms with K in the momentum equations (4.3 and 4.4) are intended to model the interfacial friction. K took values from 0.001 to 0.007. The wind stress was neglected in the model. The horizontal eddy coefficient (A) used varied from 10^3 to 10^4 cm^2/sec. The flow at the open boundaries was governed by the

constraint:

$$\partial^2 F^2/\partial n^2 = 0, \qquad 4.9$$

namely that the second derivative of the Froude number squared ($F^2=U^3/g'h^3$) normal to the boundary was to be zero. Various boundary conditions have been tried (Stronach, 1977) but this one has the advantage of allowing the flow to reverse at the boundaries. The salinities at the open boundaries were extrapolated from the neighboring inside grid points. These boundary conditions were put forward on the argument of slowly varying conditions far from the Fraser River mouth. The solid boundaries required no flow normal to them.

The main concern of this model was the effect of the tidal forcing and for this reason it was never run for more than 24 to 48 hours. Velocities and salinities were initially set to zero everywhere while the initial plume thickness was set to 150 cm.

5.2 General Modifications Of The Existing Model

The main purpose of a modelling effort in the context of this research is to relate variations of the observed "ferry" salinities to the effects of physical dynamical processes that can be quantified. As seen in the previous chapters, the ferry data most accurately define long-term variations while the tidal fluctuations are only marginally resolved. The computing effort should then emphasize the long-term variations due mainly to discharge and wind. This implies running the model for periods on the order of 10 to 20 days. In order to reduce computer cost, it was decided to sacrifice spatial resolution to a

limited extent. The grid size was increased from 2km to 3 km. This grid size still respects the stability criteria given in the appendix of Stronach's work (1977) and allows a minimum of resolution for the plume property distributions. Similarly, the area covered by the model was reduced to a minimum, namely enough to include the two ferry sections (Fig. 20). The effect of the positions of the open boundaries was investigated by running a preliminary windless model with one or two supplementary grid rows beyond the southeast and northwest ends of the model. The present positions of the open boundaries (Fig. 20) seem to leave the salinities near the ferry sections unaffected within the limit of the measurement error. The first model-geometry to be used included Boundary Bay that was located in the lower right corner of Fig. 20. It was decided to delete it from the modelling area because of computational instability arising from the open boundary conditions when a southerly wind was acting. Another solution to that problem could have been to move the southern open boundary even farther away from the river mouth but this model would have been more costly to run.

No water was allowed to go over the shallow sand flats on the south eastern side of the river mouth. The orientation of the grid points relative to the map of the Strait of Georgia was decided by aligning the southern ferry section with a row of grid points. The set of coordinates used for the numerical model is indicated in Fig. 20. This set of coordinates was used by Stronach (1977). It should be noted that this set differs from the set of coordinates defined in the previous

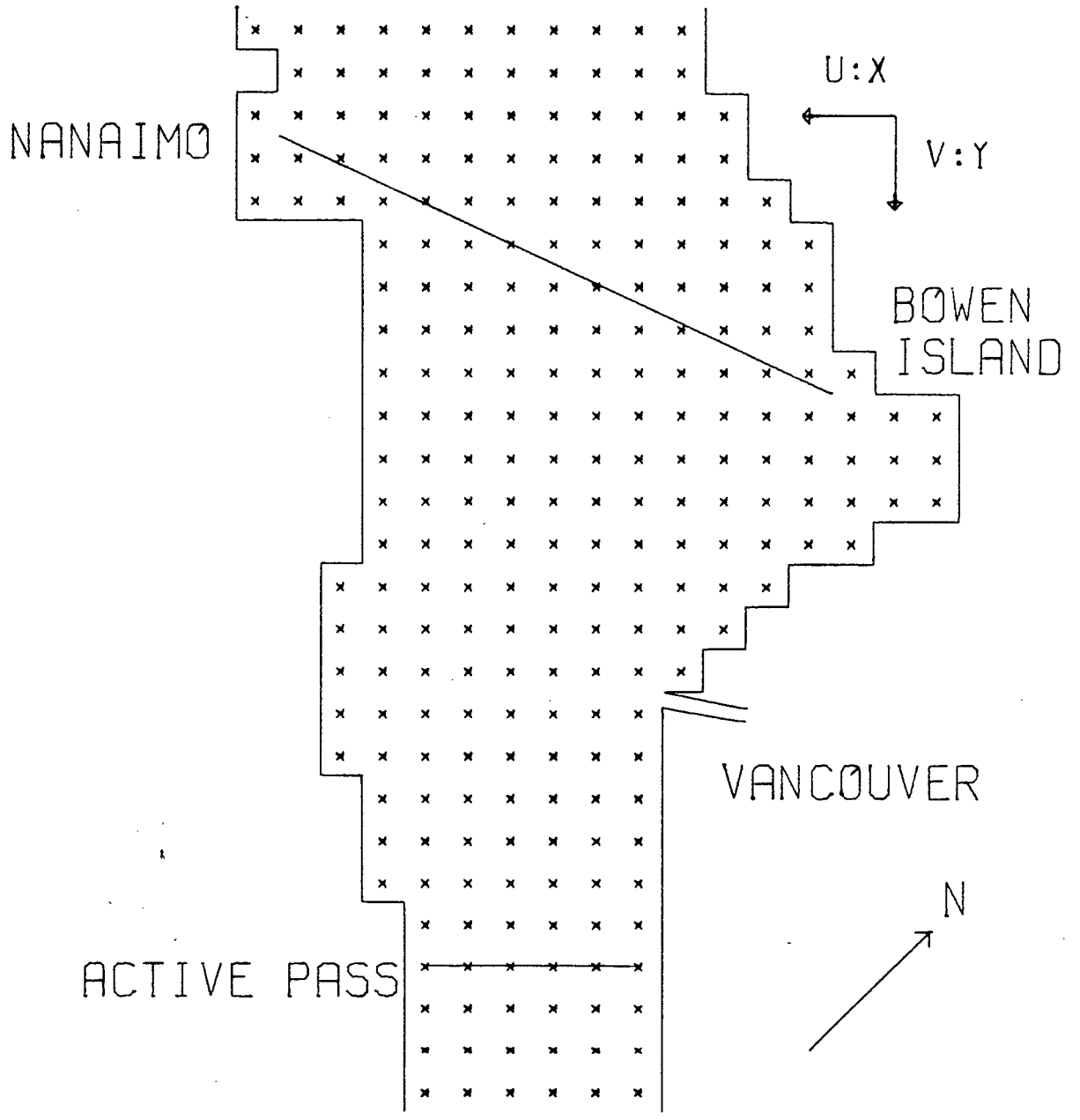

Figure 20 - Grid used by the numerical model showing the two ferry tracks and the set of coordinates used

chapters; it is rotated by 183° relative to the former. Stronach's set of coordinates was only used internally, within the framework of the model and I shall hold for the rest of the

discussion to the earlier convention.

Special care was given to the initial fields of h,U,V and S. It was felt that they should be as close as possible to "realistic" fields to avoid transient states. These initial fields should characterize the general horizontal distributions for the starting day. They were obtained by running the model with a constant river discharge of 4130 m^3/sec from constant fields (U=V=0 cm/sec, S=15 o/oo·150 cm and h=150 cm everywhere) until a steady state was reached. No tidal forcing was present in this spin-up model, meaning that the bottom layer was at rest and the tidal slopes were null. Otherwise, Stronach's model was left intact with A and K given values of 10^3 cm^2/sec and 0.001 respectively.

The distributions of salinity and velocity obtained from this spin-up model are shown in Fig. 21. They are to be used as initial conditions for further models. The action of the Coriolis force is quite evident in pushing the plume towards the northern section. From these steady state fields, the model is then run with slowly varying discharge and wind. The discharge is interpolated linearly at each time step (every 2 minutes) between the daily values monitored at Mission City starting on a day when the discharge is 4130 m^3/sec. The wind, that was set to zero during the spin-up, is brought back into the momentum differential equations at the same time as the discharge is allowed to vary slowly. The term responsible for the wind in the equations comes from the parametrization of the surface stress, a term previously neglected in Stronach's work (1977).

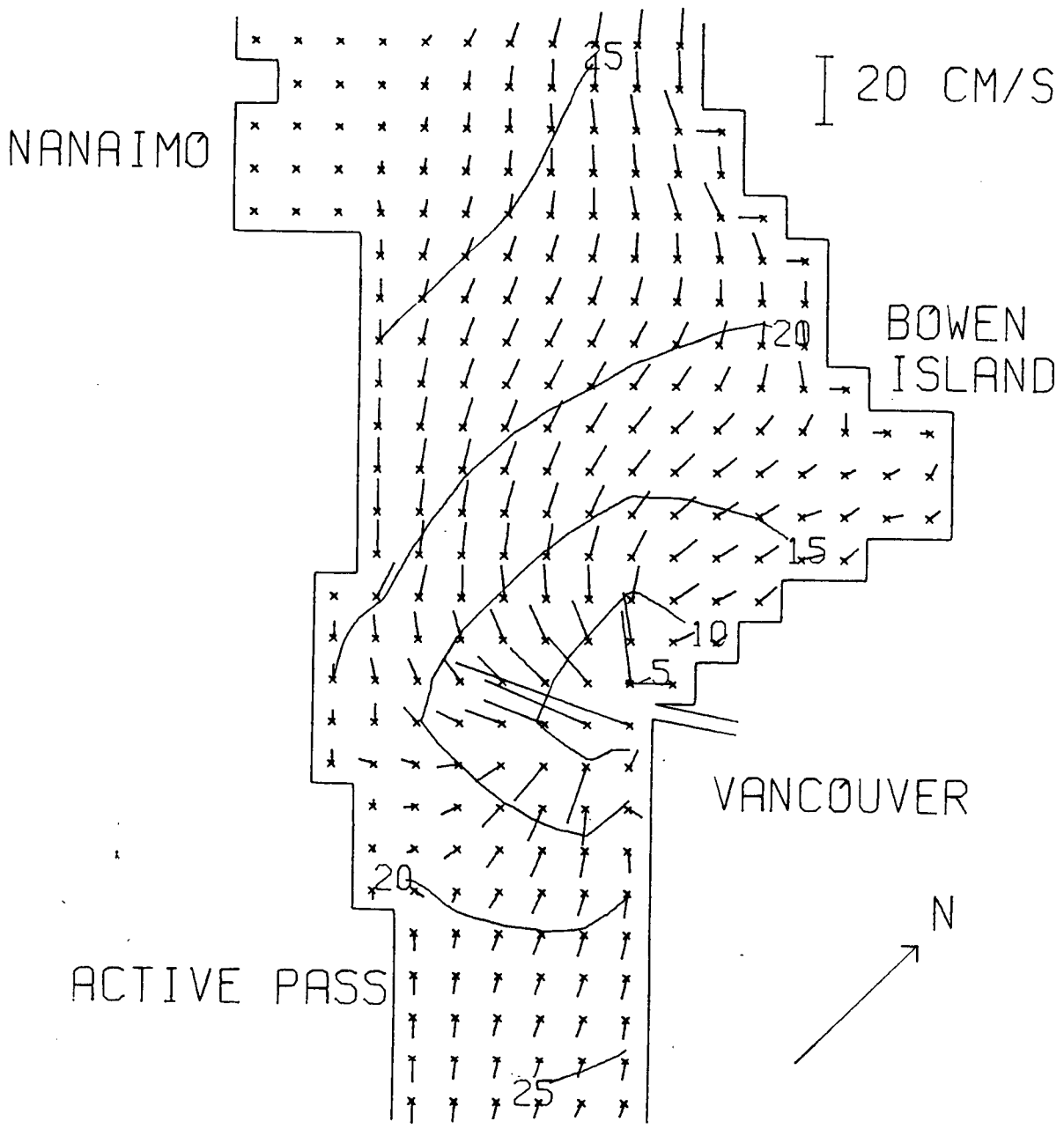

Figure 21 - Distributions of velocity and salinity used as initial conditions. The salinity contour labels have unit of o/oo and the tail of the velocity vector is located on the corresponding grid point

A few steps before getting equations 4.1 to 4.4, a term like:

$$(1/\rho)\int_{z=\xi}^{\eta}(\partial\tau_x/\partial z)dz \qquad 4.10$$

was present on the right hand side of the x-momentum equation (Stronach,1977). The surface elevation is denoted by η and ξ describes the position of the interface. This stress term can then be written as

$$(1/\rho)((\tau_x)_{z=\eta} - (\tau_x)_{z=\xi}) \qquad 4.11$$

The term $-(1/\rho)(\tau_x)_{z=\xi}$ was parametrized by the expression $-KU_R(U_R^2+V_R^2)^{1/2}/h^2$. The wind stress $((\tau_x)_{z=\eta}/\rho)$, that was neglected previously, will be replaced by the similar driving expression:

$$(C_D\rho_a/\rho)u_w(u_w^2+v_w^2)^{1/2} \qquad 4.12$$

where

u_w, v_w are the wind components in the coordinate system of the model,

ρ_a/ρ is the ratio of the air and water density (0.0013) and

C_D is the drag coefficient.

Similarily, a term like:

$$(C_D\rho_a/\rho)v_w(u_w^2+v_w^2)^{1/2} \qquad 4.13$$

is added on the right side of the y-momentum equation. The drag

coefficient has been evaluated on an open ocean stretch (Large and Pond,1981):

$$C_D = 0.0012 \quad \text{if} \quad 4<U10<11 \text{ m/sec}$$

$$C_D = 0.001(0.4+0.065\ U10) \quad \text{if} \quad 11<U10<25 \text{ m/sec} \qquad 4.14$$

where U10 is the wind speed 10 m above the sea surface. For lack of better wind measurements U10 will be substituted for the wind speed measured at Entrance Island wind station. The choice of using Entrance Island wind data instead of Sand Heads wind record should not affect the results significantly since the two data records are highly correlated for the long-term variations. Hourly wind data for each component were interpolated linearly at each time step.

In the course of running the model, the open boundary condition for the salinity along with the high velocities at the boundaries due to the wind produced upper layer salinities larger than the salinity of the bottom layer. Specifying a null first derivative of the salinity normal to the open boundary got rid of this instability.

Comparison between the output of the model and the ferry observations requires some syntheses of the salinity variations near the ferry sections. As before the average salinity along a ferry section would seem to be the appropriate characteristic for each section. An equivalent average salinity for the southern section is computed as the arithmetic average of the salinity at grid points along that section. For the northern section, fourteen values of salinity along the section are

interpolated from the surrounding grid points. These values are then arithmetically averaged to give an equivalent average salinity for the northern section. The possibility of comparing the horizontal salinity gradient was briefly investigated but the poor resolution of the numerical model along each section greatly underestimates the value of the salinity gradient. The observed magnitudes of the salinity gradient are also more scattered than the salinity measurements.

5.3 Numerical Results With Variable Discharge And Wind Forcing

With a mind to computational cost, periods with significant changes in salinity on intervals of a few days should be of more interest than slowly varying salinity. It was mentioned in chapter 3 that the increase in discharge in the spring leads to rapid salinity decreases while the decrease from that peak is somewhat slower and so are the variations in salinity. For this reason, the emphasis was put on modelling the rapid decrease of salinity in the springs. The periods to be modelled correspond to two of the cases already discussed in section 3.4, essentially the periods from Julian days 119 to 139 and from Julian days 496 to 526 for the spring of 1980 and 1981 respectively. The abnormal December Peak discharge also received modelling attention. All of these three cases started on a day when the value of the river discharge is close to 4130 m^3/s. The same initial field described in the previous section, was used for the three simulations.

As seen in section 3.4 the combined effects of the wind and

the discharge can qualitatively explain the daily variations of the average salinities. Thus the first modelling effort was to input the discharge and the wind into the model leaving out the tidal forcing. Here it was assumed that most of the tidal effect is averaged out over the period of a day. In other words, the fluctuations of salinity due to the tides oscillates about a mean set by the conditions of the discharge and the wind. A limited model which includes the tides will be the subject of the next section.

5.3.1 Comparison Of The Average Salinities

The average salinities from the ferry data are compared (Figs. 22 and 23) to the equivalent average salinities from a model that differs from the spin-up model only in that it includes variable wind and discharge. The first case (Spring 1980) became unstable at Julian day 123 and is not shown. It happened right after a period of high northerly wind (the strongest along-strait wind in the three periods studied, (Fig. 12)) that induced plume velocities on the order of 1 m/s. High values of entrainment of salt from the bottom layer follow via the direct proportionality of w_p on the plume velocities. The model stopped running because the salinity near the northern section got beyond the salinity of the bottom layer, inducing rapidly growing instabilities. Such a problem did not occur for the two other cases (Figs. 22 and 23). Nevertheless, the same process of overestimating the salinity of the plume occurred. This is especiallly true for salinity along the northern

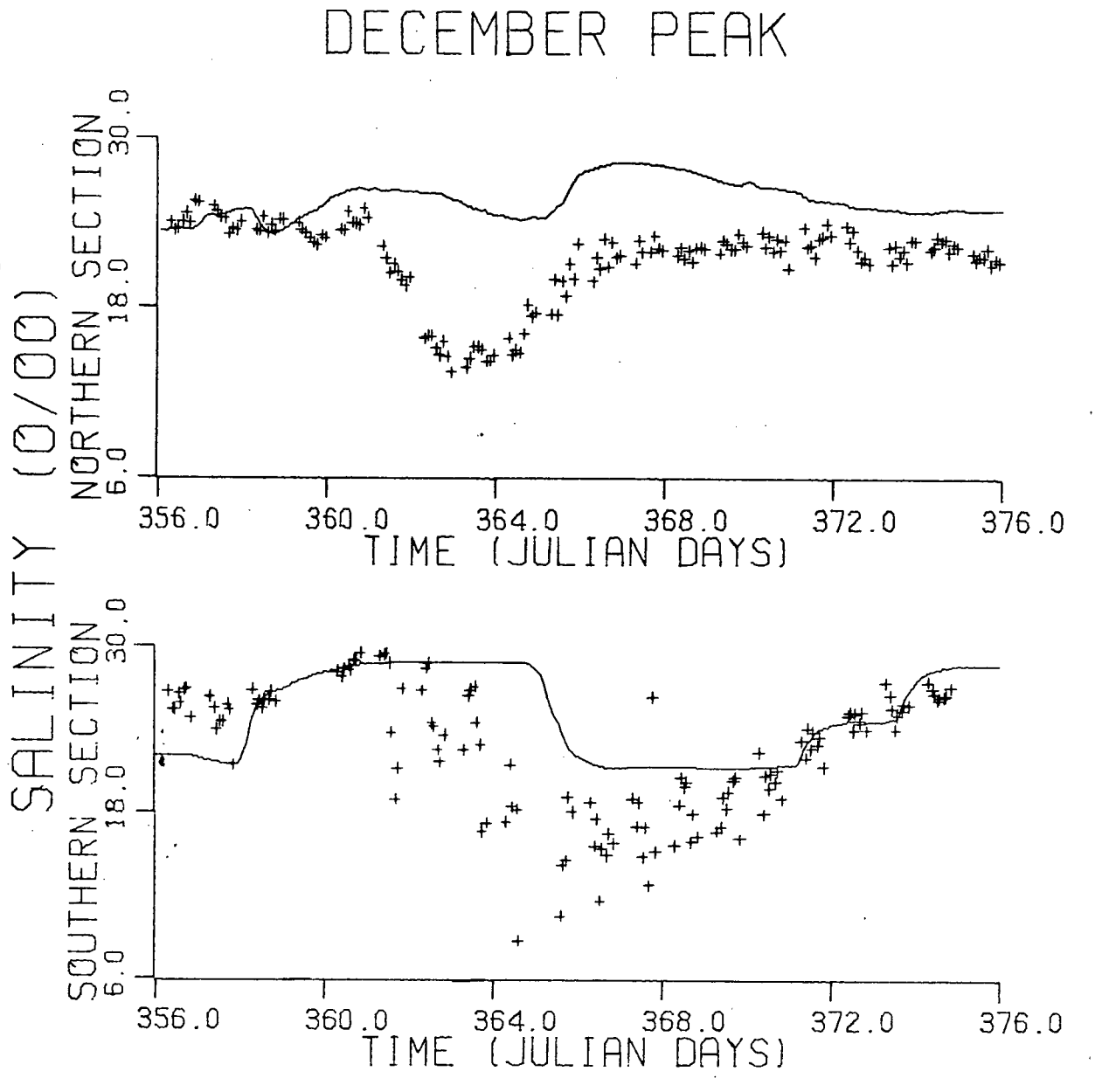

Figure 22 - Plots of the average salinity ferry data (crosses) and modelled average salinity (solid line) vs time for the December Peak using a model similar to the one of Stronach but with variable wind and discharge and no tidal forcing

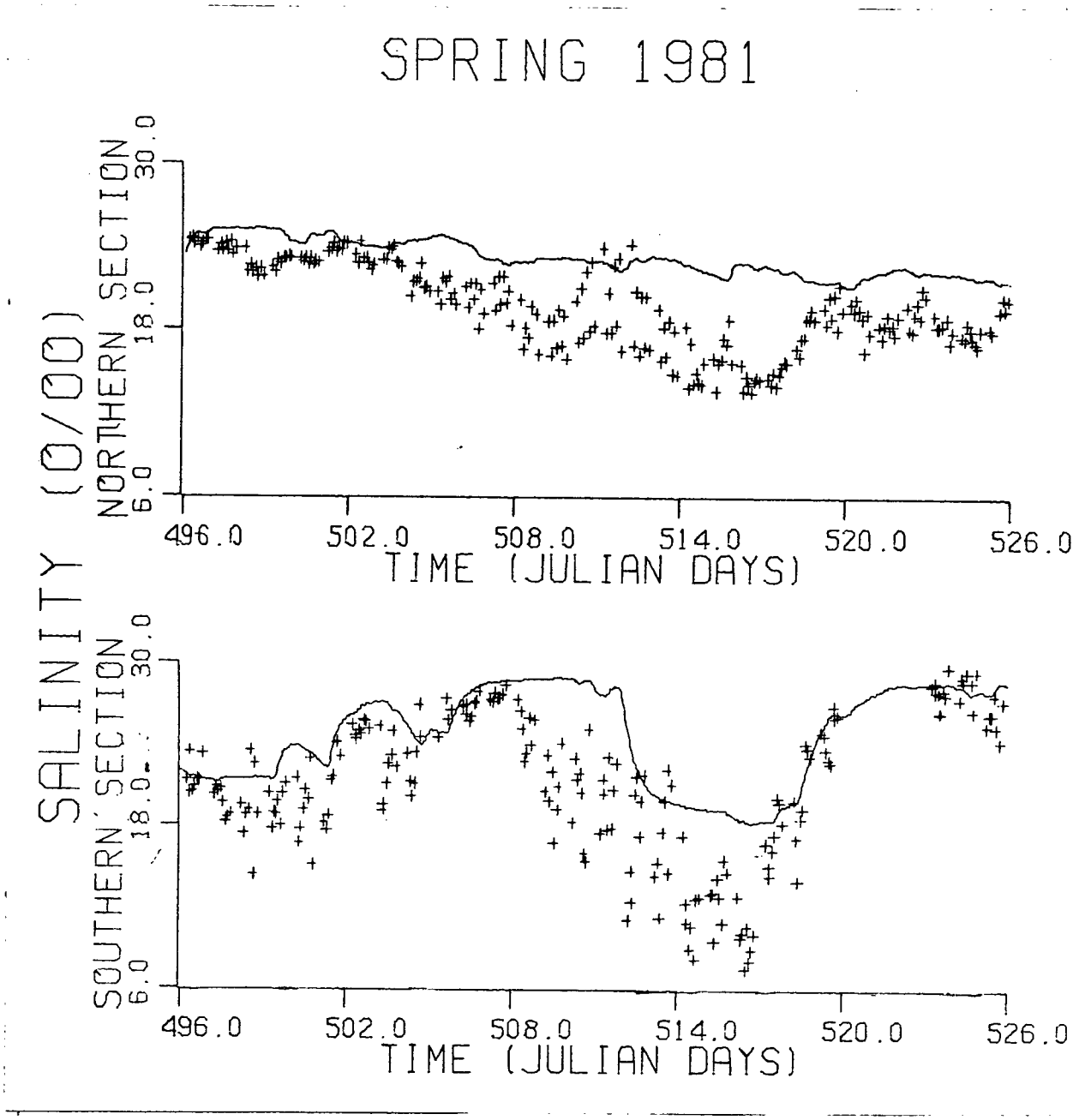

Figure 23 - Plots of the average salinity ferry data (crosses) and modelled average salinity (solid line) vs time for the Spring 1981 using a model similar to the one of Stronach but with variable wind and discharge and no tidal forcing

section. No wind or discharge effects are clearly visible in the variation of the model salinity on that section. For the southern section, the situation is much better. Overestimation of the salinity still occurred but to a lesser extent. The wind more than the discharge seems to dictate the variations of the salinity on the southern section. The rise of salinity from Julian days 502 to 503, 506 to 512, 518 to 524, 358 to 364 and finally from 372 to 376 are all associated with southeasterly winds (Figs. 13 and 14). Inversely the drops in salinity occurred during northwesterly winds. Advection due to the wind can explain these effects on the model salinity.

Clearly the model, as it is, overestimates the flux of salt into the plume. This salt can come from the bottom layer or be advected laterally through the open boundaries. The latter source of salt is not thought to be the major one because of the special form of the open boundary condition for salt. The advected salt from outside of the modelling area was set to equal the salinity just inside the open boundary. The major source of salt must then be the bottom layer. The salt is brought in the plume via the entrainment velocity that depends on the plume velocities that are themselves greatly affected by the wind.

Another conclusion resulting from the analysis of Figs. 22 and 23 is that the effect on the model of the varying discharge is minimal. The annual discharge pattern is too obvious in the observed variations of the average salinity (ref section 3.1) to be neglected, especially in the case of the December Peak for

which the abnormal drops in salinity are without a doubt due to high discharge. The model inputs the variation of the discharge through variations of the velocity and depth of the layer at the river mouth using the hypothesis that there the Froude number is one. The effect of an increased discharge of fresh water is partly erased by the increase in entrainment due to the velocity increase at the mouth. The December Peak case was run without wind input and on both sections, a drop of only 1 to 2 o/oo resulted from the sharply varying discharge.

The necessity of decreasing the entrainment velocity and providing more response to the discharge suggested a change to an entrainment velocity that depended on the stratification. Numerous studies (Long 1975 and 1978) and experiments in water tanks (Wu, 1973; Kato and Phillips, 1969; Kantha, Phillips and Azad, 1979) and under natural conditions (Kullenberg, 1977) tend to show a dependency of the entrainment on an overall Richardson number R_{i*} defined as

$$R_{i*} = g'h/u_*^2 \qquad 4.15$$

where u_* is the friction velocity. Some of the above papers suggest the expression:

$$w_p = Cu_* R_{i*}^{-1} \qquad 4.16$$

but it is questionable in the light of the more recent results of Kantha et al. (1977). The problem in using this expression is the evaluation of the friction velocity and its

relation to the cause of the turbulence. McClimmans (1980) listed sources of turbulent entrainment in plume. Wu (1973) and Kullenberg (1977) relates u_* to the wind stress but, near the river mouth, winds of the order of 100 km/hr would be needed to produce the measured entrainment (Cordes et al., 1980). If the entrainment is shear generated, u_* could be proportional to the velocity difference between the two layers as was done in Long (1975) assuming a critical flux Richardson number. Under this assumption, the entrainment depends on $g'h^3/U^3$, that is the inverse of the Froude Number squared, and the entrainment takes the form:

$$w_p = C_1 u (F^2)^n \qquad 4.17$$

where n has the value of 1. Several runs of the model for the December case were performed varying the positive exponent n. All of them failed to model the expected drop in salinity. Stronach (1977) had also noticed the failure of this expression that made the entrainment a function of the plume velocity to the power 3. A more direct dependence on the stratification was then tried using the expression:

$$w_p = 0.0001\ (U/h)\ (s/s_o)^r \qquad 4.18$$

where s is the salinity of the plume and r, an exponent to vary the dependence of w_p on the stratification. With r = 0, Stronach's expression for the entrainment velocity is recovered. The factor $(s/s_o)^r$ is always smaller than one and entrainment

values near the mouth are lower than in the far field. The introduction of this reducing factor is also consistent with the overall trend that can be seen in the entrainment coefficient of Cordes et al. (1980) according to which high ratios w_p/u are found at small salinity differences between the upper and lower layers. This expression of entrainment with r=0.75 used in a model of the December case with variable discharge, but no wind, induced a drop of salinity on the northern section of the right order of magnitude (10 o/oo). Subsequently, it was found that the drop was mainly caused by the transition between the steady state obtained with Stronach's expression to the one with reduced entrainment due to stratification. No increase in the discharge was needed to produce the drop in salinity and the fall in salinity started on the first day (356) instead of on day 361 as shown by the ferry data.

A change in the expression of the entrainment was needed to produce the expected drop which should be related to changes in the conditions of the forcing on the plume. It is suggested that the discharge could be the related forcing parameter that changes the overall effect of the stratification on the mixing and entrainment of salty water in the plume by default of a more local parameter. It should be remembered that the salinity factor in eq. 4.18 mostly affects the area near the river mouth. At a medium discharge, like the one used to get the steady state, we want the entrainment to depend weakly on the stratification and change to depend strongly on the stratification at high discharge. This is done by making the

exponent r in the expression of the entrainment (eq. 4.18) a function of the discharge. To avoid a sudden transition from the steady state fields obtained with Stronach's entrainment r will be set to zero for a discharge of 4130 m^3/s. The simplest function to use is a line:

$$r = (D-4130)/C_2 \qquad 4.19$$

where D is the discharge in m^3/s. The constant C_2 has been determined by running the spring 1981 model and trying to obtain the general trend of the northern section salinity decrease. A cut-off discharge was necessary to stop the salinity from decreasing even further. Finally, the expression for the entrainment exponent,

$$\begin{aligned} r &= 0 \quad \text{if} \quad D \leq 4130\ m^3/s, \\ r &= (D-4130)/2000 \quad \text{if} \quad 4130 \leq D \leq 5130\ m^3/s, \\ r &= 0.5 \quad \text{if} \quad D \geq 5130\ m^3/s, \end{aligned} \qquad 4.20$$

was used in the run for which the average salinities are compared with the Ferry data for the Spring 1981 in Fig. 24. The reduced entrainment mainly affects the general decrease of the salinity on the northern section. For the southern section, a more important drop in salinity between Julian days 513 and 519 is noticed if compared to the results in Fig. 23. In spite of these improvements, the general overestimation of the salinities still remains. If this expression for the entrainment velocity is applied to the December Peak case with wind input, no significant changes are observed from the results in Fig. 22. The spring 1980 case still stopped running after 5 days, just after the period of high winds. The reduced

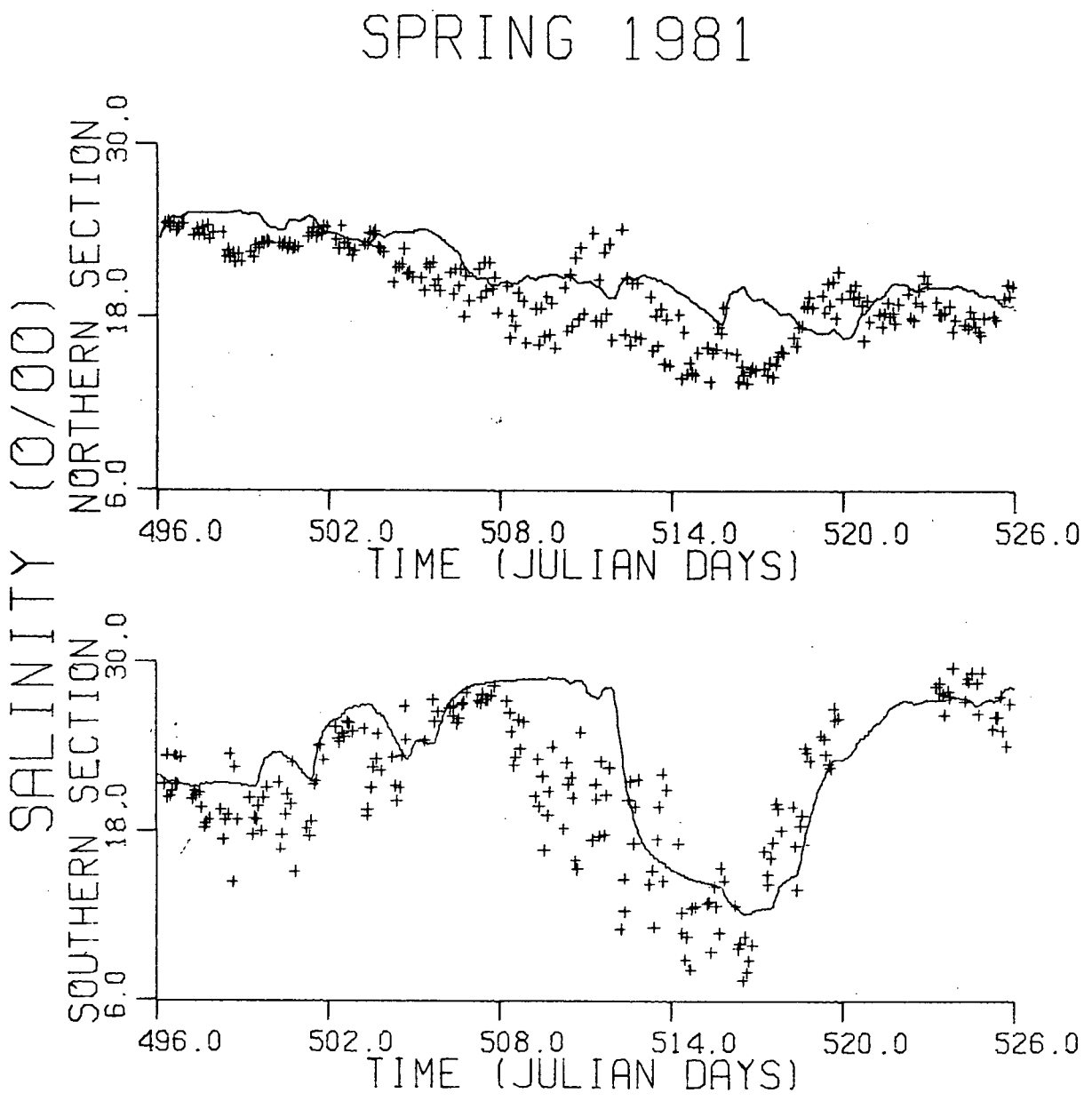

Figure 24 - Plots of the average salinity ferry data (crosses) and modelled average salinity (solid line) vs time for the Spring 1981 using a model similar to the one leading to Fig. 23 but with reduced entrainment velocity

entrainment did not help in eliminating the instabilities. This result should have been expected since they occur due to large entrainment in regions of high salinity for which the new expression of entrainment does not change anything.

The solution was found in the modification of the effect of the source of salty water entrainment i.e. the wind. A first improvement was achieved by reducing the wind input for regions of high salinity. The reason behind this change, is that for plume water with salinity close to 29 o/oo, the plume water cannot be differentiated from the bottom layer water. It was assumed so far that the wind momentum transfer is uniformly distributed in the upper layer, but in a poorly stratified situation one can imagine that the wind action could extend beyond the plume thickness so that the plume itself only gets a fraction of the momentum input from the wind. This modification is achieved by arbitrarily multiplying the drag coefficient by a factor (F_1) which depends on the salinity and goes to 0 when no stratification is present. A smoothed transition is included from a salinity of 25 o/oo and over. The general expression used for this factor is

$$F_1 = b \quad \text{if} \quad s \leq 25 \text{ o/oo}$$

$$F_1 = b - b(s-25)/4 \quad \text{if} \quad 25 \leq s \leq 29 \text{ o/oo}. \qquad 4.21$$

The instabilities for spring 1980 vanish with the introduction of this factor with b=1. The results for this case with Stronach's entrainment expression and with the reduced entrainment of equation 4.18 are displayed in Figs. 25 and 26, respectively. The two sets of curves are not qualitatively much

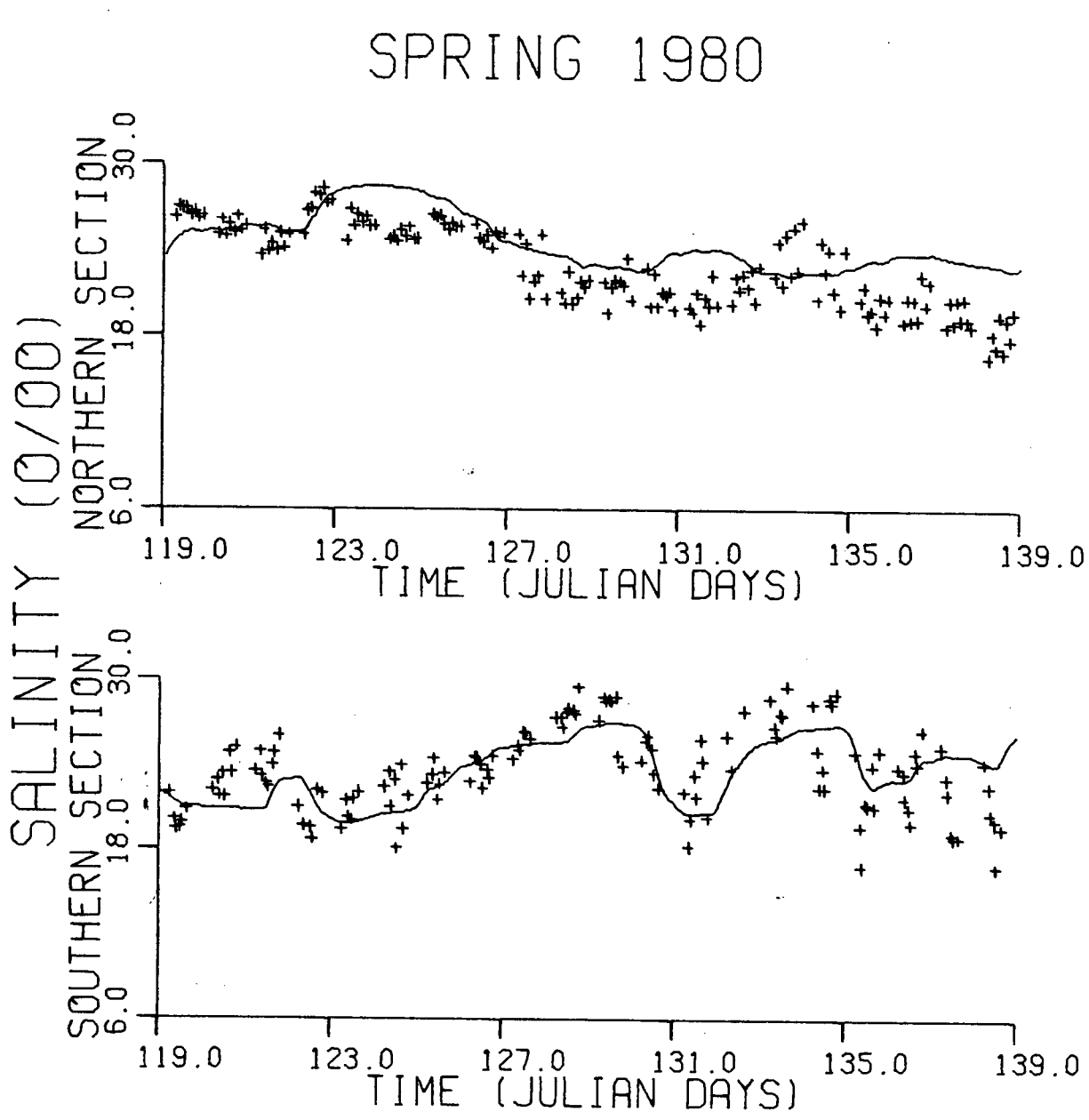

Figure 25 - Plots of the average salinity ferry data (crosses) and modelled average salinity (solid line) vs time for the Spring 1980 using a model with the entrainment velocity of Stronach and a reduced wind factor (b=1.)

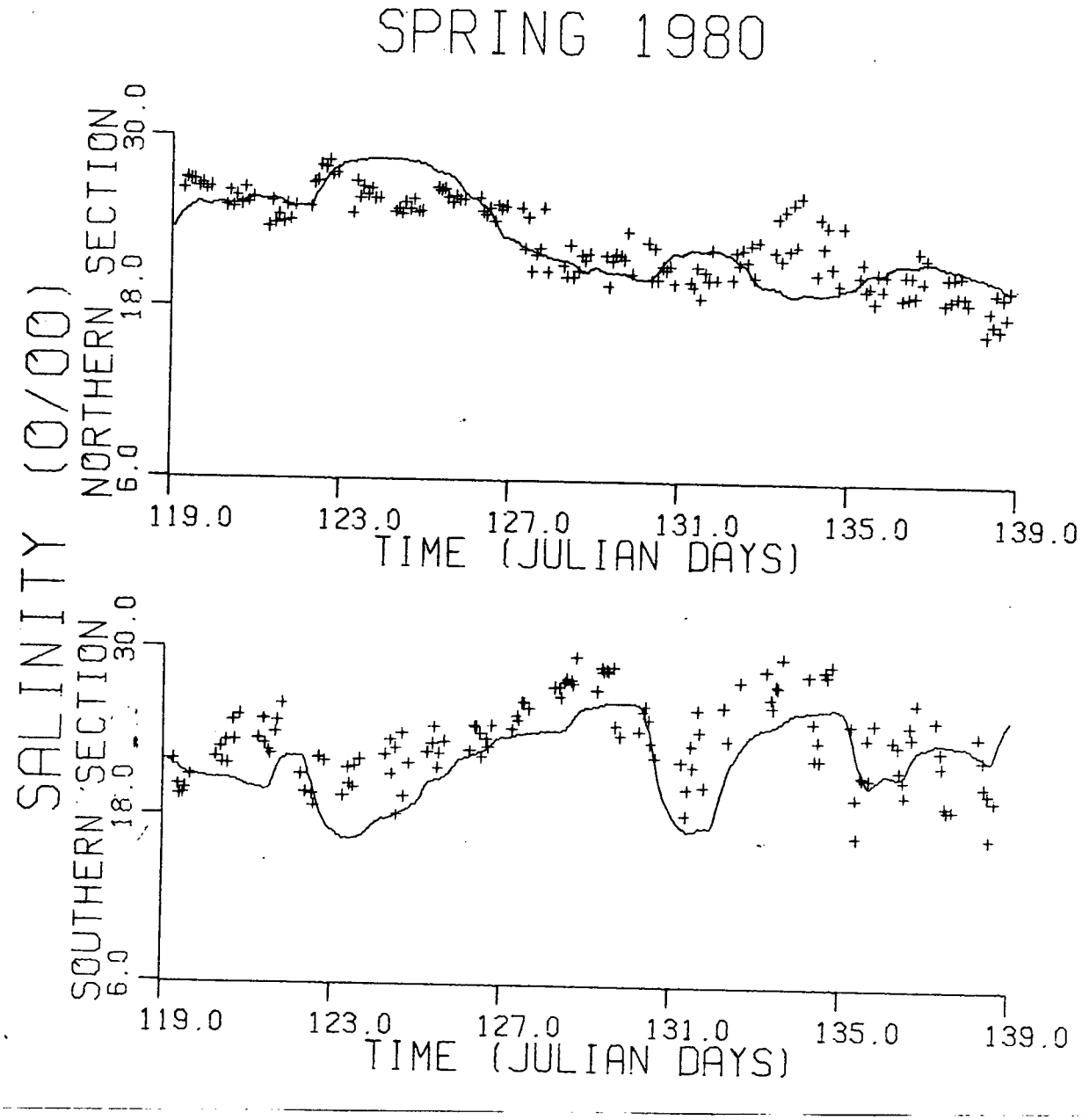

Figure 26 - Plots of the average salinity ferry data (crosses) and modelled average salinity (solid line) vs time for the Spring 1980 using a model with a reduced entrainment velocity and a reduced wind factor (b=1)

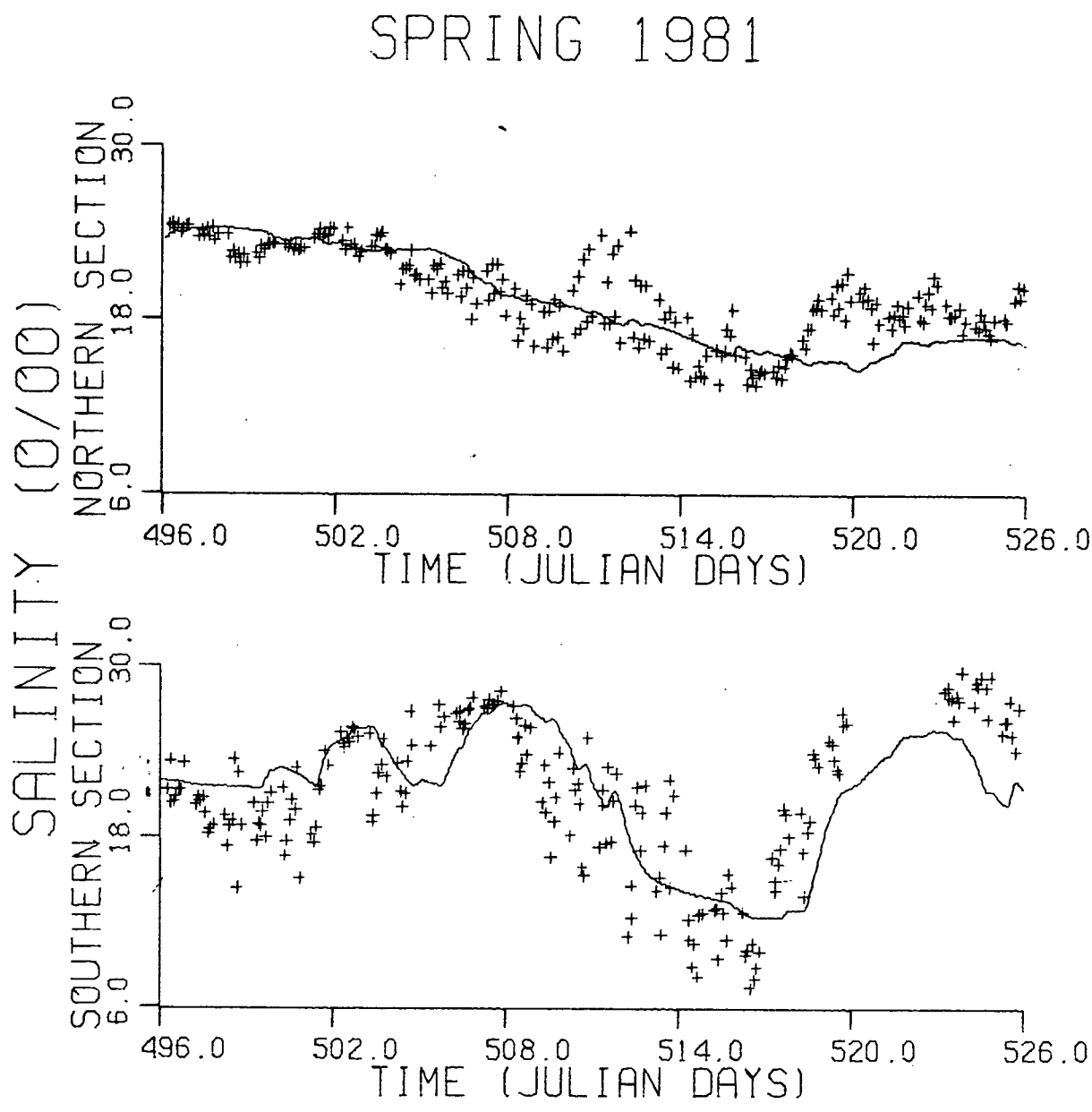

Figure 27 - Plots of the average salinity ferry data (crosses) and modelled average salinity (solid line) vs time for the Spring 1981 using a model with reduced entrainment velocity and with a reduced wind factor (b=0.5)

different from each other. The first expression of entrainment leads to a better comparison on the southern section than with reduced entrainment while the decreasing trend of salinity on the northern section seems best reproduced when the reduced entrainment is used. Both model runs fail to explain the secondary fluctuations (like the peak between Julian days 133 and 135) that are superposed on the general trend of the northern section salinity. This was also noticed for the Spring 1981 case (Fig. 24). The peak in salinity on the northern section between day 510 and 513 never appears to be modelled. These fluctuations might not be wind related. On the other hand, the model salinity on the southern section responds strongly to the wind input. The southeasterly wind during periods 125-129 and 131-134 are associated with the rise of the salinity and the drops in salinity correspond to the onset of northwesterly winds.

If the Spring 1981 case is run using the reducing factor F_1 with b=0.5 (Fig. 27), the overestimation of salinity on the southern section is reduced, especially between Julian days 508 and 513. The salinity trend on the northern section agrees better than in Fig. 24.

A "b" equal to 0.125 for the wind factor in the December Peak is necessary to achieve the agreement in Fig. 28. Again the overestimation of the southern section salinity between Julian days 361 and 366 is definitely eliminated by reducing the wind effect. The salinity drop on the northern section is modelled to some extent. An even lower entrainment velocity

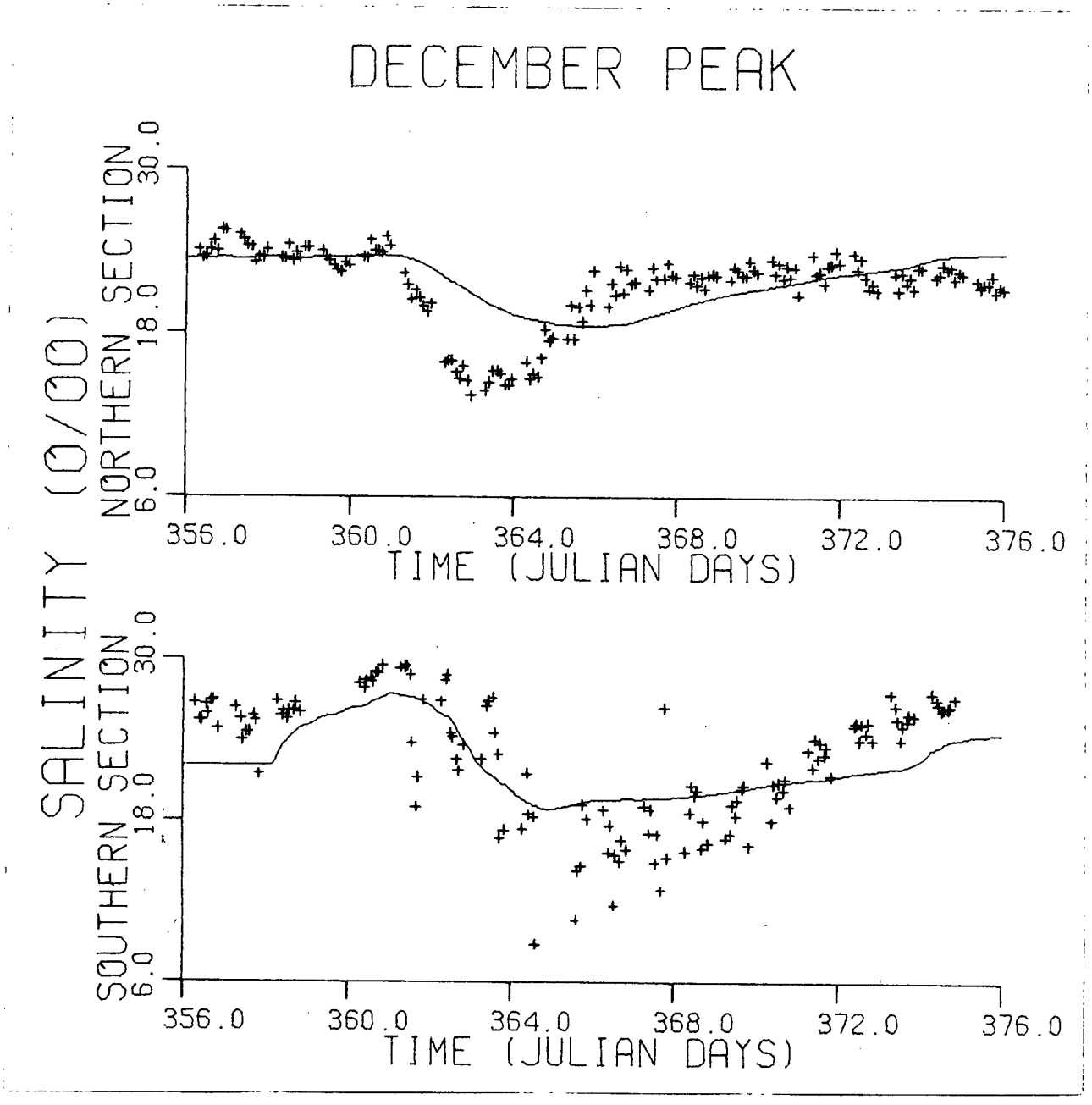

Figure 28 - Plots of the average salinity ferry data (crosses) and modelled average salinity (solid line) vs time for the December Peak using a model with reduced entrainment and with a reduced wind factor (b=0.125)

(for example with an exponent r=0.75) would be needed to simulate a drop of 10 o/oo, but the slow increase of the model salinity would still be present. The fact that the December Peak case needs a lower wind factor than the two Spring cases can be explained by remembering that during the winter wind storms destroy the stratification and more well mixed water is present than during the spring.

In trying to find the best exponent r to use in the entrainment expression, the northern section salinities were relied on because the southern section salinities were not as sensitive to changes in the entrainment velocity due to discharge fluctuations. On the other hand, the values of the coefficient b in the wind factor F_1 were found using the southern section salinities because the northern section salinities did not respond as strongly to changes in the wind factor. This seems to be in agreement with an observation made in section 4.1 according to which higher correlations between the salinity and the discharge were found on the northern section relative to the southern section while smaller correlations between the wind and the average salinity were computed on the northern section as compared to the southern section.

5.3.2 Quantitative Estimate Of The Agreement Between The Model And The Ferry Observations

The qualitative agreement between the model and the ferry measurements will be quantified in this subsection using cross-correlations between the daily average salinities (model and ferry data) and the root mean square (RMS) error between the two series. The model daily average salinity is obtained from hourly values averaged with the same filter as all other daily average estimates, namely a 48-hr Bartlett filter.

Table X summarizes the cross-correlation results for the different model runs. These are separated into three types: those with the unchanged wind and entrainment expressions, those with reduced entrainment and thirdly the ones with reduced wind and entrainment factors. The classification for the Spring 1980 case differs slightly in that all successful runs required a reduced wind input at high salinity. The two runs are then classified under the entrainment expression used. No further reduction of the wind was judged necessary for the Spring 1980 case, so that no results appear for the change of wind factor.

The first conclusion to be drawn from Table X is that the southern section is better described by the model than the northern section. This could simply be due to the fact that the southern section is closer to the Fraser River mouth and so under a more direct influence of the plume than the northern section for which other mechanisms or fresh water inputs could become important. A change in the entrainment expression does not seem to influence the correlation for the southern section

Table X - Cross-correlations and time lags between the average salinities of the model and of the ferry data

	Model with Stronach's entrainment and wind factor equal to 1	Model with reduced entrainment and wind factor equal to 1	Model with reduced entrainment and reduced wind factor
Spring 1980			
Southern section	0.84 at day lag 0	0.84 at day lag 0	the same as the model with a wind factor equal to 1
Northern section	no sig. correlation	no sig. correlation	
December Peak			
Southern section	0.68 at day lag 2	0.69 at day lag 2	0.83 at day lag 0
Northern section	no sig. correlation	no sig. correlation	0.83 at day lag 2
Spring 1981			
Southern section	0.85 at day lag 0	0.85 at day lag 0	0.89 at day lag 0
Northern section	no sig. correlation	0.67 at day lag 2	0.71 at day lag 1

salinities while a change in the wind expression has the potential of slightly increasing the correlation coefficient and improving the time lag which should be equal to 0 in the case of perfect agreement. The poor correlation encountered in the case of the northern section salinity can be attributed to the preliminary detrending of the time series previous to the cross-correlation computations. Previous qualitative agreement (ref section 4.3.1) between the average salinities (model and ferry data) could have come uniquely from the general trend, that same

Table XI - Root mean squared error (o/oo) between the model and the ferry data average salinities

	Model with Stronach's entrainment and wind factor equal to 1	Model with reduced entrainment and wind factor equal to 1	Model with reduced entrainment and reduced wind factor
Spring 1980 Southern section	1.30	2.68	the same as the model with a wind factor equal to 1
Northern section	1.97	1.68	
December Peak Southern section	5.61	5.49	3.06
Northern section	5.65	5.43	2.41
Spring 1981 Southern section	4.43	3.37	2.15
Northern section	4.12	2.22	1.73

trend that is lost during the detrending procedure. In other words, the good agreement in the northern section salinity trends can not be revealed by the cross-correlation coefficients. The effect of the reduced entrainment is seen to produce a significant correlation for the Spring 1981 northern section salinity. Even further improvement in the correlation and phase is achieved by reducing the wind by a factor of two for that spring case. For the December Peak, the introduction of a reduced wind definitely improves the correlations for both

sections. The effect of the reduced entrainment was masked by high wind effects. When these are reduced, changes in the entrainment expression can be shown to mostly affect the northern section salinity.

Cross-correlations only investigate the possible relation between the fluctuations of the two time series and disregard the amplitude of the fluctuations and the absolute values of the elements in the series. Table XI looks at the root mean square error between the model and the observed data. Successive improvements in decreasing the RMS error are achieved by introducing a reduced entrainment followed by a reduced wind input. It is only in the case of the southern section salinity for the Spring 1980 case that a worsening of the error is noticed. The cross-correlation has been seen to not have been affected by this change. On the other hand, the effect of the reduced entrainment can be seen in Table XI to improve the agreement between the model and the ferry data on the northern section for that case. The low values for the RMS error on that section reflects the good qualitative agreement of Figs. 25 and 26 that was hidden in the evaluation of the cross-correlations because of the detrending. In brief, for the spring 1980, good agreement between the observations and the model depends weakly on the entrainment velocity expression used. This is not the case for Spring 1981 for which the salinity error on the northern section is reduced by a factor of 1.9 by the use of the reduced entrainment compared to a reduction by a factor of 1.3 with the introduction of a reduced wind factor. On the other

hand, the wind factor reduces the error to a larger extent than the entrainment velocity expression for the Spring 1981 southern section comparison. For the December Peak, one should not conclude from the small improvement in the error size, coming from the change in the entrainment expression, to a deficiency of this parameter to improve the correlation. An overwhelming wind input in this case is more likely to hide any improvements brought by the modification of the entrainment velocity.

5.4 Numerical Results Including Tidal Forcing

Remembering the poor resolution of the ferry data for fluctuations at tidal frequencies, it seems unwise to proceed with an extensive and precise modelling effort to include the tides for the sake of the comparison with the ferry data. The emphasis was instead to include tidal effects in the model only as approximations of the tidal currents and the modulation of the discharge by the tides. The aim is also to check if the inclusion of the tidal forcing confirm the conclusions found so far for the effects of the discharge and the wind.

Tidal forcing in Stronach's model was input through the barotropic slopes (the terms $gh\partial\zeta/\partial x$ and $gh\partial\zeta/\partial y$ in equations 4.3 and 4.4), through the barotropic currents in the bottom layer (u_0, v_0) and the modulation of the discharge at tidal frequencies. The tidal slopes and currents were input from Crean's barotropic model every 15 minutes (Stronach,1981), but until the latter model was available, approximate amplitudes for the tidal slopes and currents were used (Stronach,1977). The

present study has made use of these approximations. Only fluctuations at the diurnal (K_1) and the semi-diurnal (M_2) periods were considered. The phases were referenced to the phases ϕ_1 and ϕ_2 of the K_1 and M_2 constituents for the sea level elevation at Point Atkinson. Phases ϕ_1 and ϕ_2 were computed from harmonic analysis of the sea level elevation for which the time origin of the analyses coincides with the starting days of the three modelling cases.

An average value of 23 cm/s for the M_2 current amplitude can be inferred from Fig. 114 of Stronach's thesis (1977). Parker (1977) reports current measurements in the Strait indicating a ratio of 0.6 between the tidal amplitudes of the K_1 and M_2 currents. The phases of the two constituents of the barotropic tidal velocity were computed from near surface current measurements on sections close to the ferry sections (Data Record of Current Observations,1969-1970). The final expression for the tidal current is

$$u_o = 0 \text{ cm/sec},$$

$$v_o = -(13.8 \cos(\omega_1 t-(\phi_1-84°)/360°) + 23 \cos(\omega_2 t-(\phi_2-75°)/360°) \text{ cm/s}, \qquad 4.22$$

where ω_1 and ω_2 are the angular frequencies of the K_1 and M_2 constituents respectively. It is assumed that the across-strait tidal current is null. As a poor approximation, geostrophy is assumed to hold for the along-strait current component so that the across-strait slope is estimated as follows:

$$\partial\zeta/\partial x = fv_o/g. \qquad 4.23$$

The along-strait slopes, on the other hand, are approximated

from the same figure of Stronach's thesis as used for the tidal currents. The amplitude of the M_2 slope has been estimated to be 5.24 cm/2 km. This slope has an out-of-phase relationship with the sea level elevation and the ratio of the amplitudes of the K_1 and M_2 slopes is the same as the ratio of the amplitudes of the sea level elevation, that is 0.94. Finally the along-strait slope is written as

$$\partial\zeta/\partial y = -(2.46\cdot10^{-6}\cos(\omega_1 t-\phi_1) + 2.62\cdot10^{-6}\cos(\omega_2 t-\phi_2))\ \text{cm/cm}. \qquad 4.24$$

Uniformity of the currents and slopes over the modelling area are a further approximation for the sake of simplicity and a reduction of the number of parameters. The modulation of the discharge by the tides is modelled by adding to the velocity at the river mouth diurnal and semi-diurnal fluctuations. The amplitude and phases of these fluctuations are obtained from the harmonic analysis of a current meter record located at the river mouth (Stronach,1977). The tidally modulated speed at the river mouth (u_m) is taken as:

$$u_m = u_c + 33\cos(\omega_1 t-(\phi_1+138°)/360°) + 48\cos(\omega_2 t-(\phi_2+152°)/360°))\ \text{cm/sec} \qquad 4.25$$

where u_c is the speed at the mouth computed from the daily discharge value.

Tidal forcing was added to the computer model and run for the three cases previously described. For each case, the wind

factor and the entrainment that gave the lowest RMS difference with the ferry data were used. No significant changes in the model average salinities were noticed if only the tidal modulation of the discharge was added. On the other hand, the entrainment velocity had to be multiplied by a factor of 0.75 in order to preserve the same general trend of the average salinity as before when the underlying current and the tidal slopes are present. No reduction of entrainment would have been necessary if the amplitude of the tidal current had been smaller than the residual velocity due to the wind and the discharge. Figs. 29, 30 and 31 show the tidally forced model average salinity in comparison to the ferry data. Perfect agreement is not reached; nevertheless, the combined effect of the discharge and the wind is still clearly visible and set, as was assumed, the average conditions of the distributions of salinity on which tidal fluctuations are superposed. This fact justifies the preceding analysis that neglected the tidal forcing as a first approach. Large tidal fluctuations of the model salinity are found to coincide with periods of high scattering of ferry data and high river discharges. This observation corresponds to the previous conclusion from Fig. 19 that the effects of high tidal amplitudes on salinity are found during periods of high river discharges.

Harmonic analysis was performed with the model salinity and the ferry data for the three cases studied and the results are compiled in table XII. Amplitudes and Phases of the model salinity fluctuations do not vary over a wide range of values

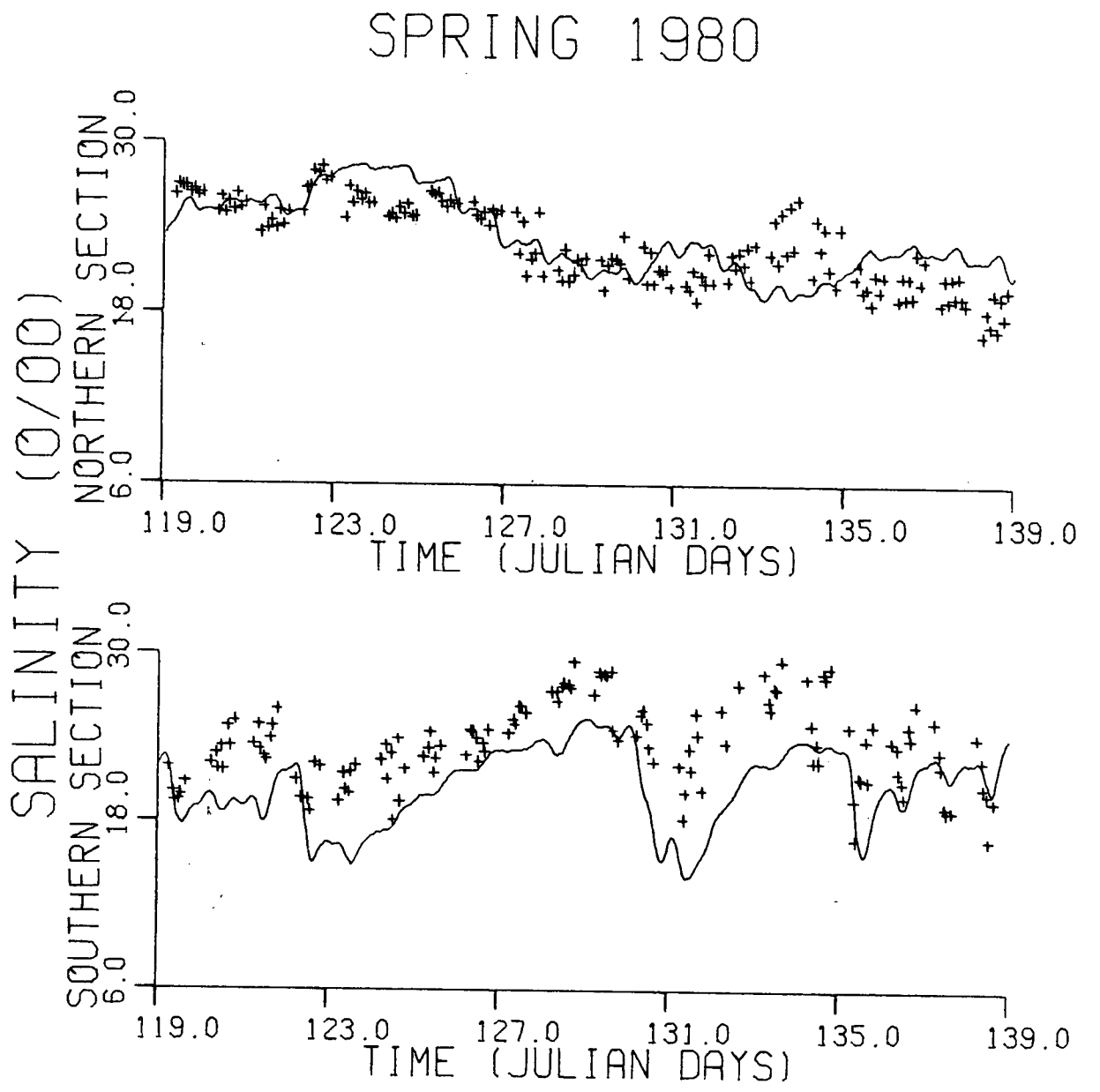

Figure 29 - Plots of the average salinity ferry data (crosses) and modelled average salinity (solid line) vs time for the Spring 1980 using a model with a reduced entrainment velocity, a reduced wind factor (b=1) and with tidal forcing

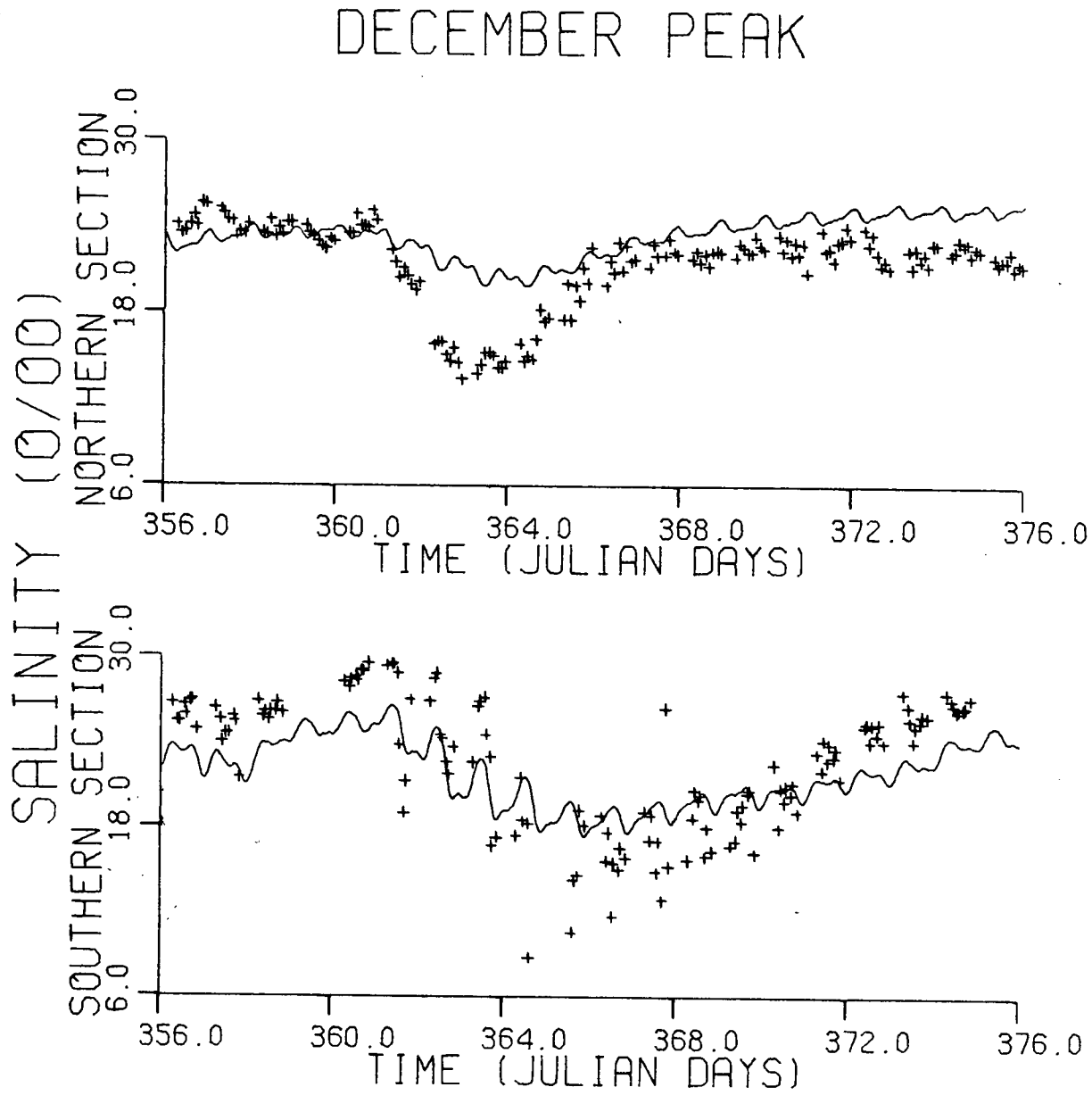

Figure 30 - Plots of the average salinity ferry data (crosses) and modelled average salinity (solid line) vs time for the December Peak using a model with a reduced entrainment, a reduced wind factor (b=0.125) and with tidal forcing

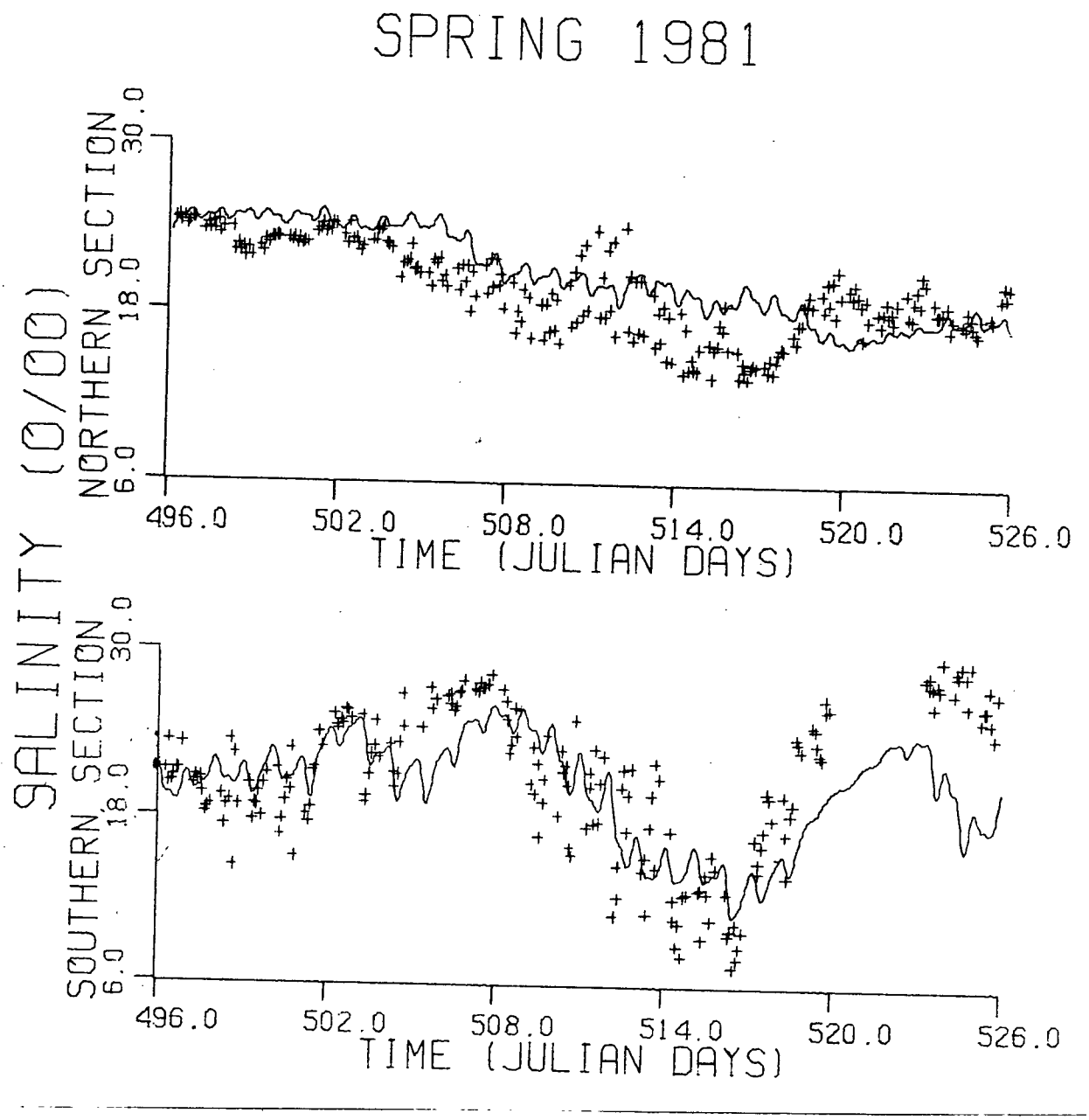

Figure 31 - Plots of the average salinity ferry data (crosses) and modelled average salinity (solid line) vs time for the Spring 1981 using a model with a reduced entrainment velocity, a reduced wind factor (b=0.5) and with tidal forcing

for the three cases for each section. The maximum difference of model salinity amplitude is 0.5 o/oo (seen between the Spring 1980 and December Peak southern section model K_1 salinity amplitude) and the maximum change in phase Amplitudes and Phases of the model salinity fluctuations do not vary over a wide range of values for the three cases for each section. The maximum difference of model salinity amplitude is 0.5 o/oo (seen between the Spring 1980 and December Peak southern section model K_1 salinity amplitude) and the maximum change in phase is 60°. The

Table XII - Amplitudes and phases from the harmonic analysis of the average salinity of the model and the ferry data

	K_1				M_2			
	Amplitude (o/oo)		Phase (degree)		Amplitude (o/oo)		Phase (degree)	
	Ferry	Model	Ferry	Model	Ferry	Model	Ferry	Model
Spring 1980								
S. Section	0.7	1.1	190.	10.	1.2	0.4	-10.	20.
N. Section	0.3	0.3	20.	140.	0.3	0.3	130.	210.
December Peak								
S. Section	0.9	0.6	-20.	-30.	0.7	0.5	-70.	20.
N. Section	0.2	0.4	180.	140.	0.2	0.2	120.	190.
Spring 1981								
S. Section	1.6	0.8	-20.	30.	1.4	0.6	-20.	-0.
N. Section	0.4	0.4	60.	140.	0.2	0.2	170.	170.

phase values agree relatively well with the phases expected from the advection of the plume by the tidal current, that is an in-phase relationship between the salinity on the southern section

and the sea level elevation and an out of phase relationship between the northern section salinity and the sea level elevation. The amplitudes indicate that, for both sections, the diurnal contribution to the salinity fluctuations is greater than the semi-diurnal one, even though the M_2 constituent is more important than the K_1 constituent for the tidal current and the sea level elevation. The dominance of the K_1 constituent over the M_2 was also noticed in the yearly harmonic analysis of the Ferry data (Table IX).

When the harmonic analysis results for the ferry data for the three cases are compared to the model harmonic results, the agreement is far from perfect. Nevertheless, the difference between the phases are usually between -90° and 90° especially for the December Peak and the Spring 1981 cases. Surprisingly, the K_1 salinity fluctuations for the Spring 1980 case of the Ferry data are almost out of phase with the same fluctuations for the model data. On the other hand, if the model harmonic phase results are compared to the ferry data phases, obtained for the two years (Table IX), it is seen that these phases agree reasonably well with the model phases; however the K_1 fluctuations at the northern section do not show the out-of-phase relationship with the sea level elevation that the model predicted. Investigating the resemblance between the amplitudes of the model and the ferry fluctuations, one can estimate that the ratio of the two amplitudes varies from 0.4 to 3 over a wide range. In general, the amplitudes of the southern section ferry salinity are greater than the corresponding model amplitudes

while the ratio of amplitudes on the northern section are usually less than or close to 1. One can presume that with a less uniform tidal current distribution, for example a distribution that would have high currents near the southern section and weak tidal currents near the northern section (as on Fig. 114 of Stronach's thesis, (1977)) that the amplitudes of the model fluctuations on the southern section would increase while the ones on the northern section would decrease and in this way more closely match the tidal amplitudes observed from the ferry data.

5.5 Horizontal Distributions Of The Plume Properties

One purpose of the model is to provide horizontal distributions of the plume properties (U,V,h and s) in the area between the ferry tracks as a function of time. Because of the localized nature of the ferry data, no such distribution can be usefully compared to the ferry observations. The only possible comparison between model horizontal distributions and observations is with the horizontal mapping of CTD surface measurements. Only two cruises were completed during the model periods, the first one during the night of May 7 to 8, 1980 (on julian days 127 and 128) and the second during May 11 to 12, 1981 (Julian days 496 and 497). To account for the non-synoptic character of the CTD measurements, the tidal numerical model of the Spring cases was run to produce distributions of the plume properties at each time a CTD station was deployed. From each distribution the salinity of the plume is interpolated at the

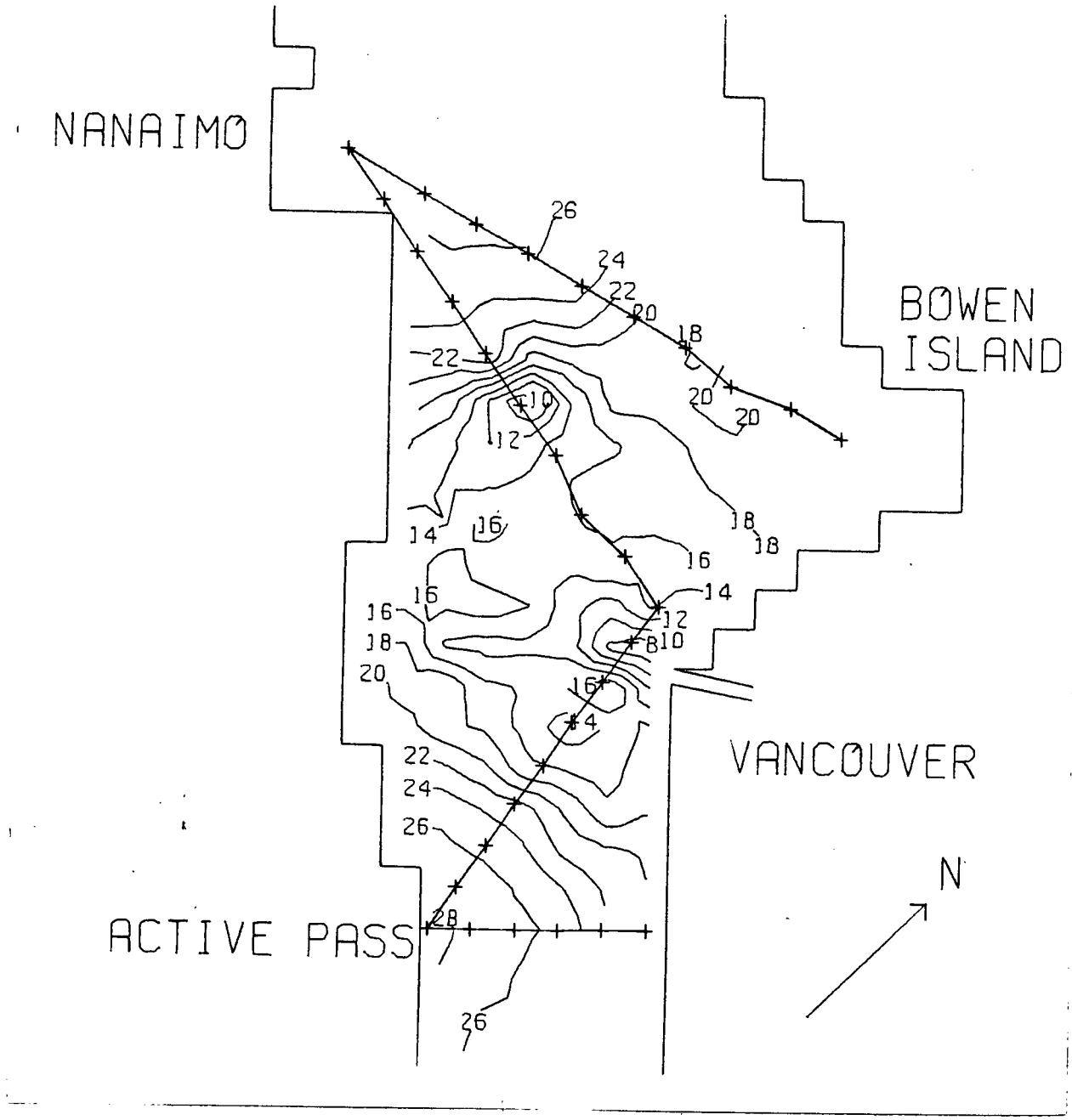

Figure 32 - Surface salinity contour (o/oo) from the CTD cruise on May 7-8, 1980 (Julian days 127-128). The crosses indicate the positions of the CTD stations

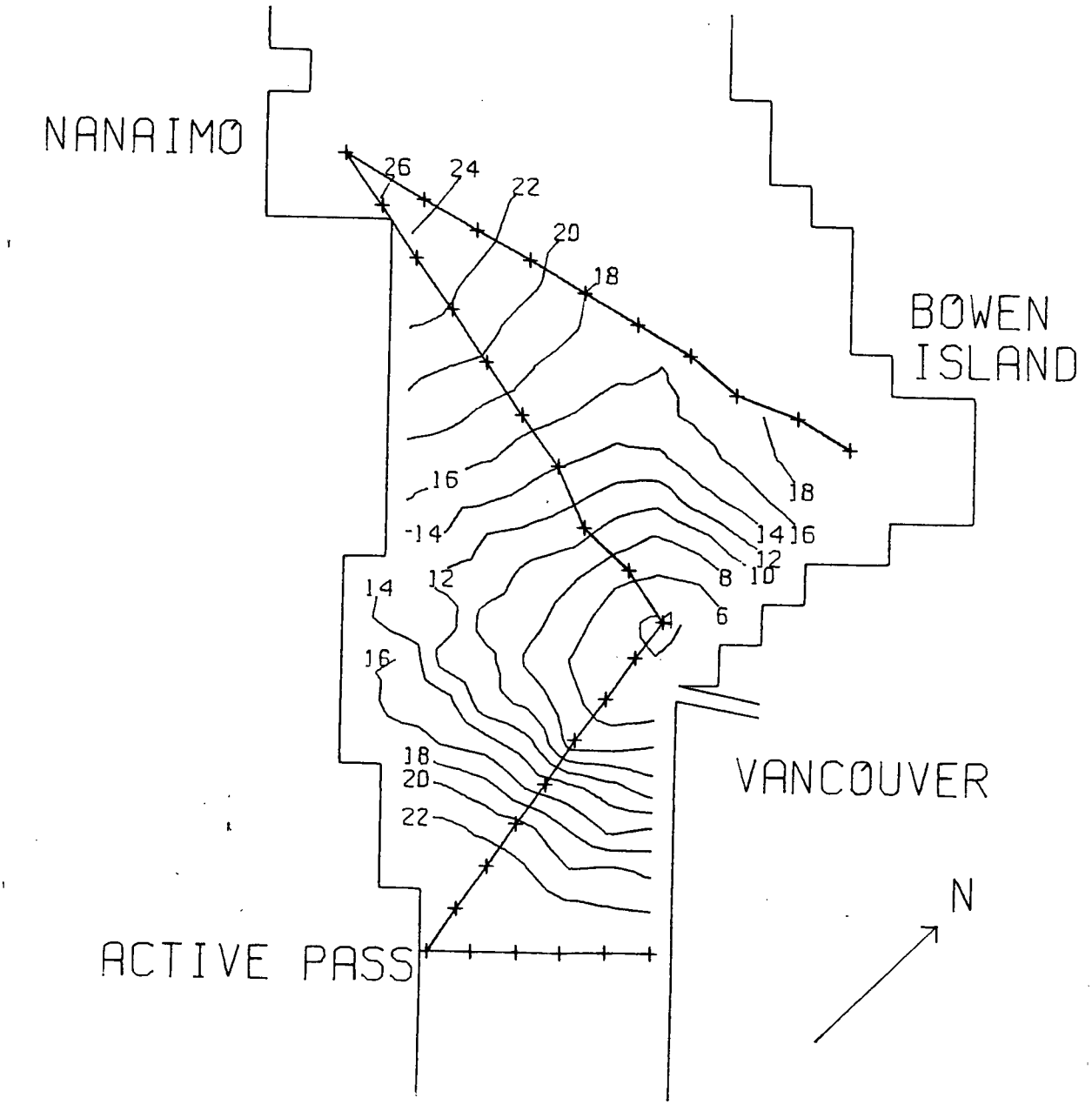

Figure 33 - Surface salinity contour (o/oo) as given by the numerical simulation of the cruise of May 7-8, 1980 (Julian days 127-128). The crosses indicate the positions of the CTD stations

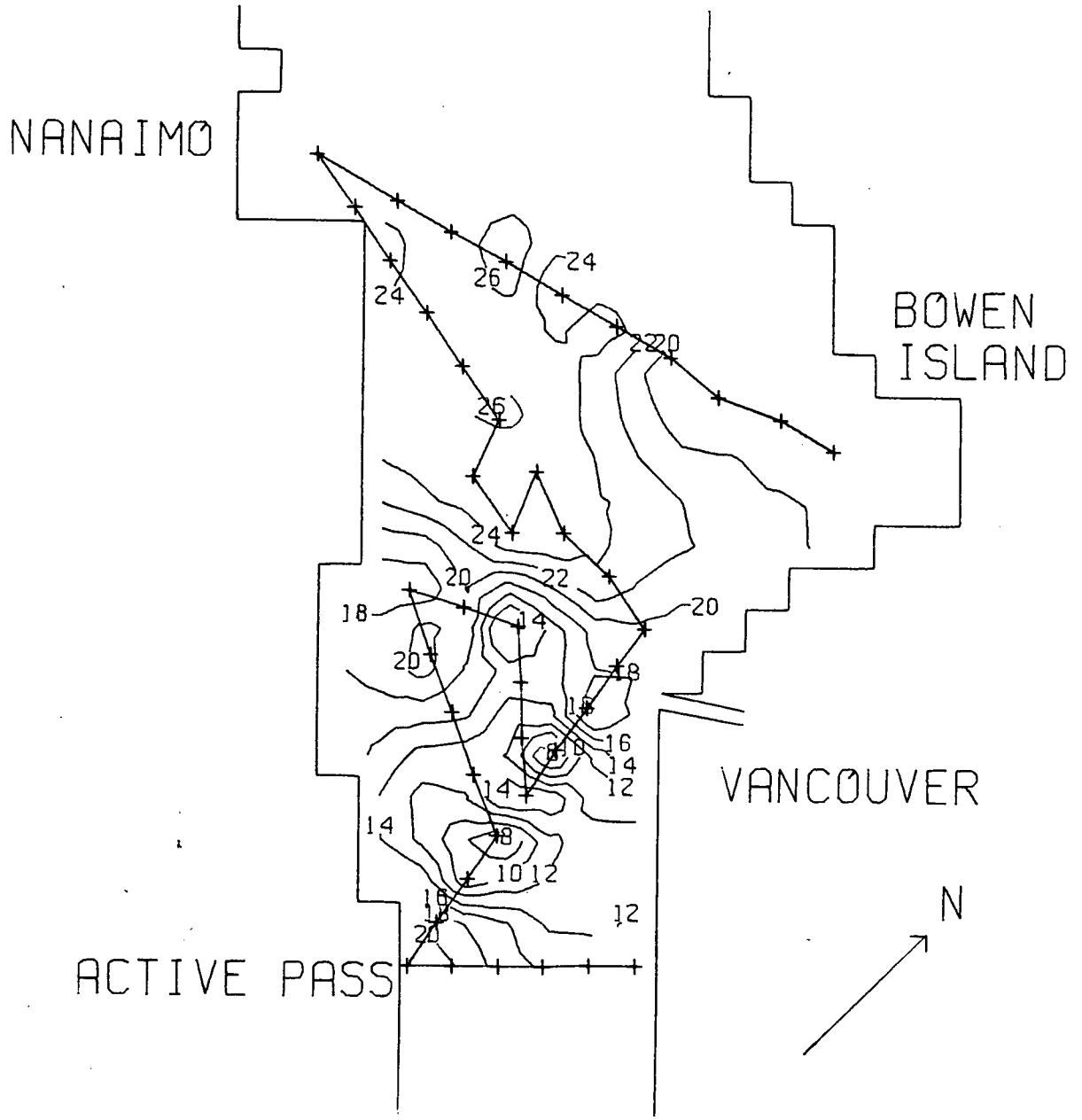

Figure 34 - Surface salinity contour (o/oo) from the CTD cruise on May 11-12, 1981 (Julian days 496-497). The crosses indicate the positions of the CTD stations

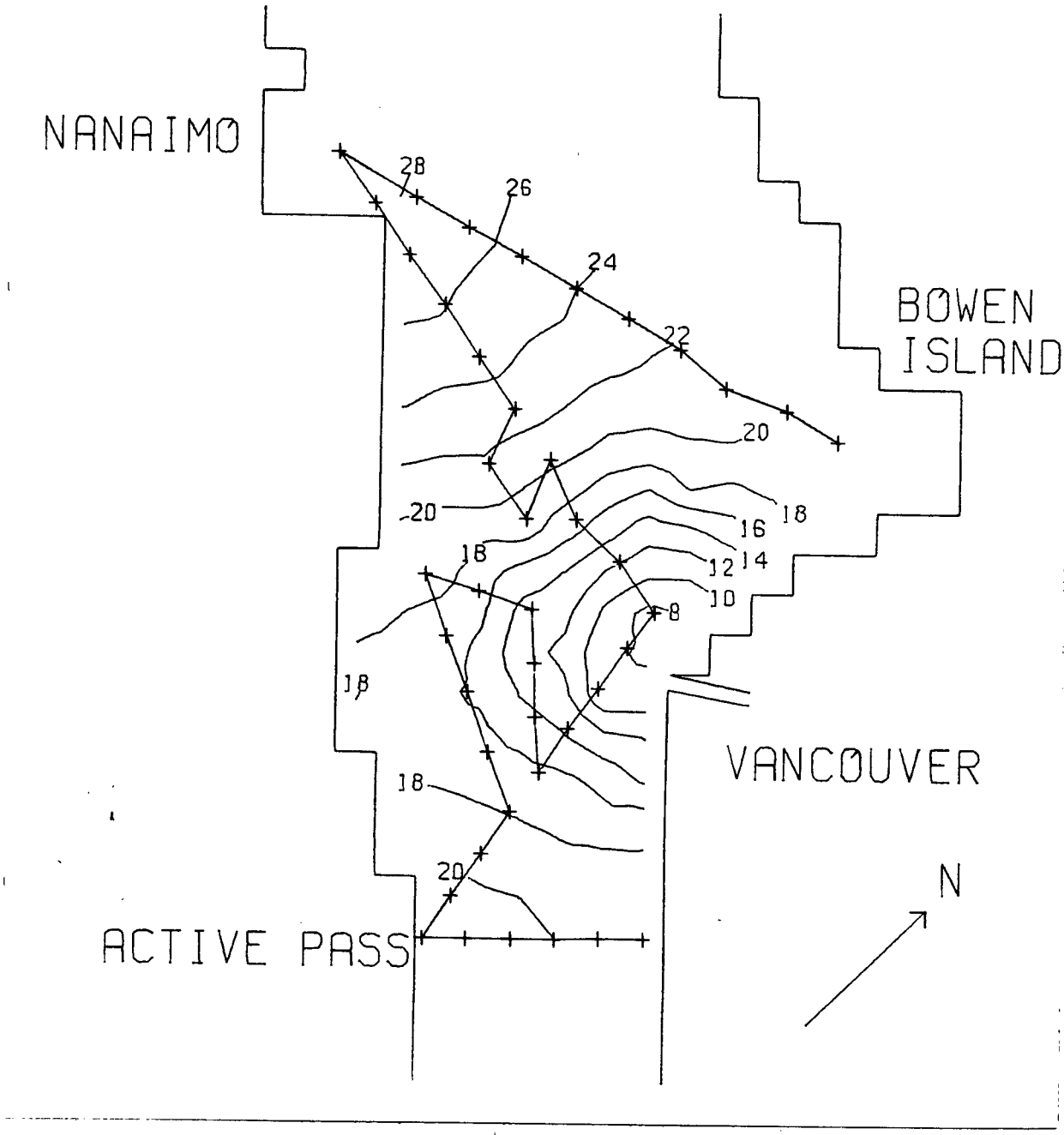

Figure 35 - Surface salinity contour (o/oo) as given by the numerical simulation of the cruise of May 11-12, 1981 (Julian days 496-497). The crosses indicate the positions of the CTD stations

position of the time corresponding to the CTD station. Contour maps of the set of these model salinities for different times and stations are shown in Figs. 33 and 35. They are compared to the corresponding contour maps from the CTD data (Figs. 32 and 34). The depth of the plume from the CTD data is assigned to be the depth at which the maximum vertical salinity gradient occurs. The analogous CTD salinity to the model is computed by averaging the salinities between the surface and this depth.

The horizontal salinity maps of Figs. 32 and 33 are the CTD and model distributions for the cruise during the Spring 1980. In general, the model produces lower salinities at the mouth than the CTD data. This suggests that a possible modification of the model would be to have the river discharge saltier than 0 o/oo. The patch of fresh water with salinity as low as 10 o/oo, near the northern section is not modeled. These low salinities are only recorded at one station so that it could come from an error in the measurement operation at that station or an erroneous estimation of the plume thickness. Without it, the horizontal salinity gradient near the northern section would be lower and compare favorably with the model salinity gradient. Near the southern section, the salinity gradients are quite similar and the positions of the 22 o/oo isohaline near this section are relatively the same.

The same conclusion about the model underestimation of the salinity at the mouth holds for the maps of the Spring 1981 case (Figs. 34 and 35). Contrary to the Spring 1980 where a quasi-symmetry seems to take place around the mouth, both model and

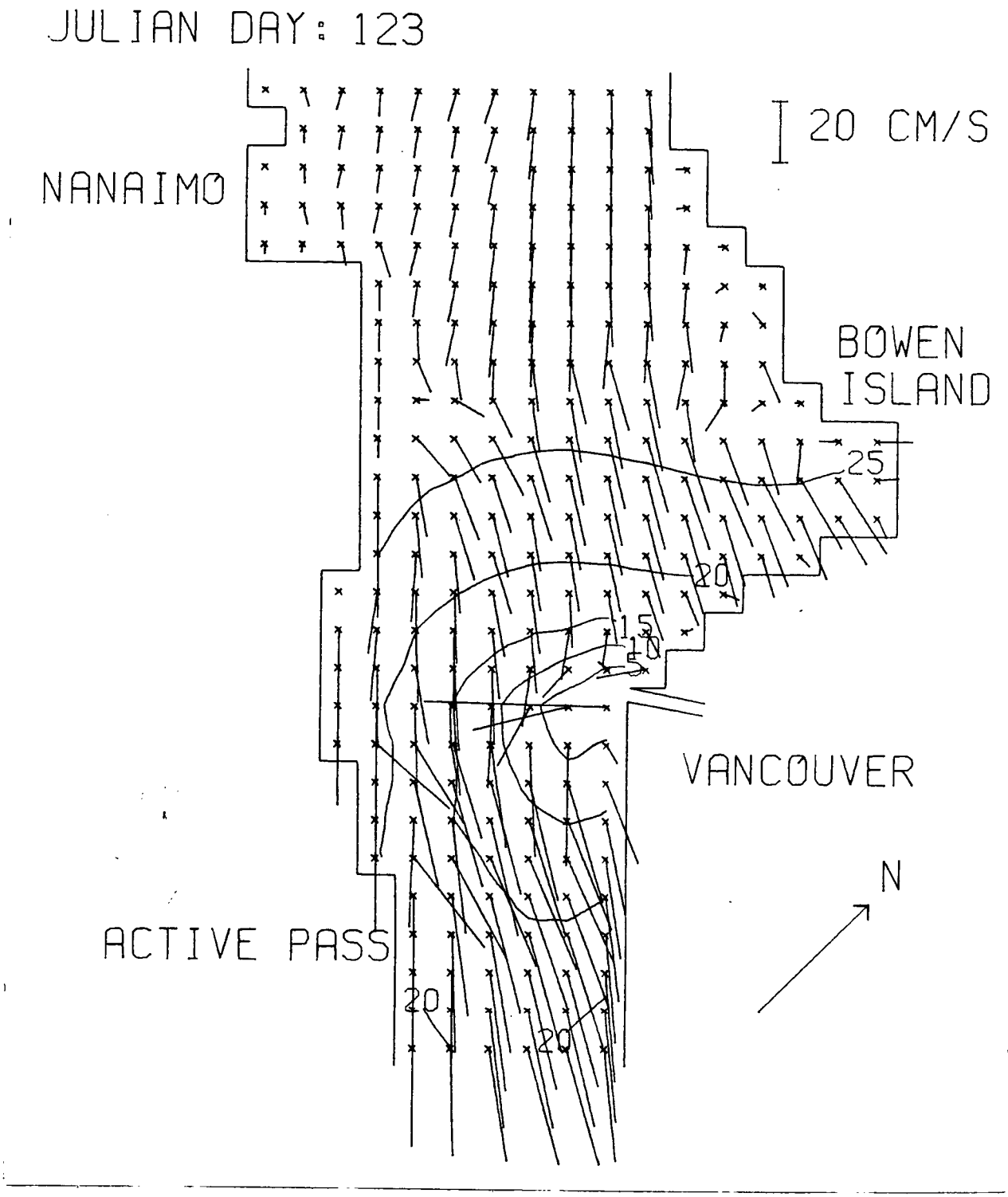

Figure 36 - Salinity (o/oo) and current distributions as given by a numerical model with variable wind and discharge on Julian day 123 (May 3, 1980)

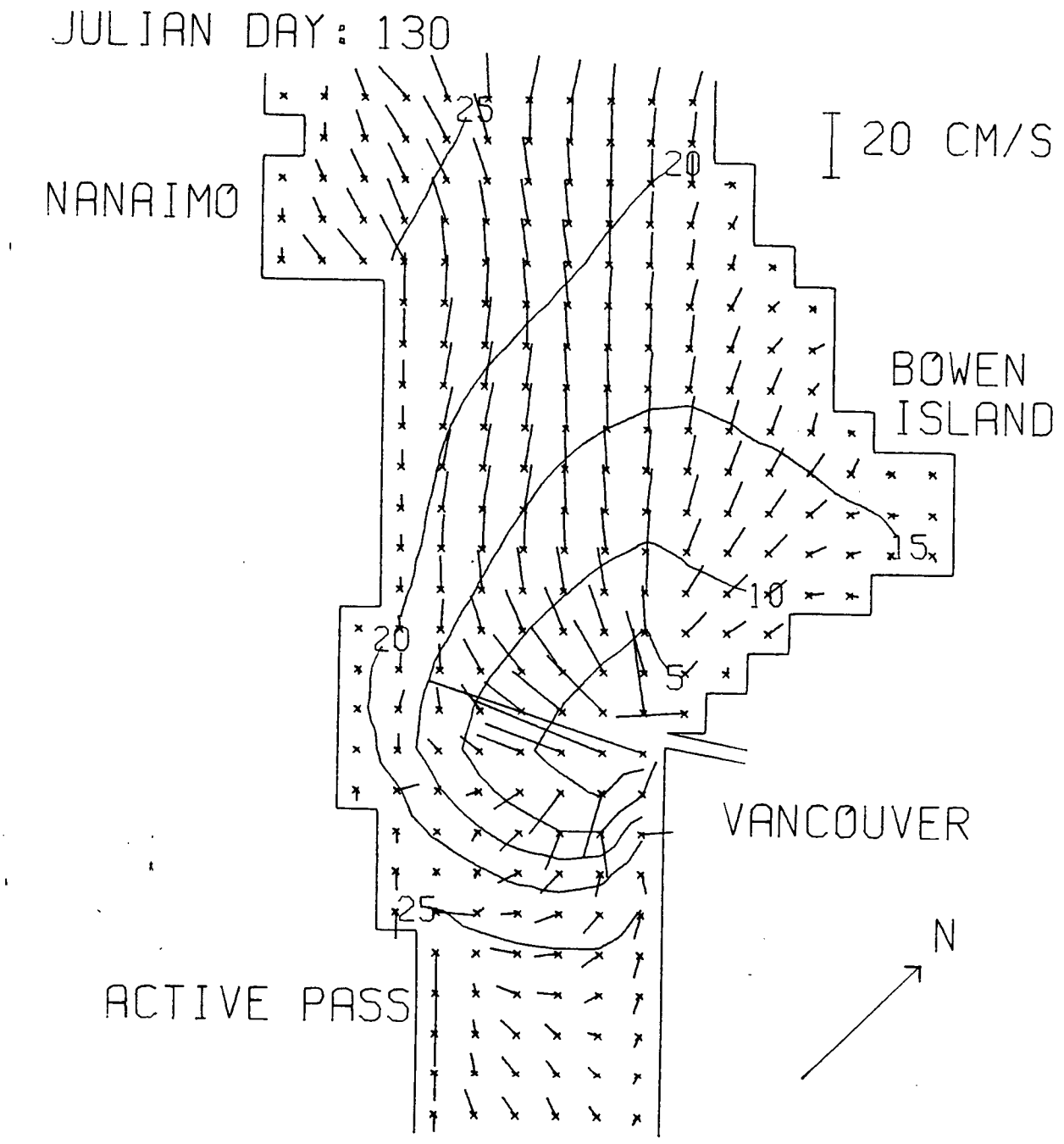

Figure 37 - Salinity (o/oo) and current distributions as given by a numerical model with variable wind and discharge on Julian day 130 (May 10, 1980)

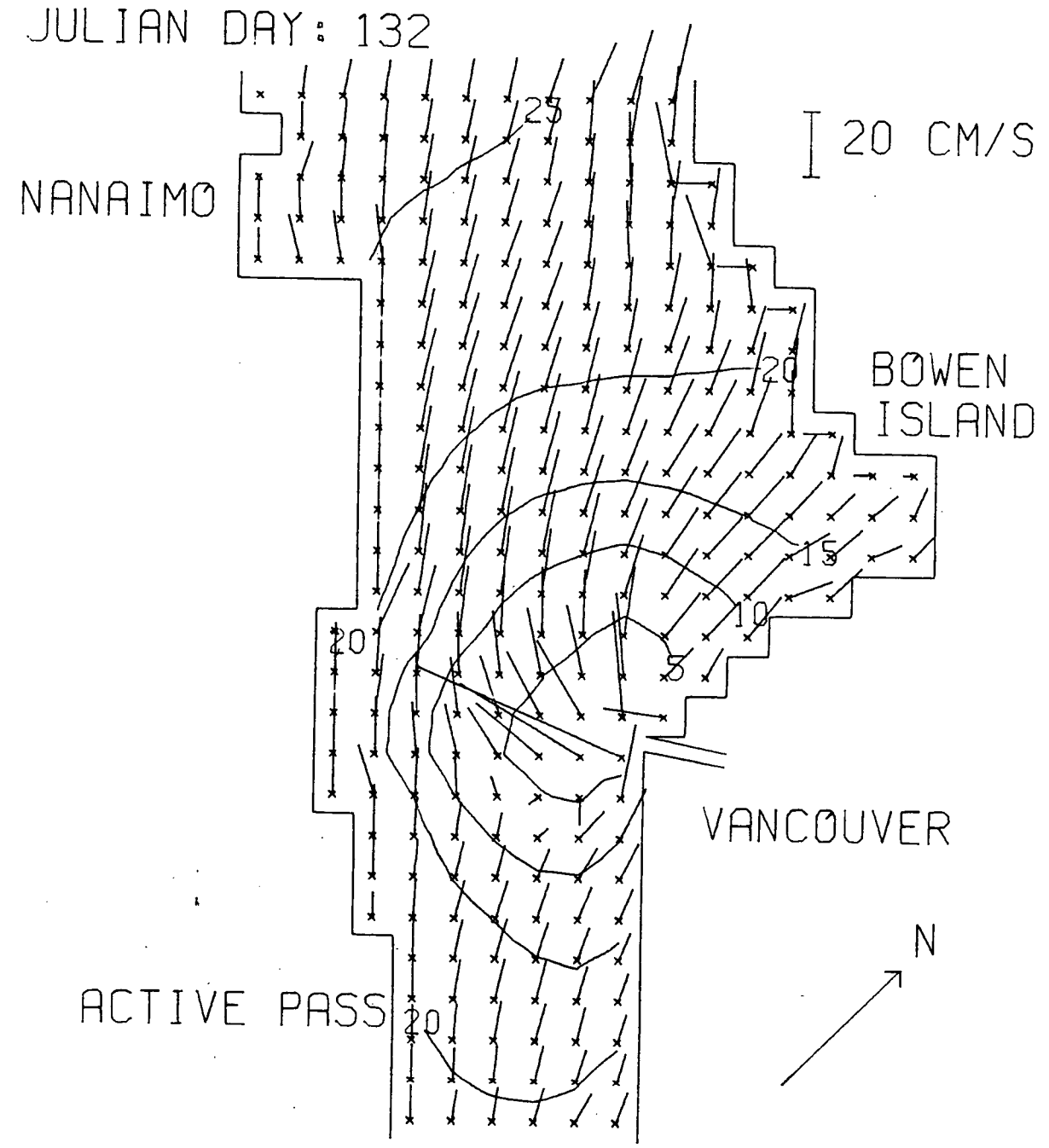

Figure 38 - Salinity (o/oo) and current distributions as given by a numerical model with variable wind and discharge on Julian day 132 (May 12, 1980)

CTD distributions of salinity show a freshening of the water towards the southern section. Considering all the limitations of the model (resolution, small area modelled, etc.), the agreement between the CTD observations and the simulations is reasonably good.

To show the time dependence of the salinity on the discharge and the wind, horizontal distributions of salinity and currents from the tideless model for the three cases are plotted in Figs. 36 to 44. Each graph corresponds to a time at which an extremum of one of the average salinities occurs. On day 123 (Fig. 36), strong northwesterly winds, of the order of 30 km/h, push the plume towards the southern section and are responsible for low salinity on the southern section and high salinity on the other section (Fig. 26). Model currents are well aligned with the direction of the wind. On the contrary, the currents on day 130 (Fig. 37) are not in the same direction as the weak wind present at that time. The current pattern as for the salinity distribution is reminescent of the southeasterly, four day long wind that ended 12 hours before. Strong positive (southeast) winds are rising again on day 132 (Fig. 38) greatly influencing the direction of the surface currents. The salinity distribution does not respond as fast and is still vaguely characterized by the negative wind advection during Julian day 130.

For the December peak case, Fig. 39 shows the plume properties during high discharge and southeasterly wind (Julian day 361). The plume has difficulty reaching the southern

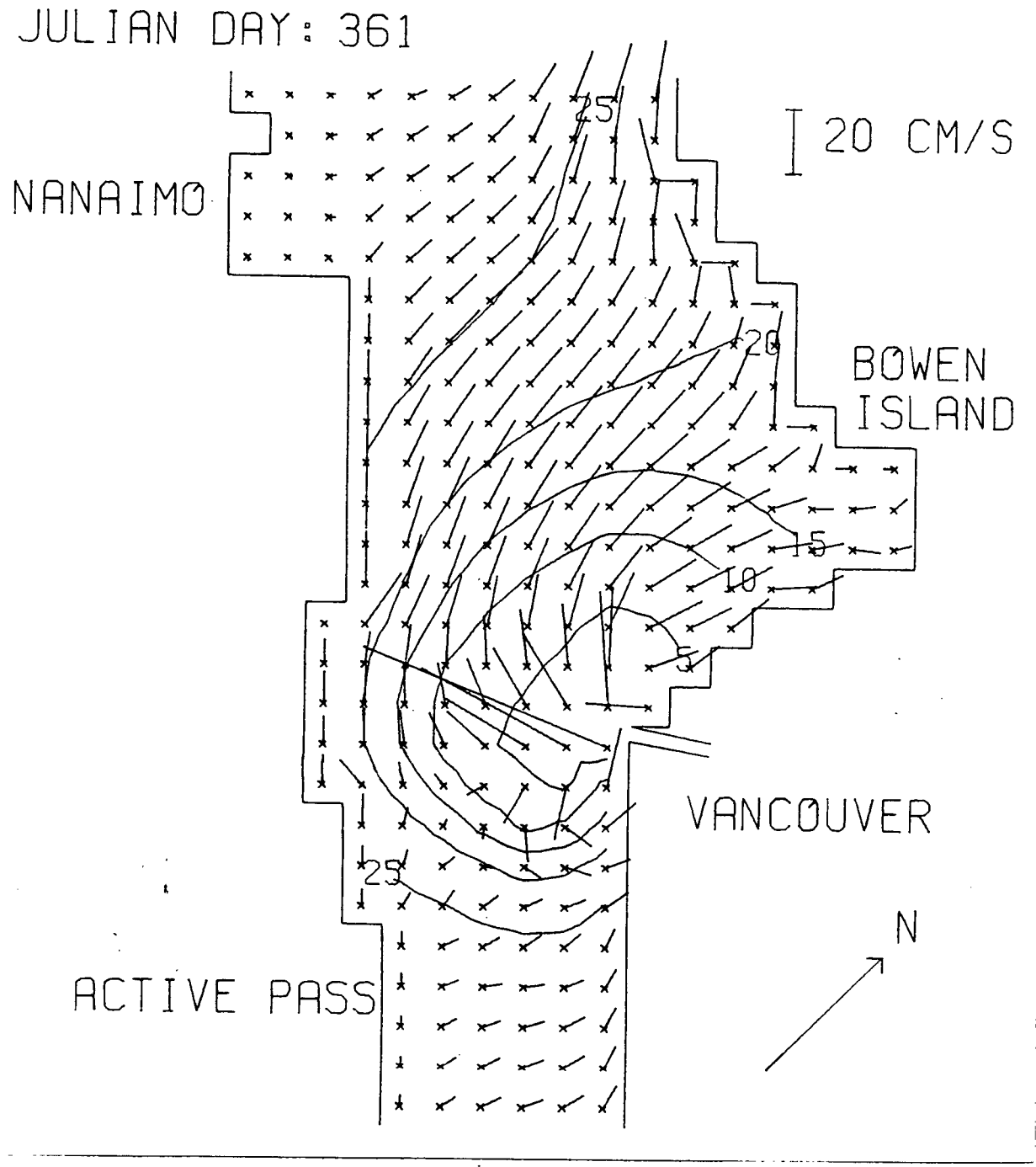

Figure 39 - Salinity (o/oo) and current distributions as given by a numerical model with variable wind and discharge on Julian day 361 (December 27, 1980)

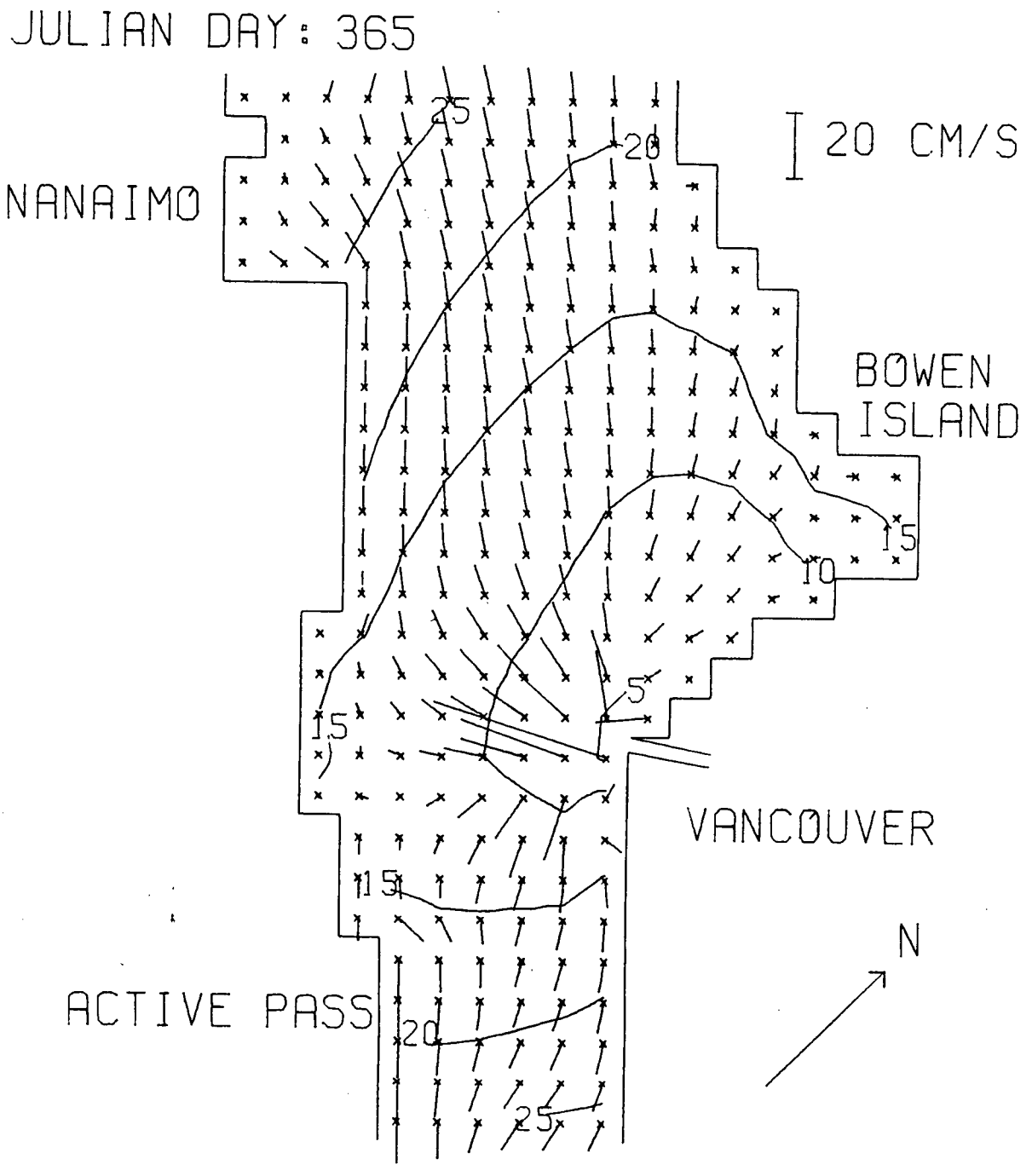

Figure 40 - Salinity (o/oo) and current distributions as given by a numerical model with variable wind and discharge on Julian day 365 (December 31, 1980)

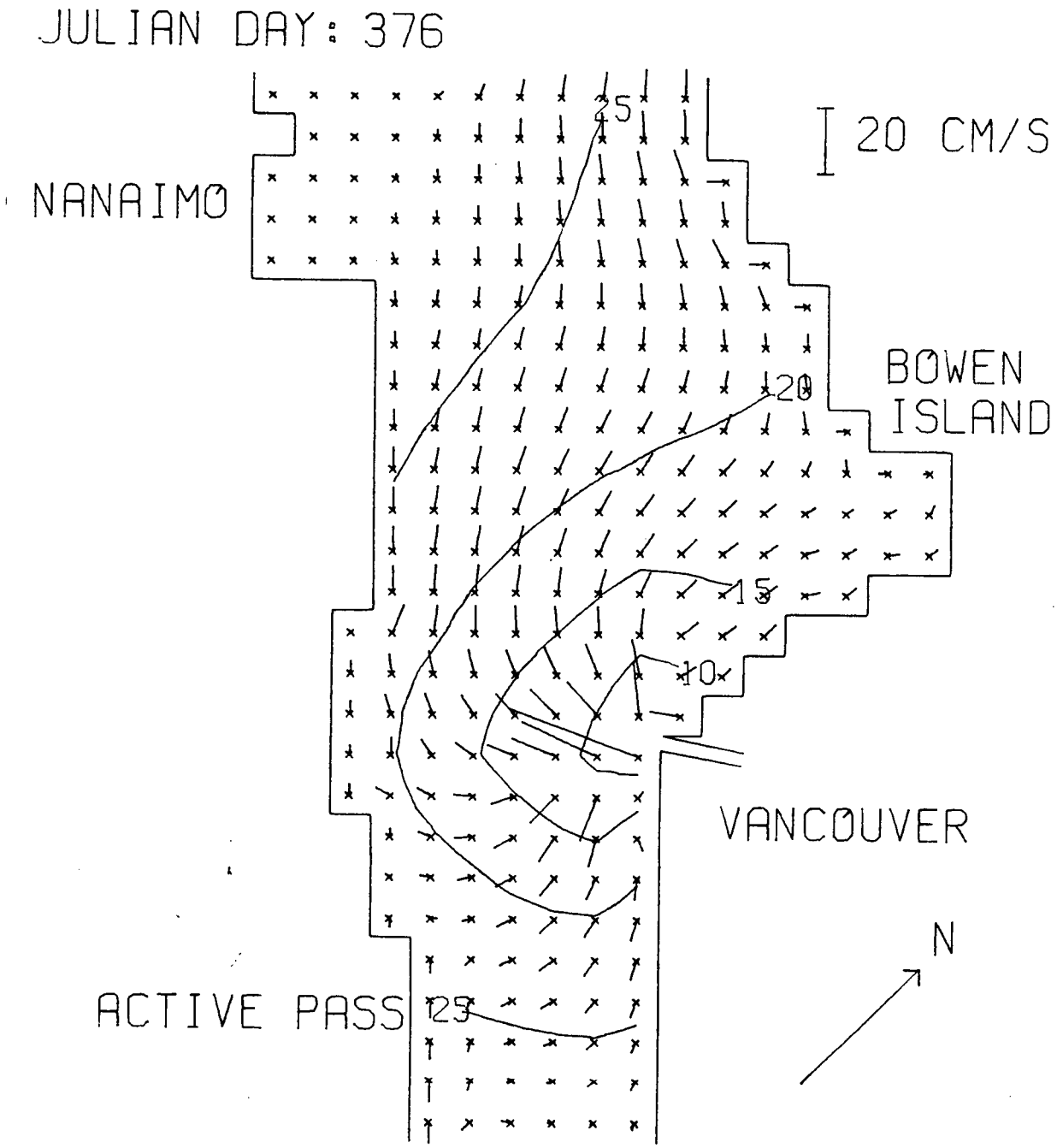

Figure 41 - Salinity (o/oo) and current distributions as given by a numerical model with variable wind and discharge on Julian day 376 (January 11, 1981)

section. It is only when the wind has changed direction (Fig. 40) on Julian day 365 that the plume spreads over all the computational area. In this case, even with strong northwesterly winds, the currents are still outward from the river mouth near the northern section. High discharge is responsible for this spreading. Fig. 41 shows the plume properties distributions on day 376 when the discharge is low again. This distribution when compared to the distribution of Fig. 21, is seen to resemble the steady state distribution.

The first chosen salinity map for the Spring 1981 case describes a situation during a period of average southerly winds (Fig. 42 for Julian day 508). The wind pattern in the current is not as apparent as it was during the Spring 1980 case for which the wind factor (F_1) was set equal to 1. Nevertheless, the salinity distribution shows signs of a northward advection, consistent with the direction of the wind. The situation depicted in Fig. 43 (for julian day 517) very much resembles the distribution of Fig. 40. Both distributions occur at a time of high discharge and negative wind. The spreading of the plume in the Spring 1981 case is more intense reflecting the higher level of the discharge. Finally on Julian day 523 (Fig. 44) the rise of high southerly wind pushes the plume north, breaking the symmetry present on day 517.

A few general observations that were discussed during the the examination of the ferry data in Chapter 3 are worth mentioning. It was noticed in that chapter that the salinity on the southern section usually had a minimum at some point in the

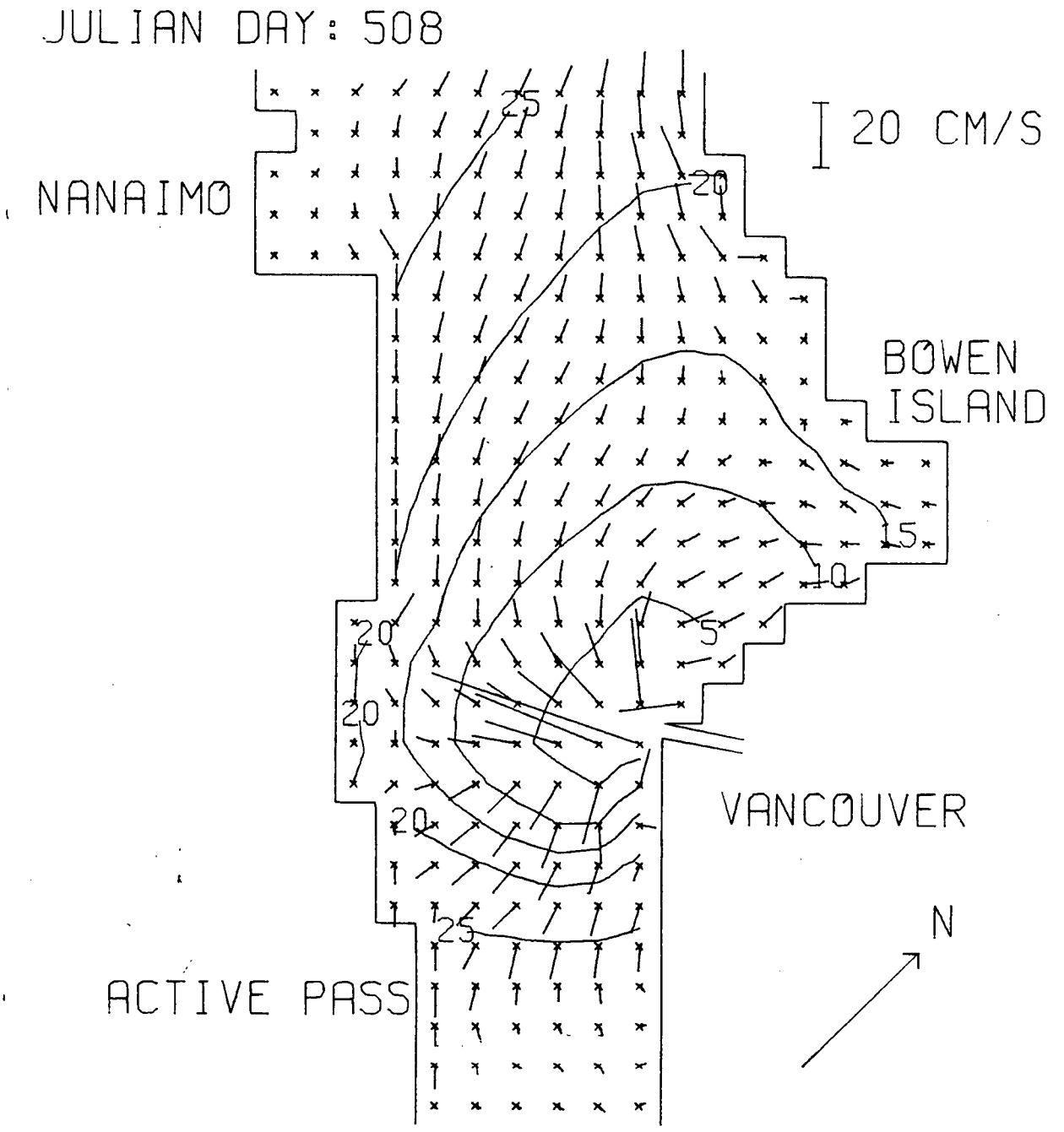

Figure 42 - Salinity (o/oo) and current distributions as given by a numerical model with variable wind and discharge on Julian day 508 (May 23, 1981)

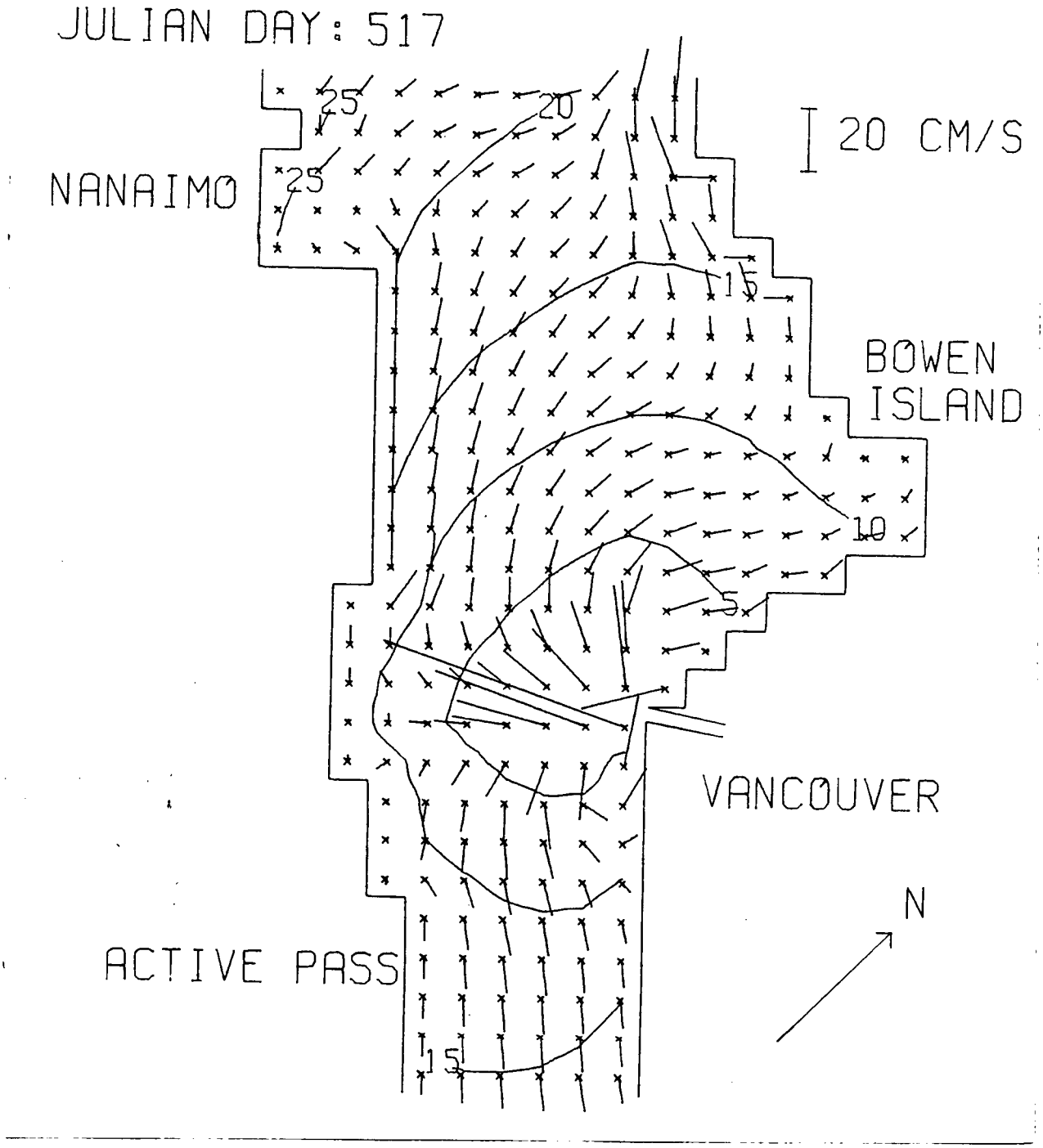

Figure 43 - Salinity (o/oo) and current distributions as given by a numerical model with variable wind and discharge on Julian day 517 (June 1, 1981)

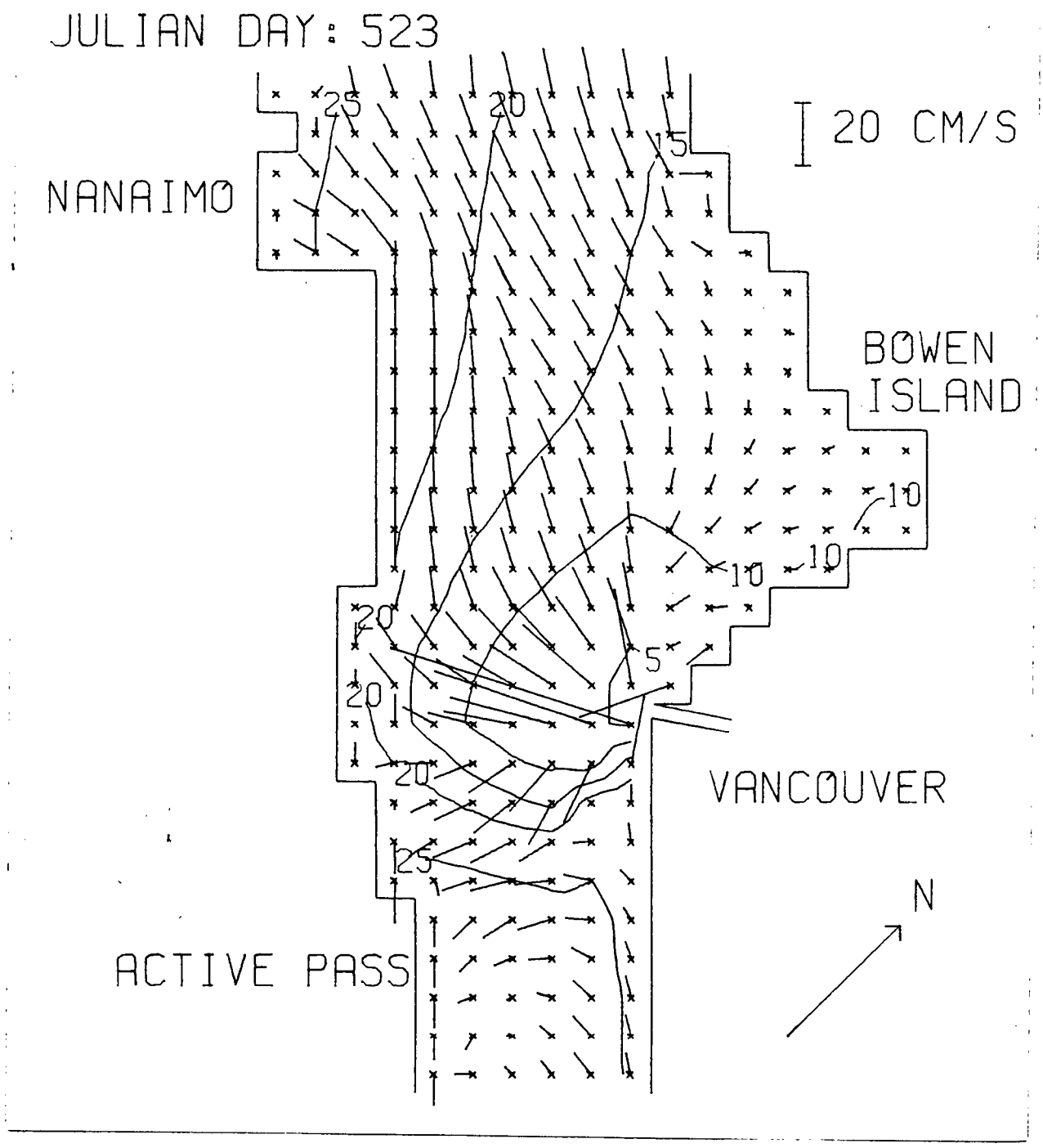

Figure 44 - Salinity (o/oo) and current distributions as given by a numerical model with variable wind and discharge on Julian day 523 (June 7, 1981)

middle of the section and not at x=1, as one might have assumed from the proximity of this point to the river mouth. Most of the distributions of figs. 36 to 44 also indicate a high salinity at x=1 on the southern section compared to a point in the middle of the section. In contrast, the distributions show a monotonic decrease of salinity along the northern section except possibly on day 365 (Fig. 40) for which it was already mentioned that during the December peak discharge, the lowest salinity and the highest daily variance were not found at x=1.

VI. CONCLUSIONS

Comparisons between time series of average salinity, maximum salinity gradient and river discharge demonstrate that, for both northern and southern ferry sections, low salinities and high horizontal salinity gradients correspond to peaks in the river discharge. Cross-correlations and cross-spectra (coherence and phase) comfirm this relationship especially at lower frequencies. In general the salinity increases along each section towards Vancouver Island. In terms of daily variance in the north the plume appears to progress towards Vancouver Island during the June increase in discharge. No such progression is seen along the southern section.

In terms of frequency, possible wind and discharge contributions to plume variability are well separated. Cross-correlations and cross-spectra between the plume characteristics and the along-strait wind are compatible with the along-strait advection of the plume. A positive wind (blowing from the southeast) will drive the plume to the northwest, raising the average salinity and lowering the salinity gradient at the southern section; at the same time this advection will sharpen the salinity gradient and lower the salinity at the northern section.

A linear combination of the effects of wind and discharge was found to substantially improve the correlations between the plume characteristics and the driving forces. Better qualitative agreement was achieved using a non-linear combination where the wind contribution depends on the discharge

level.

Harmonic analysis confirmed the combined effects of tidal advection and tidal modulation of the river discharge, at least for the salinity fluctuations on the southern section. During ebb-tide, tidal currents advect the plume towards the southern section and the slack tide allows maximum river discharge. For a flood-tide the reverse is true, so that while the tidal currents move the plume northward, the tide is gradually restricting the river outflow. Thus for the northern section, the two processes oppose each other leading to uncertain statistical results. The tidal salinity amplitudes reflect the discharge level.

By modifying the entrainment velocity expression so as to make it dependent on the stratification and by reducing the momentum transfer to the plume from the wind, the numerical model can be seen to have the potential to reproduce the long-term fluctuations of the plume caused by the discharge and the wind. This agreement between observations and model results signals two major accomplishments. First, the Ferry data constitute the first extensive set of observations that can be readily compared to Stronach's numerical model and be used to calibrate it. The need for calibration and verification was mentioned in Stronach's paper (1981) and again in LeBlond's review (waiting publication). Out of two years of Ferry data, only three periods covering a total of 70 days, received modelling attention. These three periods were all characterized by high discharge levels. There is still a large portion of the

data obtained during a somewhat lower level of discharge, that could be used for further model calibration and verification. Secondly, the fact that the wind is seen for the first time to have a definite effect on the plume both in the observations and in the model results, contradicts previous assumptions according to which the wind influence was neglected.

In view of the inability of the ferry data to properly resolve tidal fluctuations, no significant improvement in simulation was expected when tidal forcing was added to the numerical model. Nevertheless, results from a simple model including tidal forcing reproduced for the southern section salinity, relative to the sea-level elevation, the phase relationship expected from the advection of the plume by tidal currents. In spite of the large magnitudes of the tidal currents, the fluctuations of the plume salinity, along the ferry sections, seem to be a superposition of small tidal variations and a mean set by wind and discharge. Horizontal distributions of the plume properties from CTD surveys compared favorably with corresponding numerically obtained distributions.

Improvements in the numerical model are needed to clarify some of the assumptions introduced herein. The physical processes that determine the variations of the wind factor (F_1) still have to be found. The area covered by the model could be extended to include the region of water exchange with the Pacific Ocean at the northern end of the Strait. This extension might prevent fresh water from getting out of the system at the northern boundary. Modulation of the discharge by the tides is

often thought to produce successive fronts within the plume. In the present version of the model, this process is not observed and this could follow from an underestimation of the variations of the river current at the mouth. A non-uniform distribution of tidal current over the Strait or, even better, a direct input of the tidal currents would clearly improve and detailed view of the Fraser River plume fluctuations.

BIBLIOGRAPHY

1. CANADIAN TIDE AND CURRENT TABLES, 1980, Juan de Fuca and Georgia Straits, Government of Canada, Fisheries and Oceans. Vol 5, 72 pp.

2. CANADIAN TIDE AND CURRENT TABLES, 1981, Juan de Fuca and Georgia Straits, Government of Canada, Fisheries and Oceans. Vol 5, 72 pp.

3. CORDES, R.E. 1977. Measurements of the velocity field in the Fraser River Plume. M.SC. Thesis, University of British Columbia, 137 pp.

4. CORDES, R.E., S. POND, B.R. de LANGEBOOM and P.H. LEBlOND, 1980. Estimates of entrainment in the Fraser River plume, British Columbia. Atmosphere-Ocean, 18(1),pp 15-26

5. CREAN, P.B. 1976. Numerical model studies of the tides between Vancouver Island and the mainland coast. J. Fish. Res. Board Can. 33:2340-2344.

6. CREAN, P.B. 1978. A numerical model of barotropic mixed tides between Vancouver Island and the mainland and its realtion to studies of the estuarine circulation. In: Hydrodynamics of estuaries and fjords, J.C. Nihoul (Ed.) Elsevier, New York, pp 283-314

7. DATA RECORD OF CURRENT OBSERVATIONS, 1969-1970, Gabriola Island to Gower Point, Manuscript Report Series. Vol X, Department of the Environment, Marine Sciences Directorate, Pacific region, 153 pp.

8. DATA RECORD OF CURRENT OBSERVATIONS, 1969-1970, Samuel Island to Point Robert, Manuscript Report Series. Vol XII, Department of the Environment, Marine Sciences Directorate, Pacific region, 96 pp.

9. DUFFUS, H.J. and M.A. TILLEY, 1978. Satellite observations of the Fraser River plume. Coastal Marine Science Laboratory, manuscript report 78-2 (unpublished manuscript), 18 pp.

10. ELLISON, T.H. and J.S. TURNER, 1959. Turbulent entrainment in stratified flows. J. Fluid Mech. Vol. 6, pp. 423-448

11. FEELY, R.A. and M.F. LAMB, 1979. A study of the dispersal of suspended sediment from the Fraser and Skagit Rivers into Northern Puget Sound using Landsat imagery. Interagency Energy/Environment R. and D. Program report EPA-600/7. 46 pp.

12. FOREMAN, M.G.G. and R.F. HENRY, 1979. Tidal analysis based on high and low water observations. Pacific Marine Science Report 79-15. Institute of Ocean Sciences, 39 pp.

13. GARVINE, R.W. 1974. Physical features of the Connecticut River outflow during high discharge. Journal of Geophysical Res. Vol. 79(6), pp. 831-846

14. GARVINE, R.W. 1977. Observations of the motion field of the Connecticut River plume. Journal of Geophysical Res. Vol. 82(3), pp. 441-454

15. GARVINE, R.W. 1979a. An integral hydrodynamic model of upper ocean frontal dynamics, Part I: Development and analysis. Journal of Phys. Oceanography. Vol. 9, pp. 1-18

16. GARVINE, R.W. 1979b. An integral hydrodynamic model of upper ocean frontal dynamics, Part II: Physical characteristics and comparison with observations. Journal of Phys. Oceanography. Vol. 9, pp. 19-26

17. GARVINE, R.W. 1980. The circulation dynamics and thermodynamics of upper ocean density fronts, Journal of Phys. Oceanography. Vol. 10, pp. 2058-2081

18. GARVINE, R.W. and J.D. MONK. 1974. Frontal structure of a river plume. Journal of Geophysical Res. Vol. 79(5), pp. 2251-2259

19. GIOVANDO, L.F. and S. TABATA. 1970. Measurements of surface flow in the Strait of Georgia by means of free-floating currents followers. Tech. Rep. No. 163, Fish. Res. Board Can., 69 pp.

20. GROVES, G.W. and E.J. HANNAN, 1968. Time series regression of sea level on weather, Reviews of Geophysics, Vol 6(2), pp 129-174

21. JENKINS, G.M. and D.G. WATTS. 1968. Spectral Analysis and its applications. Holden Day, San Fransisco, 525 pp.

22. KANTHA, L.H., O.M. PHILLIPS and R.S. AZAD, 1977. On turbulent entrainment at a stable density interface. J. Fluid Mech. Vol. 79 part 4, pp. 753-768

23. KATO, H. and O.M. PHILLIPS, 1969. On the penetration of a turbulent layer into a stratified fluid, J. Fluid Mech. Vol. 37, pp. 643-655

24. KEULEGAN, G.H. 1966. The mechanics of an arrested saline wedge. Estuary and coastline hydrodynamics, A.T. Ippen (Ed.), McGraw-Hill, New York, pp. 546-574

25. KULLENBERG, G. 1977. Entrainment velocity in natural stratified vertical shear flow. Estuarine and Coastal Marine Science, 5:329-338

26. LARGE, W.G. and S. POND. 1981. Open ocean momentum flux measurements in moderate to strong winds, Journal of Physical Oceanography, Vol 11 No. 3, pp 324-336

27. LEBLOND, P.H. 198X. The Strait of Georgia: functional anatomy of a coastal sea. Can. J. Fish. Aquat. Sci. (Waiting publication)

28. LONG, R.R. 1975. The influence of shear on mixing across density interfaces. J.F.M. 70:305-320

29. LONG, R.R. 1978. A theory of mixing in a stably stratified fluid. J. Fluid Mech. Vol. 84 part 1, pp. 113-124

30. MCCLIMANS, T.A. 1980. Energetics of mixing processes in fjords. Fjords oceanography, H.J. Freeland, D.M. Farmer and C.D. Levings (Ed.) Plenum Press, New York, pp. 215-218

31. PARKER, B.B. 1977. Tidal hydrodynamics in the Strait of Juan de Fuca-Strait of Georgia. NOAA Tech. Rep. NOS 69, U.S. Department of Commerce, 56 pp.

32. SPATH, H. 1969. Exponential spline interpolation. Computing, 4:225-233.

33. STRONACH, J.A. 1977. Observational and modelling studies of the Fraser River Plume. Ph.D. Thesis, University of British Columbia, 221 pp.

34. STRONACH, J.A. 1981. The Fraser River Plume, Strait of Georgia. In: Ocean Management 6, Elsevier Scientific Publishing Company, pp. 201-221.

35. TABATA, S. 1972. The movement of the Fraser River-influenced water from a series of aerial photographs. Marine Sciences Branch, Pacific Region, Pacific Mar. Rep. No. 72-6, 69 pp.

36. TULLY, J.P. and A.J. DODIMEAD, 1957. Properties of the water in the Strait of Georgia and influencing factors. J. Fish. Res. Bd. Can. Vol. 14, pp. 241-319

37. WALDICHUK, M. 1957. Physical oceanography of the Strait of Georgia, British Columbia. J. Fish. Res. Board Can. 14:312-486.

38. WRIGHT, L.D. and J.M. COLEMAN, 1971. Effluent expansion

and interfacial mixing in the presence of a salt wedge, Mississipi River Delta. J. Geophysical Res. Vol. 76, pp. 8649-8661

39. WU, J. 1973. Wind-induced turbulent entrainment across a stable density interface. J. Fluid Mech. Vol. 61 part 2, pp. 275-287